Combining Surface Analytical and Computational Techniques to Investigate Orientation Effects of Immobilized Proteins

Elisa Turla Harrison

A dissertation submitted in partial fulfillment of the

requirements for the degree of

Doctor of Philosophy

University of Washington

2017

Reading Committee:

David G. Castner, Chair

Gianluca Interlandi, Co-Chair

Buddy Ratner

Program Authorized to Offer Degree:

Department of Chemical Engineering

University of Washington

Abstract

Combining Surface Analytical and Computational Techniques
to Investigate Orientation Effects of Immobilized Proteins

Elisa Turla Harrison

Chair of the Supervisory Committee:
Professor David G. Castner
Departments of Chemical Engineering and Bioengineering

Controlling how proteins are immobilized (e.g. controlling their orientation and conformation) is essential for developing and optimizing the performance of *in vitro* protein-binding devices, such as enzyme-linked immunosorbent assays. The objective of this work is to develop new methodologies to study proteins and complex mixtures of proteins immobilized onto surfaces. The focus of this study was to control and characterize the orientation of protein G B1, an IgG antibody-binding domain of protein G, on well-defined surfaces as well as measure the effect of protein G B1 orientation on IgG antibody binding using a variety of surface analytical and computational techniques.

The surface sensitivity of time-of-flight secondary ion mass spectrometry (ToF-SIMS) was used to distinguish between different proteins and their orientation by monitoring the changes in intensity of characteristic amino acid mass fragments. Amino acids distributed asymmetrically were used to calculate peak intensity ratios from ToF-SIMS data to determine the orientation of five different cysteine mutants of protein G B1 covalently attached to a maleimide surface.

To study the effect of protein orientation on antibody binding, we formed multilayer protein films by binding IgG to protein G B1 films. Quartz crystal microbalance with dissipation monitoring (QCM-D) detected protein coverages of 69 – 130 ng/cm^2 (theoretical mass of a monolayer of protein G B1 is 110 – 160 ng/cm^2). QCM-D and

X-ray photoelectron spectroscopy analysis revealed that packing density along with orientation affected the antibody binding process. Spectra from ToF-SIMS using large Ar gas cluster ion sources distinguished between different proteins in multilayer protein systems.

A Monte Carlo algorithm was developed to predict protein orientation on surfaces. Two distinct orientations of protein G B1 adsorbed onto a hydrophobic surface were found and characterized as two mutually exclusive sets of amino acids on the outermost β-sheets contacting the surface. This prediction was consistent with sum frequency generation (SFG) vibrational spectroscopy results. In fact, theoretical SFG spectra calculated from an equal combination of the two predicted orientations exhibited reasonable agreement with measured spectra of protein G B1 on polystyrene surfaces. These results show that computational methods to study proteins on surfaces can complement surface analytical data.

TABLE OF CONTENTS

LIST OF FIGURES

LIST OF TABLES

ACKNOWLEDGEMENTS

Firstly, I would like to express my sincere gratitude to my advisor Prof. David Castner for his support of my PhD study and research. I am grateful for the motivation, enthusiasm, and immense knowledge he provided along the way. I cannot imagine a better advisor and mentor for my PhD study.

I am grateful to my mom and dad, who have provided endless motivation and emotional support in my life. I am also grateful to my other family members, near and far, for encouraging me along the way.

A very special thank you goes out to my fellow Chemical Engineers for brainstorming, complaining, and helping to keep my sanity during my graduate career. I don't know what I would do without coffee breaks and happy hours.

I can't forget all the friends I have made along the way. I am forever grateful for their love and support. I am grateful for all the book clubs, band practices, yoga sessions, etc. for maintaining a life outside the lab.

Finally, last but not least, I am grateful to everyone in the NESAC/Bio group for their support and assistance. It was great sharing a laboratory and office with all of you.

Chapter 1. INTRODUCTION

1.1 GENERAL OVERVIEW

1.1.1 *PROTEIN/SURFACE INTERACTIONS*

A full understanding of the interactions between proteins and surfaces, especially at the molecular level, is essential in the development of many diverse applications including biosensors, medical devices, pharmaceutical drugs, and environmental test devices [1-6]. Since proteins will immediately adsorb onto any material when it comes in contact with a biological fluid, the function of the material may be affected by the structure, activity, and orientation of immobilized proteins.

Many proteins undergo orientation or conformation changes upon adsorption. For example, large, globular proteins are known to unfold or denature on hydrophobic surfaces to expose hydrophobic amino acids that would otherwise be buried when surrounded by solvent molecules [7-10]. On the contrary, some proteins, such as the LKα14 peptide, only form an ordered secondary structure upon adsorption onto a surface and will lose their structure if kept in solution for long periods of time [11].

Control of the immobilization of proteins on the surface is essential for the development of *in vitro* binding protein devices, such as enzyme-linked immunosorbent assays (ELISA) and protein microarrays [12-14]. Controlled adsorption of proteins on surfaces, via hydrophobic interactions, electrostatic interaction, or covalent attachment, has been used to improve the antibody binding capabilities of binding assays. Specifically, the orientation of proteins can play a vital role in the function and performance of such binding assays [14-22].

The need to control the immobilization of proteins on surfaces motivates the necessity for developing methods capable of fully analyzing protein-surface interactions. Thus, surface analytical and computational techniques are being developed to gain a more detailed understanding of immobilized proteins.

1.1.2 *Surface Analytical Instrumentation*

Qualitative techniques are currently used to obtain information about immobilized proteins on surfaces. In binding assays, such as sandwich ELISAs, the structure and activity of proteins are indirectly determined by measuring how the proteins bind to other proteins and/or antibodies [4, 5, 22, 23]. Oftentimes, many layers of proteins and antibodies are formed on top of the protein of interest or labels are required before any information can be gathered. Proteins that would otherwise be ruled out because of a lack of signal may, in fact, be useful if researchers could fully control the structure and activity of the adsorbed protein. To take the empirical trial and error aspect out of the design of diagnostic tools, highly sensitive, quantitative, and label-free tools are required.

Quantitative techniques, such as nuclear magnetic resonance (NMR) and X-ray diffraction (XRD), have been developed to analyze the structure of proteins in solution or in its crystalline phase [24-29]. The Research Collaboratory for Structural Bioinformatics (RCSB) protein databank contains protein structures of over 116,000 proteins [www.rcsb.org] [30]. Unfortunately, a databank for adsorbed protein structures has not been established because the structure of proteins adsorbed onto a surface is not well understood. This particular lack of scientific data emphasizes the need for techniques to analyze immobilized proteins.

Surface analytical techniques, such as X-ray photoelectron spectroscopy (XPS), time-of-flight secondary ion mass spectrometry (ToF-SIMS), quartz crystal microbalance with dissipation monitoring (QCM-D), and sum frequency generation (SFG), can provide information on the composition, mass of adsorbed proteins, orientation, activity, and adsorption/binding kinetics of immobilized proteins [6, 12, 31-49]. While not one technique can provide a full understanding of protein-surface interactions, combining many label-free, surface-sensitive techniques can provide the molecular-level information of protein-surface systems lacking in other techniques that rely on indirect measurements, the use of labels, or comparison to solution or crystalline phases.

1.1.3 *Computational Analysis of Proteins on Surfaces*

Development of computational methods to study proteins on surfaces can complement surface analytical data. Computational methods, such as molecular dynamics (MD) simulations, can provide atomic-level information on interactions between proteins and surfaces that may not be accessible with experimental techniques [50-53]. However, because of the vast conformational space and large number of degrees of freedom when describing protein-surface interactions, classical MD is limited to time scales that may not be sufficient to sample enough orientations of the protein on the surface.

Monte Carlo (MC) techniques, on the other hand, allow the sampling of protein orientations on surfaces at a lower computational cost than conventional MD simulations. The widely used MC-based method, Rosetta, was developed to efficiently sample the conformational space of a protein [54, 55]. However, Rosetta relies on a knowledge-based scoring function, and currently not enough examples of protein-surface systems have been characterized at atomic-level detail to correctly optimize Rosetta's scoring function. Thus, it is necessary to develop approaches that do not rely on the existence of fully characterized protein-surface models.

1.1.4 *Specific Aims*

The goal of this work is to develop new methodologies to study proteins and complex mixtures of proteins on surfaces. The goal is to stress the importance of using a multi-technique approach, combining both surface analytical and computational methods, to fully characterize proteins on surfaces. This work focuses on determining the orientation, conformation, and binding of immobilized proteins on a variety of surfaces and studying how the orientation of immobilized proteins affects the immobilization/binding of subsequent proteins and antibodies.

The work outlined here focuses on two main aspects of protein immobilization: (1) orientation of immobilized proteins and (2) the formation of complex, multicomponent protein films. The aims of this work are as follows:

Specific Aim 1: Predict the orientation of protein G B1 on hydrophobic surfaces using Monte Carlo simulations combined with surface analytical techniques, including QCM-D and SFG [56]. (Biointerphases, 2017. **12**(2): p. 02D401.)

Chapter 3 discusses Monte Carlo simulations to predict the orientation of proteins on a hydrophobic surface. Monte Carlo simulations can be extended to predict the orientation of proteins on more complex surfaces, such as hydrophilic and charged surfaces.

Specific Aim 2: Control the orientation of cysteine mutants of protein G B1 via covalent attachment to a surface and use surface analytical methods such as XPS, QCM-D, and ToF-SIMS to characterize the protein films.

Chapter 4 discusses the controlling of protein G B1 orientation, using point mutations to control the site of attachment, and using XPS and QCM-D to determine the amount of adsorbed protein and ToF-SIMS to determine the protein orientation.

Specific Aim 3: Analyze the effect of protein G B1 orientation on antibody binding in complex, multilayer protein systems using complementary techniques of XPS, QCM-D, and ToF-SIMS. This work can be extended to depth profile through complex multilayer protein films formed from protein G B1 and the immunoglobulin (IgG) antibody using ToF-SIMS with larger Ar cluster ions.

Chapter 5 discusses work using QCM-D to study antibody binding to the initial layer of immobilized protein G B1 cysteine mutants and introduces effects of the addition of secondary antibodies in the formation of more complex multicomponent films in a step-wise fashion. Chapter 5 also discusses developing methodology to distinguish between the different proteins using the J105 ToF-SIMS.

Appendix: The appendix discusses the study of the denaturation and orientation of adsorbed plasma proteins on bare gold and sodium styrenesulfonate (NaSS) grafted surfaces using ToF-SIMS and XPS. For full text, see ref. [40].

Chapter 2. METHODS AND MATERIALS

2.1 PROTEIN IMMOBILIZATION

2.1.1 *SURFACE PREPARATION AND MODIFICATION*

When developing methods to understand protein-surface interactions, e.g., controlling immobilization, orientation, conformation and binding activity, it is best to start with simple, model systems and then increase in complexity. Surfaces can be modified to control protein immobilization through interactions such as hydrophobicity, charge-charge, ligand binding and covalent bonding [39, 57-62]. Self-assembled monolayers (SAMs) are commonly used for surface modification because of their ease of preparation, precision of surface control, and wide variety of possible surface chemistries [35, 58, 60, 63-69]. The thiol groups on one end of the molecules bind strongly to a gold surface and self assembles into a well-ordered monolayer due to Van der Waal interactions between the alkane chains. The headgroup on the other end of the thiol molecule is then accessible to the surrounding environment and can be modified to optimize protein immobilization. Poly(ethylene glycol) (PEG) chains are often used between the thiol anchors and the headgroup to reduce nonspecific adsorption as well as inhibiting unfolding of the targeted protein as it is immobilized onto the surface [50, 60, 64].

The SAM substrates used in this work were prepared by submerging gold-coated silicon substrates in a solution of 1 mM maleimide-terminated (MEG) disulfide (HO-EG4-C11-S-S-C11-EG6-NHCO-Maleimide, Prochimia, Sopot, Poland) in 200-proof ethanol (Fisher Scientific) for at least 16 hours. The substrates were then rinsed with 200-proof ethanol and sonicated in ethanol to remove unbound molecules. To prepare bare gold substrates, the gold-coated substrates were submerged in 200-proof ethanol in a separate hood to avoid vapor deposition of thiols or disulfides.

Gold-coated silicon wafers and gold-coated quartz crystal sensors were used as substrates for protein immobilization studies. Gold-coated silicon wafers were used for XPS and ToF-SIMS studies and gold-coated quartz crystal sensors were used in QCM-

D experiments. Silicon wafers (Silicon Valley Microelectronics Inc., San Jose, CA) were diced into 1×1 cm^2 substrates using a diamond saw. Gold substrates were fabricated by depositing a 5 nm titanium adhesion layer followed by depositing a 100 nm gold layer onto the diced and cleaned silicon substrates via electron-beam deposition at room temperature and pressures <1 $x10^{-6}$ torr. Gold-coated quartz crystal sensors (Q-Sense, Gothenburg, Sweden) were cleaned using the UV-Ozone cleaner for 10 minutes and a 75˚C heated piranha solution (5:1:1 water:hydrogen peroxide:ammonium hydroxide solution; caution: piranha solution reacts violently with organic compounds) for 5 minutes prior to surface modification. Polystyrene-coated gold quartz crystals, used as a hydrophobic surface (described in Chapter 3), were purchased by Q-Sense and used without any further sample preparation (Q-Sense, Sweden).

2.1.2 *PROTEIN SYNTHESIS*

Protein G B1, a 6 kDa, 56 amino acid immunoglobulin (IgG) binding domain of protein G, was used to study the effect of orientation on antibody binding. This protein was chosen because of its stability, both in solution and immobilized on surfaces, and the availability of experimental data [25, 31, 32, 53, 70-76]. The five cysteine mutants listed in Table 2.1 were synthesized to vary the site of immobilization.

Table 2.1. Five cysteine mutants synthesized for this work.

Amino acid replaced	Abbreviation
Threonine 11	T11C
Valine 21	V21C
Asparatic-acid 35	D35C
Glutamic-acid 42	E42C
Threonine 49	T49C

Protein G B1, wildtype and the various cysteine point mutants, used in this work were synthesized by the Baker group (Protein Design, University of Washington, Seattle, WA). Recombinant protein G B1 was expressed in E. coli and purified using IMAC and the SMT3/ULP1 protease to cleave the 10xHis tag, then verified for identity using intact mass spectrometry. The amino acids chosen for the point mutations were selected

based on location, ease of synthesis, and predicted binding site of protein G B1 to the IgG antibody. The predicted binding site of protein G B1 to the Fc region of the IgG antibody is shown as a cartoon in Figure 2.1.

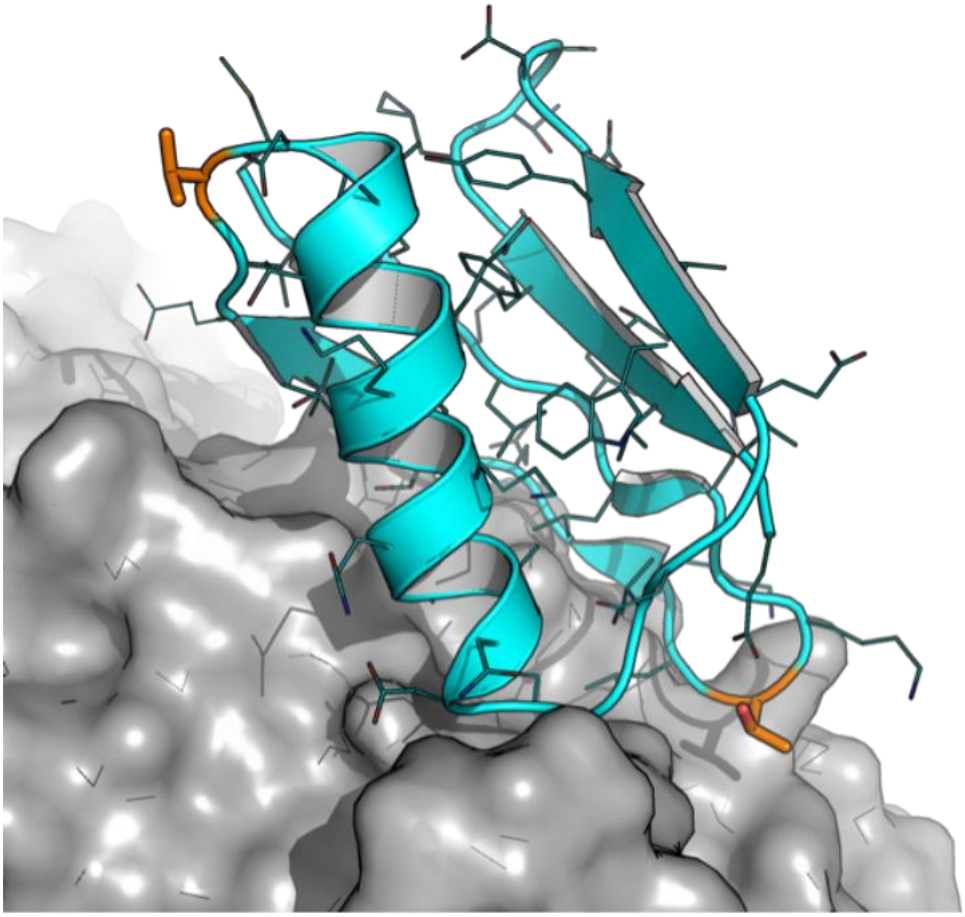

Figure 2.1. Proposed binding of protein G B1 (cyan) to the Fc region of the IgG antibody (grey). Two of the cysteine mutants (top left: T11C and bottom right: V21C) are highlighted in orange.

Protein G B1 for the sum frequency generation (SFG) experiments was expressed and purified as described elsewhere [32]. Whole IgG (H+L) antibody and F(ab')$_2$ fragment of the IgG antibody were purchased from Jackson ImmunoResearch (West Grove, PA).

2.1.3 *Protein Immobilization Methods*

Depending on the instrument used, protein immobilization was done in either a static or flow mode. Protein immobilization for X-ray photoelectron spectroscopy (XPS) and time-of-flight secondary ion mass spectrometry (ToF-SIMS) studies was done using static

adsorption while protein immobilization for quartz crystal microbalance with dissipation monitoring (QCM-D) studies was done in a flow regime.

Phosphate buffered saline (PBS) solution (0.01 M phosphate, 0.138 M sodium chloride, 0.0027 M potassium chloride, pH 7.4) was purchased from Sigma (Sigma-Aldrich, St Louis, MO). Bicarbonate/carbonate buffer (50mM, pH 9.5) was prepared by adding 1.59 g of sodium carbonate and 2.93 g of sodium bicarbonate in 1 L of deionized water. The buffer was filtered, degassed, and sonicated for 1 hour prior to use. Protein G B1 and IgG solutions were prepared in bicarbonate/carbonate buffer (50 mM, pH 9.5). The protein G B1 used in this work were the wildtype and five cysteine mutants: threonine11 to cysteine (T11C), valine21 to cysteine (V21C), asparatic-acid35 to cysteine (D35C), glutamic-acid42 to cysteine (E42C), and threonine49 to cysteine (T49C).

Substrates used for static protein immobilization were hydrated in 0.5 mL degassed buffer in a 24-well plate for 30 min at room temperature prior to adding protein solution and then allowing the immobilization to occur for at least 16 hours at 4˚C, 2 hours at 37˚C, or 2 hours at room temperature. After protein immobilization, substrates were rinsed by serial dilution in buffer and then submerged in a series of two buffer and three water solutions for 5 min each while mixing with a stir bar. Substrates were then dried and stored under nitrogen gas. Substrates were analyzed by XPS and ToF-SIMS within a week of preparation. Replicates were prepared on different days using freshly prepared protein solutions.

Protein/antibody multilayer substrates were prepared similarly. After Protein G B1 immobilization and rinsing, 1 mg/mL IgG antibody was added for at least 16 hours at 4˚C, 2 hours at 37˚C, or 2 hours at room temperature. Substrates were again rinsed by serial dilution in buffer and then submerged in a series of two buffer and three water solutions for 5 min each while mixing with a stir bar. Substrates were then dried and stored under nitrogen gas. Substrates were analyzed by XPS and ToF-SIMS within a week of preparation. Replicates were prepared on different days using freshly prepared protein solutions.

Additional protein layers, including $F(ab')_2$ fragment of IgG antibodies and another layer of whole (H+L) IgG antibodies, were prepared in a similar fashion. A cartoon of the

multilayer protein system is shown in Figure 2.2. Modifications in the protein adsorption protocol, such as bovine serum albumin (BSA) blocking, might be required in future experiments to avoid nonspecific adsorption as the system increases in complexity.

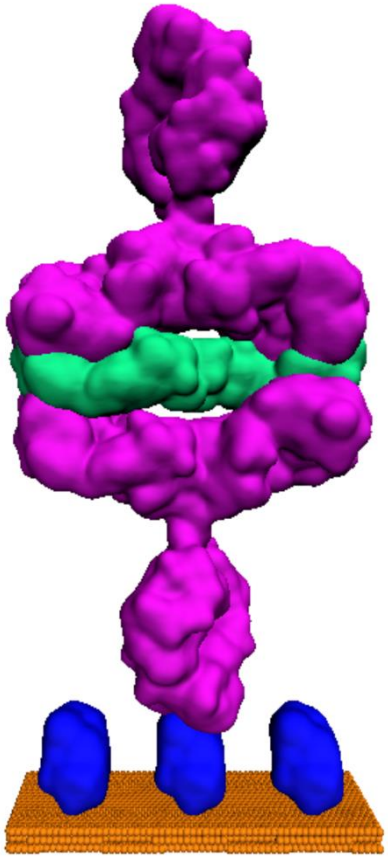

Figure 2.2. Cartoon of multilayer protein system consisting of a surface (gold), protein G B1 (blue), whole (H+L) IgG antibody (magenta), and F(ab')$_2$ fragment of IgG antibody (green).

Sum frequency generation (SFG) was used to validate computational results. Calculated SFG spectra based on Monte Carlo predicted orientations were compared with experimental data of protein G B1 adsorbed onto polystyrene. Details of the SFG setup are published elsewhere and will only be briefly discussed here [28]. One side of the CaF2 prism was spin coated with a 100 nm polystyrene film according to a procedure described in Ref. [28]. The polystyrene side was then brought into contact with the PBS buffer solution, and the interface was probed through the backside of the prism. A 0.1 mg/ml protein solution in 1 PBS buffer and pH 7 was injected into the flow cell, replacing the clean buffer inside the cell.

2.2 SURFACE ANALYTICAL METHODS

2.2.1 *X-RAY PHOTOELECTRON SPECTROSCOPY*

XPS can determine the elemental composition of the top 10 nm of the substrate surface [42, 77]. In this work, XPS was used to verify the quality of the substrates and to quantify protein adsorption. In the development of a multi-layer protein film, each layer was fully analyzed using XPS in a step-wise fashion. This way, we can determine the quality of the SAMs formed and how much protein was adsorbed.

XPS is based on the photoelectric effect. X-rays bombard the sample and electrons from the atoms' core and valance bands, called photoelectrons, are ejected and analyzed [77]. The kinetic energy (*KE*) of the photoelectrons is measured and the binding energy (E_B) of the photoelectrons is calculated using the X-ray photon energy (*hv*), which is a fixed, known energy. The binding energy electrically conductive samples placed in direct contact with the spectrometer is given by:

$$E_B = h\nu - KE - \phi_{sp} \tag{2.1}$$

Where the work function (Φ) is the minimum energy required to eject an electron into the vacuum from the highest occupied energy level. The spectrometer work function (Φ_{sp}) can be calibrated using a clean bare gold sample and remains constant as long as the spectrometer maintains in ultra-high vacuum (UHV). Insulating samples require charge neutralization using a low-energy (<20 eV) electron flood gun. However, the samples prepared in this study were conducting and did not require charge neutralization during XPS analysis. If the overlayer becomes too thick (>10 nm), charging may occur. Careful experimental design will be needed when forming multilayer protein films thicker than 10 nm.

The atomic percentage of each element is calculated from the photoelectron yield for a particular orbital (e.g., C1s). The binding energy of the photoelectrons depends on the type and environment of the atom. Therefore, high-resolution XPS spectra can be used to determine, for example, the quality of SAMs based on the presence and ratio of bound and unbound S2p peaks [78].

XPS data were acquired on a SSI S-Probe XPS system (Surface Science Instruments, Mountain View, CA) using a monochromatic Al $Ka_{1,2}$ X-ray source (*hv* =1486.6eV). Survey and detailed scans were collected with analyzer pass energy of 150 eV and a 100 ms dwell time. The survey step size was 1 eV, while 0.4 eV was used for detail scans. High-resolution spectra were acquired with analyzer pass energy of 50 eV and a step size of 0.065 eV. Binding energy scales were calibrated by setting the CH_x peak in the C1s region to 284.6 eV, and a linear background was subtracted for all peak area quantifications. Elemental compositions (atomic percentages) were calculated using the Hawk Data Analysis 7 software (Service Physics, Inc., Bend, Oregon). The C1s, O1s, and Au4f peak areas were obtained from the survey spectra (0-1100 eV). The N1s (390-410 eV) and S2p (155-173 eV) peak areas were obtained from the detailed scans.

For protein adsorption, the atomic percentage of N1s was monitored since the protein (~14 atomic % N) has a larger nitrogen concentration compared to the SAM (~3 atomic % N) or bare gold substrate (no N). The gold signal is monitored to access the overlayer thickness and coverage since the gold signal will be attenuated as the overlayer thickness or coverage increases. The C1s, O1s, N1s, and S2p atomic percentages are renormalized to 100 % to remove the Au4f signal and investigate the organic overlayer composition.

2.2.2 *Quartz Crystal Microbalance with Dissipation Monitoring*

Quartz crystal microbalance with dissipation monitoring (QCM-D) can be used to measure changes in mass and viscoelastic properties of immobilized proteins and antibodies as a function of time [3, 4, 37, 38, 63, 79]. In this work, protein G B1 and IgG antibodies (both whole (H+L) IgG antibody and $F(ab')_2$ fragments of the IgG antibody) were immobilized onto a variety of surfaces, including bare gold, SAMs on gold, and polystyrene. A cartoon of the multilayer protein system is shown in Figure 2.2. The impact of surface properties on binding kinetics was monitored using changes in amount of protein G B1 immobilized and IgG antibodies bound.

QCM-D is based on the piezoelectric effect. When a voltage is applied to a piezoelectric quartz crystal, the material begins to oscillate. The frequency of oscillation will change depending on the amount of material deposited onto the quartz crystal. The dissipation is monitored by measuring decay as the voltage to the quartz crystal is turned off. Viscoelasticity, or the rigidity of the deposited layer, will cause the voltage to decay at different speeds [2, 5, 80, 81].

Adsorption and binding of protein G B1 and IgG antibodies was monitored using the E4 QCM-D (Q-Sense, Gothenburg, Sweden) system. Frequency and dissipation measurements were made on gold quartz crystals with fundamental frequencies of 4.95 MHz (Q-Sense, Gothenburg, Sweden). Replicates were conducted for each protein and substrate combination. The temperature was maintained at 22˚C. During the course of a typical QCM-D experiment, protein G B1 was immobilized onto the sensors at a concentrations ranging from 50 µg/mL to 1000 µg/mL in buffer at a flow rate of 300 µL/min. Following protein G B1 adsorption, the system was rinsed with buffer at 300 µL/min to remove any excess protein. IgG antibodies were then immobilized at a concentration of 50 µg/mL in buffer at a flow rate of 300 µL/min. Again, the system was rinsed with buffer at 300 µL/min to remove unbound antibodies. Additional layers were formed similarly. Prior to the QCM-D experiment, the temperature was stabilized for at least 30 min and the buffer baseline was established for at least 30 min.

The mass adsorbed, in ng/cm^2, can be calculated using both the Sauerbrey and Voigt model. Analysis for these measurements used the seventh overtone for calculating the Sauerbrey mass and the third, fifth, seventh, ninth, and eleventh overtones for calculating the viscoelastic Voigt mass. The Sauerbrey model assumes an inverse relationship between the change in frequency (Δf) and mass (Δm):

$$\Delta f = \frac{2f_0^2}{A\sqrt{\rho_q \mu_q}} \Delta m \qquad (2.2)$$

Where f_0 is the resonant frequency, A is the quartz crystal area, ρ_q is the density of quartz (2.648 g/cm^3), and μ_q is the shear modulus of quartz for AT-cut crystal (2.947x10^{11} g·cm^{-1}·s^{-2}) [82]. This model can only be used when the dissipation change is low, typically less than 5% of the change in frequency. In this case, the protein is

considered rigid. The Sauerbrey model was also used if all overtones of the frequency overlapped. If dissipation occurs, the Sauerbrey model will underestimate the mass. If the dissipation is too large to use the Sauerbrey model, the Voigt model can be used, which models the changes in viscoelastic properties as a damper and spring [83-85].

The estimated number of IgG antibodies bound to each protein G B1 was calculated by taking the ratio of the changes in frequency and multiplying by the ratio of molecular weights of the protein G B1 (PG) and IgG antibodies [38].

$$\frac{N_{IgG}}{N_{PG}} = \frac{\Delta f_{7,IgG}}{\Delta f_{7,PG}} \frac{MW_{PG}}{MW_{IgG}} \tag{2.3}$$

where MW_{PG} = 6 KDa and MW_{IgG} = 150 KDa. This analysis assumes that the water content of protein G B1 and IgG antibodies does not change upon binding.

Another method of interpreting the QCM-D frequency and dissipation data is by plotting the frequency versus the dissipation. The slope of this line provides information about protein adsorption over the time. If a change in the slope is observed, this indicates a change in the way the protein is adsorbing or the way the IgG antibodies are binding. An increased slope indicates a change to a softer overlayer, while a decreased slope suggests a change to a more rigid layer.

2.2.3 *Time of Flight Secondary Ion Mass Spectrometry*

The orientation of immobilized protein films can be determined using time-of-flight secondary ion mass spectrometry (ToF-SIMS) [12, 31, 32, 70, 86-88]. A primary ion beam bombards the surface causing a collision cascade that sputters molecular fragments from the top 1-3 nm of the sample surface. A small fraction of these molecular fragments are ionized, called secondary ions, and are extracted into the time-of-flight mass analyzer. Both positive and negative secondary ions can be analyzed [33, 89-92].

Negative and positive secondary ion spectra were acquired on a TOF.SIMS 5-100 instrument (ION-TOF, Munster, Germany) using a pulsed 25 keV Bi^{3+} primary ion beam under static conditions (primary ion dose < 10^{12} ions/cm^2). Spectra were collected from five 100 µm x 100 µm regions for each sample. Secondary ions were collected over a

range of 0–800 m/z at a mass resolution (m/Δm) between 4000–8000. Positive spectra m/z values were mass calibrated using CH_3^+, $C_2H_3^+$, and $C_3H_5^+$ peaks, and negative spectra using CH^-, OH^-, C_2H^-, C_3^-, C_4H^- and C_5^- peaks. Mass calibration errors were typically below 20 ppm.

Secondary ion spectra were also acquired with large Ar gas cluster ion beams (GCIBs) to increase the surface sensitivity when analyzing protein films [93-95]. Since all the proteins and antibodies used in this work are comprised of the same twenty-one amino acids, the increased surface sensitivity of the Ar clusters was important for distinguishing between the proteins [96-103].

Positive ion spectra produced from Ar GCIBs were acquired using a J105 imager (Ionoptika, Southhampton, UK). The GCIB was operated at 40 keV using argon 4000 clusters, containing 15% CO_2 to improve cluster formation (Matheson Tri-Gas, Fife, Washington). Spectra were collected from a 500 micron x 500 micron area with an ion dose of ~$3.6x10^{11}$ ions/cm^2). The instrument was mass calibrated using peaks at masses m/z 219, 527, and 731 from a thin film of Irganox 1010. Calibration errors were below 5 ppm. Depth profiles were acquired by taking sequential spectra using these same settings with the exception that the dose was kept at $9.3x10^{10}$ ions/cm^2 per layer.

Multivariate analysis techniques, such as principal component analysis (PCA), can be used to extract useful information from ToF-SIMS spectra that typically contain hundreds of peaks. PCA can identify differences between samples and help determine sources of these variances. A series of scripts written by NESAC/BIO for MATLAB (MathWorks, Inc., Natick, MA) was used for analysis. A list of protein-relevant peaks derived from amino acid fragments was compiled [87, 88]. The data was normalized by the sum of selected peaks, mean centered, and square root transformed to insure that variance within the data set was due to differences in sample variances rather than in sample means. Peaks that could originate from both the proteins and from the self-assembled monolayer substrates were eliminated from the data set prior to analysis. Also, samples where the intensity of the sodium ion peak was greater than 1% of the total intensity were not included in the ToF-SIMS analysis [104].

Peak ratio analysis of ToF-SIMS spectra used a peak list consisting of only protein amino acid-derived mass fragments. Ratios of intensities of peaks from amino acids on opposite ends of the protein can be used to suggest a preferred protein orientation when immobilized onto a surface [22, 31, 32, 70]. Peak intensity ratios were calculated as the sum of intensities of chosen amino acids from the C-terminus divided by the sum of intensities of chosen amino acids from the N-terminus.

2.2.4 *Sum Frequency Generation*

Sum frequency generation (SFG) spectroscopy can be used to determine the orientation of adsorbed protein [48]. For SFG vibrational spectroscopy, visible and infrared light beams are overlapped in time and space at a surface or interface. The sum frequency signal is generated at locations without inversion symmetry (e.g., interfaces) due to nonlinear optical frequency mixing. When the vibrations of interfacial species satisfy the SFG-selection rules (e.g., both Raman and IR active), the SFG signal is enhanced [105]. Owing to the nonlinear optical selection rules of SFG, only ordered protein layers at the interface are detected. Disordered proteins, either on the surface or nearby in solution, are not detected. In analogy to Raman or infrared spectroscopy, the amide I modes can provide detailed information about the folding and structure of interfacial proteins.

SFG spectra can be calculated using the method described in ref. [106]. The couplings between the amide groups can be determined from atom coordinates in protein structure files. Nearest neighbor couplings between amide groups can be calculated using *ab initio* methods that give the coupling as a function of the dihedral angle between the neighboring amide moieties. Non-nearest neighbor couplings are calculated with a coulomb-like transition dipole coupling model. After diagonalizing the Hamiltonian, the IR and Raman modes of the protein can be calculated from the eigenvalues and eigenvectors, and then their outer product can be used to calculate the vibrational SFG response [48, 56].

2.3 COMPUTATIONAL METHODS

2.3.1 *CHARMM22 FORCE FIELD IMPLEMENTED IN GROMACS PROTEIN SIMULATION PACKAGE*

Molecular dynamics has become a widely used method to study large bio-molecular systems such as proteins. However, the calculations involved have become increasingly complex as the complexity of the studied systems grows. So, the development of protein simulation packages has been essential. The GROningen MAchine for Chemical Simulation (GROMACS) open-access simulation package was developed for the simulation of biological (macro)molecules in aqueous solution [107, 108] and includes a suite of analysis tools to interpret the molecular dynamics trajectories [109]. However, it is important to note that the simulation package cannot be treated as a “black-box software” since parameters must be chosen carefully depending on the system simulated. This will be especially important for simulations of proteins on surfaces.

Choosing an accurate force field is a vital component in protein simulations to gain realistic and useful information from protein simulations [52]. The CHARMM PARAM22 force field is widely used in biomolecular simulations, especially with the simulations of proteins [110]. Forces and energies calculated as a part of a force field include bonded and non-bonded interactions.

$$E_{total} = E_{bonded} + E_{non-bonded} \quad (2.4)$$

$$E_{bonded} = E_{stretching} + E_{bending} + E_{torsion} + E_{improper} \quad (2.5)$$

$$E_{non-bonded} = E_{VanderWaals} + E_{Columbic} + E_{Solvation} \quad (2.6)$$

Two-, three-, or four-particle interactions are included in stretching, bending, and torsion energies, respectively, for the calculation of the bonded interaction energy. The improper energy term is mainly used to maintain planarity in a molecular structure [111]. The non-bonded energy includes Van der Waals (VDW), Coloumbic/electrostatics, and solvation terms. The VDW potential combines the attractive and repulsive forces between two non-bonded atoms. The electrostatic interaction, or Coloumbic interaction,

models charge distributions in a molecule. The distribution is represented as point charges localized in the nuclei of the atoms in the molecule [108, 112].

An accurate representation of the solvent surrounding the biomolecules is essential for realistic simulations. The aqueous environment can either be simulated explicitly, where all water molecules are included in the molecular dynamics simulation, or implicitly, where solvation effects are taken into account by means of a potential of mean force. Including water molecules explicitly is computationally very expensive. For this reason, implicit solvation models were based on the solvent accessible surface area [113] or on the amount of excluded water [114, 115]. Recent more accurate implicit solvation models are based on implementations of the Generalized Born equation, such as Still [116], HCT (Hawkins–Cramer–Truhlar) [117] and OBC (Onufriev–Bashford–Case) [116] Simulating solvation, whether it is explicitly or implicitly, can become computationally expensive.

2.3.2 *Monte Carlo Simulations*

Monte Carlo simulations allow the protein to sample many orientations on the surface at a lower computational cost [118, 119]. The predictions from the Monte Carlo simulations can then be used to complement results from surface analysis experiments that do not provide atomic detail. Also, the predictions can be used to start more accurate explicit solvent molecular dynamics simulations to study conformational changes of the protein at the interface with a surface.

Monte Carlo simulations must satisfy ergodicity, requiring that the local minimum be accessible using a finite number of random sampling steps [118-120].We chose to randomly make translational and rotational moves of a rigid protein for each sampling step and to keep the surface frozen. Periodic boundary conditions are applied to simulate an infinite surface. After a move, the total energy of the system is evaluated and the move is accepted or rejected according to a Metropolis criterion [120]. The accepted orientations thus satisfy the Boltzmann distribution.

The effective energy of the system, used in a Metropolis acceptance criterion, includes a VDW interaction term and a solvent accessible surface area (SASA) solvation term to account for the hydrophobic effect.

$$E_{Effective} = E_{VanderWaals} + E_{Coulombic} + G_{Solvation} \quad (2.7)$$

The VDW energy term was calculated using the program Gromacs 4.6 [107-109, 121] with the CHARMM22 force field [110, 122]. A graphene surface was chosen in the initial development of the Monte Carlo algorithm because Coulombic interactions could be ignored since graphene does not contain electrostatic charges. However, electrostatics will need to be included in future versions when simulating surfaces with polar groups.

$G_{Solvation}$ consists of a polar and a non-polar component:

$$G_{Solvation} = G_{polar} + G_{non-polar} \quad (2.8)$$

Since graphene is inert, we can ignore the polar solvation term (G_{polar}). For future versions when simulating surfaces with hydrophilic head groups, the Gpolar term will be included. For example, as shown in ref. [114], the $E_{Coulombic}$ term could be divided by the dielectric constant of water:

$$E_{Coulombic(with\ Solvation)} = {}^{E_{Coulombic}}/_{78.5} \quad (2.9)$$

The implicit solvation module currently available in Gromacs is based on a Generalized Born method, which assumes a compact system, like an unbound globular protein. Thus, we introduced a non-polar solvation term based on the solvent accessible surface area (SASA). This allowed us to penalize orientations where hydrophobic atoms, in both the protein and surface, are exposed to the solvent [24]. The non-polar solvation energy term was calculated by multiplying the surface tension (σ) by the solvent accessible surface area (A_{SASA}) for each atom.

$$G_{non-polar} = \sigma \times A_{SASA} \quad (2.10)$$

The SASA was calculated using a 1.4 Å probing radius. A surface tension of 100 kJ/mol/Å^2 was used for hydrophobic groups and -100 kJ/mol/Å^2 was used for hydrophilic groups.

Scripts were written in Tcl code and run using the program Visual Molecular Dynamics (VMD) [123]. Prior to a Monte Carlo simulation, the protein was energetically minimized in a Generalized Born implicit solvent using the steepest descent algorithm in Gromacs.

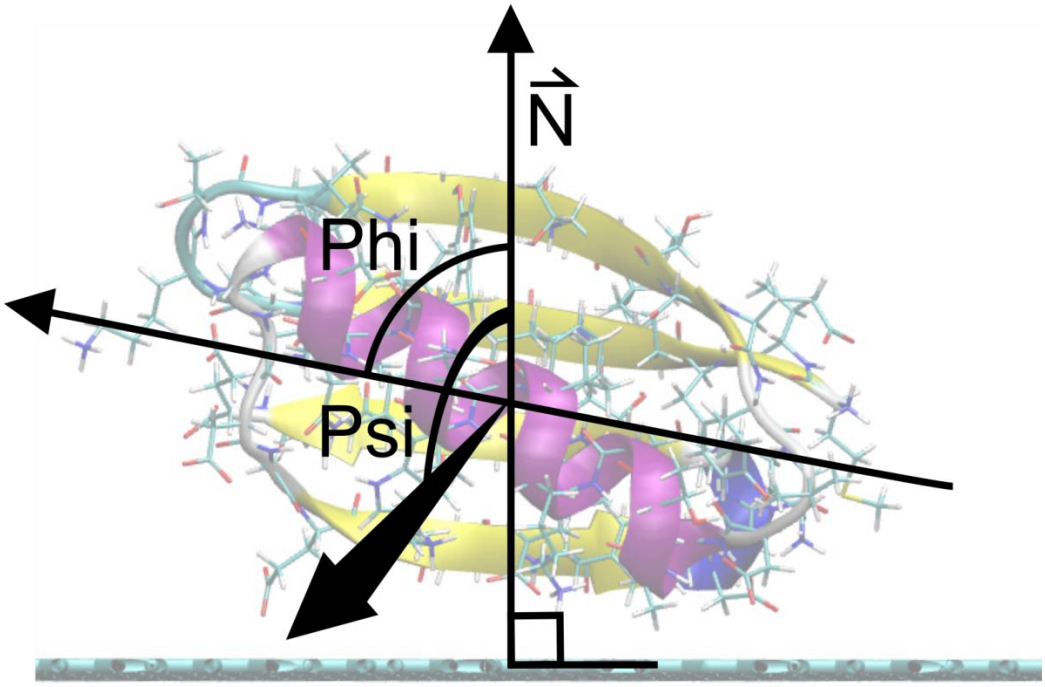

Figure 2.3. Schematic of principal axis angle analysis. The first two principal axis angles, Phi and Psi, are shown on one of the predicted orientations for protein G B1 on graphene. Phi and Psi are the angles between the principal axes and the surface normal vector, N.

The angle of orientation and the interaction between each residue and the surface was calculated for each Monte Carlo simulation. The angle of orientation is determined by calculating the angle between two principal axes, phi and psi, of the protein and the surface normal vector, as shown in Figure 2.3. The angles can be visualized using a heat map in ranges of 10 degrees [56]. The interaction between each residue and the surface was determined by calculating the number of times each residue is within 6 Å of the surface. This data was represented using a histogram of the normalized number of times the residue is within 6 Å of the surface for each residue of the protein. This data can also be visualized using a color heat map on the protein using Visual Molecular Dynamics (VMD).

2.3.3 *Molecular Dynamics Simulations*

Molecular dynamics (MD) simulations can evaluate the stability of a predicted orientation. The MD simulations were performed using the program Gromacs 4.6 [107] with the CHARMM22 force field [124] containing the CMAP correction [125, 126]. Although the force field used here is known to overestimate the stability of α-helical structures, we do not expect a significantly different outcome of the simulations even when using the latest available CHARMM36 force field, where this issue has been corrected [127], since the protein is shown here to be rigid when adsorbed. The protein G B1 and the graphene surface were placed in a 47.96 x 42.6 x 70 $Å^3$ water box containing 3,666 TIP3P water molecules and 4 Na^+ ions. The system was minimized using 1,000 steps of steepest descent. After minimization, positional restraints were applied to heavy atoms (all atoms excluding hydrogen atoms) of the protein and the system was simulated for 200 ps, during which the temperature of the system was ramped from 5 to 300 K and the water molecules equilibrated around the surface of the protein.

After this equilibration phase, the positional restraints were released and the system was simulated for a total of 50 ns. During the dynamics, the translation of the center of mass was removed and three-dimensional periodic boundary conditions were applied. The graphene surface atoms were kept fixed during the dynamics. Electrostatic and VDW interactions were calculated within a cutoff of 10 Å while long range electrostatic effects were taken into account by the Particle Mesh Ewald summation method [128]. The Nosé-Hoover thermostat [129, 130] with a time constant of 0.4 ps was used to maintain the temperature at 300 K. All bonds involving hydrogen atoms were kept fixed using the LINear Constraint Solver (LINCS) algorithm [131]. The dynamics were integrated with a time step of 2 fs and snapshots were saved every 10 ps.

Chapter 3. PREDICTING THE ORIENTATION OF PROTEIN G B1 ON HYDROPHOBIC SURFACES USING MONTE CARLO SIMULATIONS

Elisa T. Harrison
Department of Chemical Engineering, University of Washington, Seattle, Washington 98195

Tobias Weidner
Department of Chemistry, Aarhus University, 8000 Aarhus C, Denmark and Max Planck Institute for Polymer Research, 55128 Mainz, Germany

David G. Castner
Department of Chemical Engineering, University of Washington, Seattle, Washington 98195 and Department of Bioengineering, University of Washington, Seattle, Washington 98195

Gianluca Interlandi
Department of Bioengineering, University of Washington, Seattle, Washington 98195

(Received 25 August 2016; accepted 18 November 2016; published 6 December 2016)

Biointerphases 12 (2), 02D401

3.1 ABSTRACT

A Monte Carlo algorithm was developed to predict the most likely orientations of protein G B1, an immunoglobulin G (IgG) antibody-binding domain of protein G, adsorbed onto a hydrophobic surface. At each Monte Carlo step, the protein was rotated and translated as a rigid body. The assumption about rigidity was supported by quartz crystal microbalance with dissipation monitoring experiments, which indicated that protein G B1 adsorbed on a polystyrene surface with its native structure conserved and showed that its IgG antibody-binding activity was retained. The Monte Carlo simulations predicted that protein G B1 is likely adsorbed onto a hydrophobic surface in two

different orientations, characterized as two mutually exclusive sets of amino acids contacting the surface. This was consistent with sum frequency generation (SFG) vibrational spectroscopy results. In fact, theoretical SFG spectra calculated from an equal combination of the two predicted orientations exhibited reasonable agreement with measured spectra of protein G B1 on polystyrene surfaces. Also, in explicit solvent molecular dynamics simulations, protein G B1 maintained its predicted orientation in three out of four runs. This work shows that using a Monte Carlo approach can provide an accurate estimate of a protein orientation on a hydrophobic surface, which complements experimental surface analysis techniques and provides an initial system to study the interaction between a protein and a surface in molecular dynamics simulations.

3.2 INTRODUCTION

Materials in contact with the biological environment will immediately become coated with proteins and this adsorbed protein layer thus becomes the interface between the material and species in the surrounding environment, such as proteins, antibodies, antigens, lipids, and cells [45, 132]. The orientation of the adsorbed proteins may influence the interaction of the material with the biological environment [12]. For example, exposing active sites of binding proteins may increase efficiencies of *in vitro* diagnostic devices such as enzyme-linked immunosorbent assays (ELISAs) [133]. However, one main challenge for developing and improving devices like ELISA is determining the conformation and orientation of the proteins when adsorbed onto a surface, especially when multicomponent protein films are present. In fact, besides the possibility of undergoing conformational changes, protein molecules adsorbed onto surfaces might also align in an ordered manner with respect to the surface. In this manuscript, the orientation of a protein is characterized by which amino acids contact the surface and by the angle between the two major axes of symmetry and the surface normal. As the need for the improvement and the complexity of devices such as ELISA increases, so does the need for the development of techniques that can provide a complete understanding of protein–surface interactions. This includes characterizing

both how proteins are ordered (i.e., their orientation with respect to the surface) and any conformational changes the proteins might undergo upon adsorption.

Proteins immobilized onto surfaces have been extensively studied using experimental methods [35, 60, 61, 134-137]. Techniques such as quartz crystal microbalance with dissipation monitoring (QCM-D), surface plasmon resonance, and ellipsometry can provide useful information such as binding efficiencies and kinetics of adsorbing proteins, but can only indirectly suggest orientation information since many other factors influence protein binding [12, 41]. The surface sensitivity and the chemical specificity of time-of-flight secondary ion mass spectrometry (ToF-SIMS) can provide conformation and orientation information by tracking changes in secondary ion intensities from amino acid fragments unevenly distributed throughout the protein [43, 44, 86]. However, while this technique can provide orientation information, the conformation and structure of immobilized proteins may change upon being dried and subjecting them to ultrahigh vacuum prior to analysis. Sum frequency generation (SFG) vibrational spectroscopy provides orientation information since it relies on order within the sample, and samples can be analyzed in solution [138-140]. However, many of these techniques require that all proteins are uniformly oriented on the surface and are limited to providing an average orientation. For example, if multiple orientations of the protein exist on a given surface, extracting the different orientations from the experimental data becomes increasingly difficult as the number of orientations increases.

To complement and more completely interpret experimental results, the development of computational methods is needed to predict the structure of proteins on surfaces. Classical molecular dynamics (MD) simulations can provide atomic-level information on interactions between proteins and surfaces that may not be accessible with experimental techniques [141, 142]. However, because of the vast conformational space and large number of degrees of freedom present when describing protein–surface interactions, classical MD simulations are limited to time scales that may not be long enough to sample all protein orientations on the surface. The Monte Carlo-based method, Rosetta, has been developed to efficiently sample the conformational space of a protein [54], and it has been recently applied to study the interaction between the protein statherin and hydroxyapatite [55]. However, Rosetta relies on a knowledge-

based scoring function, and currently not enough examples of protein–surface systems have been characterized at the level of detail required to correctly optimize Rosetta's scoring function. Thus, there is the necessity to develop approaches that do not rely on the existence of fully characterized protein–surface models.

In this work, we have developed a method to predict the orientation of proteins on surfaces based on Monte Carlo simulations and an implicit solvation model. The developed algorithm was applied to determine the orientation of the LKα14 peptide and protein G B1 on a graphene surface. The LKα14 peptide is a 14 amino-acid model peptide consisting of only leucine and lysine residues that was designed to form an α-helical secondary structure when immobilized onto either hydrophobic or hydrophilic surfaces [143]. Since its orientation on surfaces is known, it was used here as a benchmark. The second, more complex system is protein G B1, a 6 kDa domain of protein G which binds to the Fc region of immunoglobulin (IgG) antibodies. This protein was chosen for this study because of its stability, both in solution and immobilized on surfaces, and the availability of experimental data [70]. The predictions from Monte Carlo simulations with protein G B1 were validated through SFG experiments. Finally, MD simulations in explicit solvent investigated the conformational stability of protein G B1 on graphene surfaces. The present work highlights how Monte Carlo simulations allow the sampling of protein orientations on surfaces at a lower computational cost than conventional MD simulations. The predictions can then be used to complement results from surface analysis experiments that do not provide atomic level detail or to start explicit solvent MD simulations to study conformational changes of the protein at the interface with a surface.

3.3 Materials and Methods

3.3.1 *Monte Carlo Simulations*

The Monte Carlo simulations performed here are based on the Metropolis criterion [120, 144]. At each Monte Carlo step, the protein was randomly translated and rotated as a rigid body while the surface was kept frozen. Periodic boundary conditions were applied to simulate an infinite surface. After a move, the total energy of the system was

evaluated, and the move was accepted or rejected according to the Metropolis criterion [120, 144]. The accepted orientations thus satisfy the Boltzmann distribution. The total energy of the system consisted of a van der Waals (VDW) interaction term and a solvation term to account for the hydrophobic effect. The VDW energy term was calculated using the program GROMACS 4. 6 [107] with the CHARMM22 force field [124]. Electrostatic interactions did not need to be calculated because graphene consists of only carbon atoms with neutral charges. Future versions of the algorithm that include surfaces with polar groups will need to consider also electrostatic interactions.

To take solvation effects into account, we introduced a nonpolar solvation term based on the solvent accessible surface area (SASA). This allowed us to penalize orientations where hydrophobic atoms, in both the protein and surface, are exposed to the solvent [113]. The nonpolar solvation energy term was calculated by multiplying a surface tension parameter (r) by the SASA of the groups of atoms listed in Table 3.1. The SASA was calculated using a 1.4 A˚ probing radius by means of the GROMACS package.

Table 3.1. Surface tension parameters (σ) used in the evaluation of the non-polar solvation term.

Group	Description	σ (kJ/mol/Å^2)
Hydrophobic sidechain	Residue name: Gly, Ala, Val, Leu, Ile, Met, Pro, Phe, Trp, and the aromatic ring of Tyr	100
Hydrophilic sidechain	Residue name: Ser, Thr, Asn, Gln, Cys, Arg, Asp, His, Lys, Glu, and the hydroxyl group of Tyr	-100
Hydrophobic backbone atoms	Cα-H and carbonyl carbon (C)	100
Hydrophilic backbone atoms	Carbonyl oxygen (O) and amide group (N-H)	-100
Hydrophobic surface atoms	Carbon (C)	100

The script is written in TOOLKIT command language and runs using the program VISUAL MOLECULAR DYNAMICS (VMD) [123]. The crystallographic structure of protein G B1 (PDB code 1PGA) was used. Prior to the Monte Carlo simulation, the coordinates of the protein were minimized in a generalized Born implicit solvent [145, 146] with 1000 steps of steepest descent by means of the program GROMACS [107].

Three Monte Carlo simulations were run for the LKα14 peptide and 13 Monte Carlo simulations were run for protein G B1. Each simulation was run for a total of 10,000 accepted moves, during which all but one simulation with protein G B1 converged to a stable orientation.

3.3.2 *Molecular Dynamics Simulations*

The MD simulations were performed using the program GROMACS 4.6 [107] with the CHARMM22 force field [124] containing the correction map (CMAP) correction [125, 126] (this is generally referred to as the CHARMM22/CMAP force field). Although the force field used here is known to overestimate the stability of a-helical structures, we do not expect a significantly different outcome of the simulations even when using the latest available CHARMM36 force field, where this issue has been corrected [127], since the protein is shown here to be rigid when adsorbed. The protein G B1 and the graphene surface were placed in a 47.96 × 42.6 × 70 $Å^3$ water box containing 3,666 TIP3P water molecules and four Na^+ ions. The system was minimized using 1,000 steps of steepest descent. After minimization, positional restraints were applied to heavy atoms (all atoms excluding hydrogen atoms) of the protein and the system was simulated for 200 ps, during which the temperature of the system was ramped from 5 to 300 K and the water molecules equilibrated around the surface of the protein.

After this equilibration phase, the positional restraints were released, and the system was simulated for a total of 50 ns. During the dynamics, the translation of the center of mass was removed, and three-dimensional periodic boundary conditions were applied. The graphene surface atoms were kept fixed during the dynamics. Electrostatic and van der Waals interactions were calculated within a cutoff of 10 A˚ while long range electrostatic effects were taken into account by the particle mesh Ewald summation method [128]. The Nose-Hoover thermostat [129, 130] with a time constant of 0.4 ps was used to maintain the temperature at 300 K. All bonds involving hydrogen atoms were kept fixed using the LINear Constraint Solver algorithm [131]. The dynamics were integrated with a time step of 2 fs, and snapshots were saved every 10 ps.

3.3.3 *Quartz Crystal Microbalance with Dissipation Monitoring*

Adsorption and binding of protein G B1 and IgG antibody onto polystyrene surfaces was monitored using the E4 QCMD (Q-Sense, Sweden) system. Frequency and dissipation measurements were made on polystyrene-coated gold quartz crystals with fundamental frequencies of 4.95 MHz (Q-Sense, Sweden). The analysis for these measurements used the fifth and seventh overtone. Experiments were repeated three times. The temperature was maintained at 22˚C.

During the course of each QCM-D experiment, protein G B1 was adsorbed onto the polystyrene-coated gold sensors from a 5 µg/ml phosphate buffered saline (PBS) solution (0.01 M phosphate, 0.138 M sodium chloride, and 0.0027 M potassium chloride) at a flow rate of 150 µl/min and a pH of 7.4. Following protein G B1 adsorption, the system was rinsed with PBS buffer at a 150 µl/min flow rate to remove any excess protein. IgG antibodies were then immobilized to adsorbed protein G B1 from a 5 µg/ml PBS solution at a flow rate of 150 µl/min and a pH of 7.4. Again, the system was rinsed with PBS buffer at a 150 µl/min flow rate to remove unbound antibodies. Dissipation was monitored to ensure that protein G B1 did not undergo significant viscoelastic changes upon adsorption.

3.3.4 *Sum Frequency Generation Spectroscopy*

Details of the SFG setup are published elsewhere and will only be briefly discussed here [28]. The visible beam from an EKSPLA Nd:YAG laser with a wavelength of 532 nm and the tunable IR beam from an EKSPLA optical parametric generation/ amplification unit were focused at the sample with energies of 120 and 180 µJ per pulse for the visible and the IR beams, respectively. The spectra were collected with 200 shots per data point in 4 cm^{-1} increments. The SFG spectra were normalized by the product of the intensities of the IR and visible pump beams, which were tracked with photodiodes. The input angles of the visible and IR beams after entering the prism were 47 and 58 with respect to the surface normal.

One side of the CaF2 prism was spin coated with a 100 nm polystyrene film according to a procedure described in Ref. [28]. The polystyrene side was then brought into contact with the PBS buffer solution, and the interface was probed through the backside of the prism. A 0.1 mg/ml protein solution in 1 PBS buffer and pH 7 was injected into the flow cell, replacing the clean buffer inside the cell.

3.3.5 *SFG Spectra Calculations*

SFG spectra were calculated using the method described in Ref. [147]. From the atom coordinates in the protein structure files from the Monte Carlo simulations, we determined the couplings between the amide groups: nearest neighbor couplings are calculated using *ab initio* methods that give the coupling as a function of the dihedral angle between the neighboring amide moieties; non-nearest neighbor couplings are calculated with a coulomb-like transition dipole coupling model. After diagonalizing the Hamiltonian, we calculated the IR and Raman modes of the protein from the eigenvalues and eigenvectors, and then take their outer product to calculate the vibrational SFG response. The background phase was kept at 3.5 and 1.5 rad for ssp (s-polarized SFG, s-polarized visible, and p-polarized IR) and ppp, respectively, which gave the best results, and thus these values were used for all spectra calculations.

3.3.6 *Materials*

Recombinant protein G B1 was expressed in Escherichia coli and purified using IMAC and the SMT3/ULP1 protease to cleave the 10xHis tag, then verified for identity using intact mass spectrometry. Protein G B1 for the SFG experiments was expressed and purified as described elsewhere [32]. IgG antibody and PBS solution (0.01 M phosphate, 0.138 M sodium chloride, and 0.0027 M potassium chloride, pH 7.4) was purchased from Sigma (Sigma-Aldrich, St. Louis, MO).

3.4 RESULTS

3.4.1 *TESTING THE MONTE CARLO ALGORITHM USING THE LKA14 PEPTIDE*

The LKα14 peptide, which consists of only leucine and lysine residues (Figure 3.1), was used as a benchmark because its orientation on hydrophobic surfaces has been determined experimentally in previous studies [11, 31, 52, 148]. When adsorbed onto either a charged or hydrophobic surface, this peptide assembles into an alpha-helical secondary structure where all the leucine residues lie on one side of the α-helix and all the lysine residues lie on the other side [52]. Thus, the LKα14 peptide has a predictable conformation and orientation on hydrophobic surfaces, such as polystyrene and methyl-terminated self-assembled monolayers, and its orientation and structure has been extensively studied with a wide variety of experimental and simulation techniques, including solid state NMR, SFG, and MD [11, 28, 52, 149]. This makes LKα14 on graphene a good benchmark system for testing the Monte Carlo method for protein orientation studies.

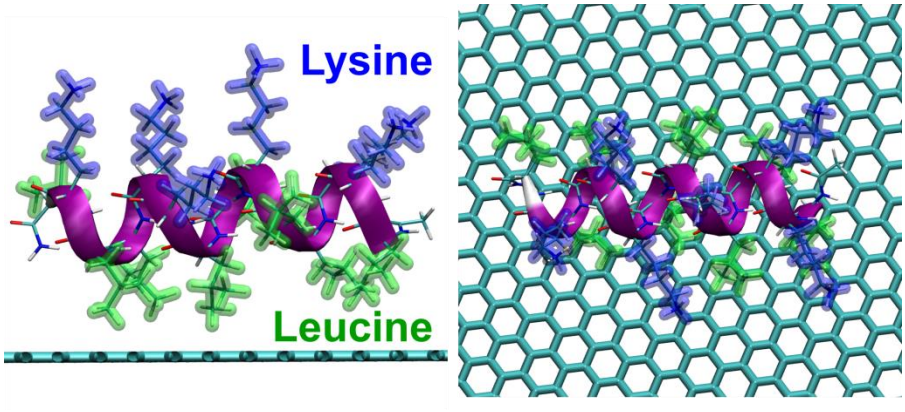

Figure 3.1. Two different views of the LKα14 peptide on a graphene surface.

For this purpose, three simulations of 10,000 accepted moves each were started with the LKα14 peptide near the graphene surface. The LKα14 peptide was generated using VMD [123] and each of the simulations started with the lysine amino acid residues closest to the surface. By the end of all three simulations, the LKα14 peptide flipped its orientation with the leucine amino acid residues closest to the surface. The total energy was monitored along the trajectories [Figure 3.2(a)]. The time series of the total energy revealed that the three simulations converged to one minimum. Previous SFG studies suggested an average orientation angle between the peptide backbone and the surface normal to be 80˚, or almost parallel to the surface [48]. In its most frequently sampled orientation, the angle between the principal axis of the peptide and the surface normal vector for the MC simulations was ~86˚ [Figure 3.2(b)], consistent with the SFG results. The agreement between the Monte Carlo and SFG results suggest that the Monte Carlo algorithm developed in this study can correctly describe the orientation of LKα14 adsorbed onto graphene surfaces.

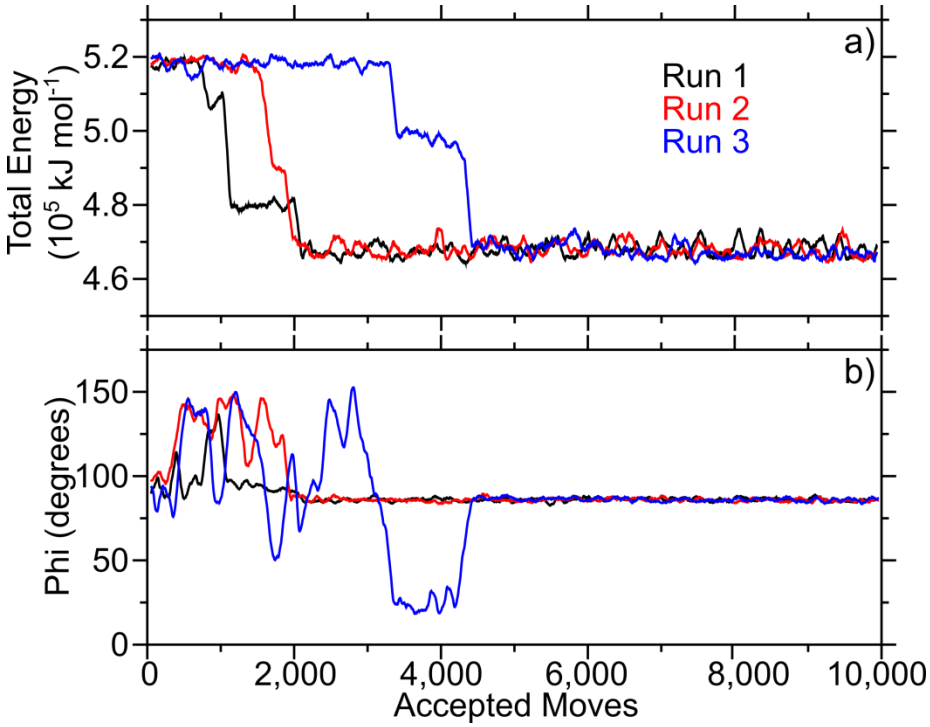

Figure 3.2. Total energy (a) and principal axis angle (b) of the LKα14 on graphene over the course of 10,000 accepted moves in three Monte Carlo simulations (shown in black, red, and blue). The simulations were started with the LKα14 peptide oriented such that the lysine residues were closest to the graphene surface. All plots show a 100-pt running average.

3.4.2 *Predicting the Orientation of Protein G B1 on a Graphene Surface*

The Monte Carlo algorithm was applied to a more complex, but widely studied, IgG antibody-binding domain of protein G, protein G B1. This 6 kDa binding domain consists of 56 residues and, when in solution, it adopts a secondary structure consisting of two β-sheets and one α-helix [Figure 3.3(a) and Figure 3.3(b)]. Like with the LKα14 peptide, Monte Carlo simulations were performed with protein G B1 on a graphene surface.

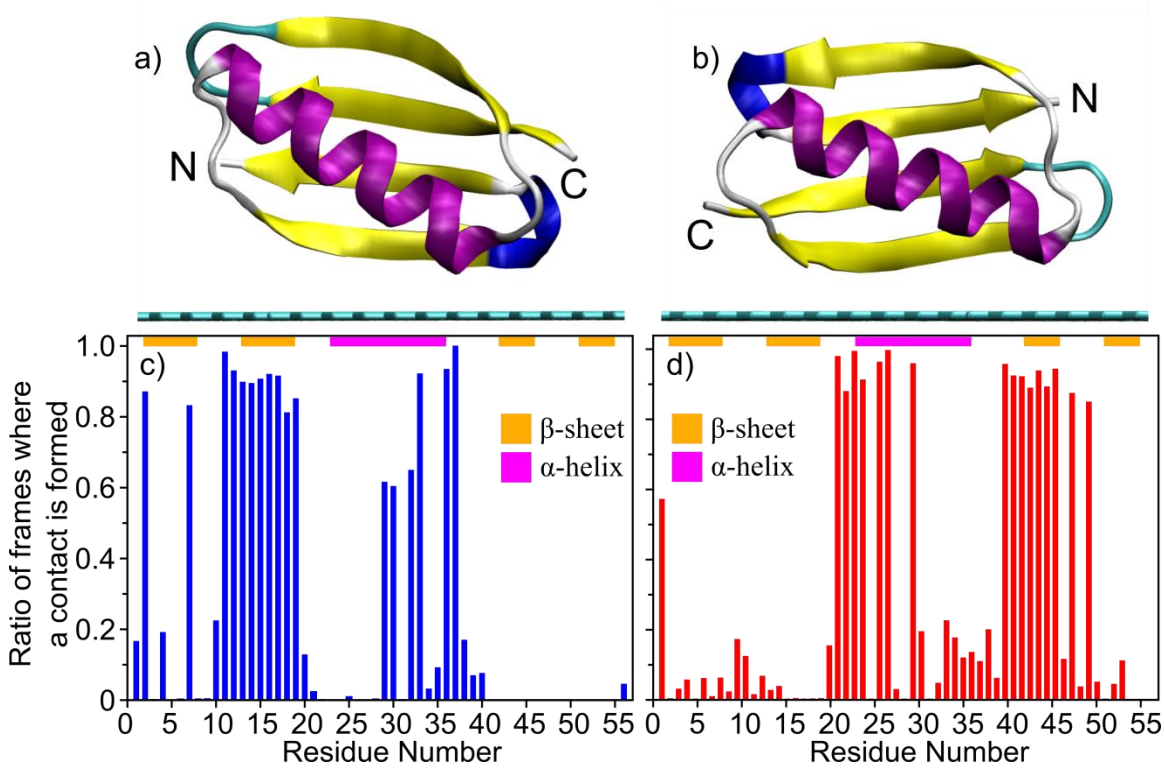

Figure 3.3. Predicted orientations of protein G B1 on a graphene surface through Monte Carlo simulations. The runs converged towards either the orientation represented in (a) or the orientation represented in (b). The graphene surface is colored in cyan and it is visible below the protein. The N- and C-termini of the protein are labeled. (c) and (d) Ratio of accepted Monte Carlo moves (referred to here as frames) where a particular residue is within 6 Å from the surface in the runs that converged either towards the orientation in (a) or in (b), respectively. The ratio is calculated with respect to the total number of sampled orientations where any atom of the protein is within 6 Å from the surface (prior to the calculation, the frames from all runs that converged towards either the orientation in (a) or in (b) were merged). In the plots, the secondary structure regions are indicated with horizontal bars and colored in magenta for α-helices or orange for β-sheets, respectively.

In total, 13 MC simulations were run using the same starting conformation. In one of the 13 simulations, the protein moved away from the surface and did not return during the course of the simulation, so this run was discarded. In the remaining 12 simulations, the protein converged to a stable orientation. The total energy was monitored along the trajectories. The time series of the total energy (Figure 3.4) revealed that each of the remaining 12 simulations converged to one of two energy minima, which corresponded to two distinct orientations of protein G B1 on the surface [Figure 3.3(a) and Figure 3.3(b)]. Runs 1, 3, 5, 8, 9, and 12 converged to one [Figure 3.3(a) and Figure 3.3(c)] while runs 2, 4, 6, 7, 10, and 11 converged to the other minimum [Figure 3.3(b) and Figure 3.3(d)].

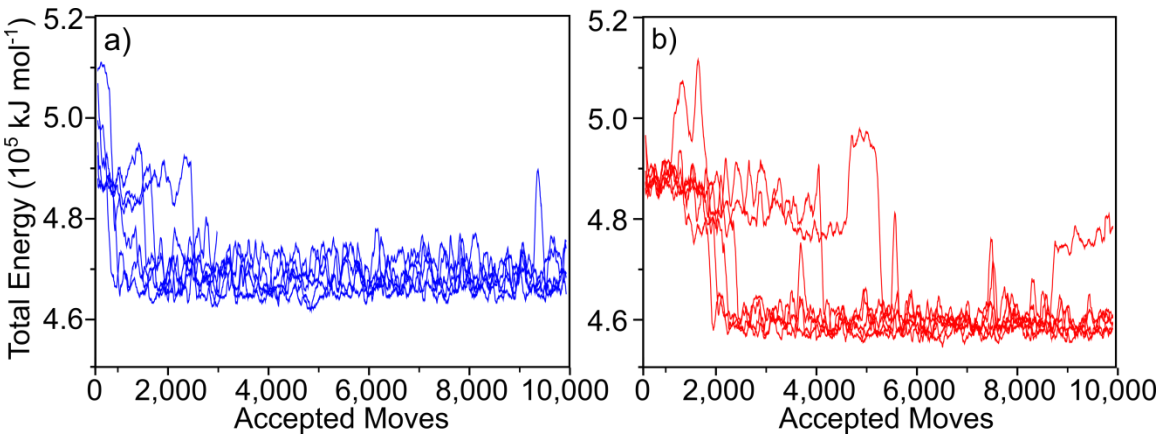

Figure 3.4. Total energy of the system over the course of 10,000 accepted moves. The two minimums were reached an equal number of times. (a) Orientation predicted in runs 1,3,5,8,9, and12. (b) Orientation predicted in runs 2,4,6,7,10, and 11. All plots show 100-pt running average.

The visual analysis of the PDB structures corresponding to the minima revealed that part of the α-helix and either one of the outermost β-strands contact the surface [Figure 3.3(a) and Figure 3.3(b)]. The predicted orientations differ from each other by a rotation of 180˚ around the second largest principal axis of the protein [Figure 3.3(a) and Figure 3.3(b)]. This can be quantitatively described by calculating the ratio of frames where a particular residue is in contact with the surface with respect to the total number of frames where the protein contacts the surface in simulations that converged toward either minimum [Figure 3.3(c) and Figure 3.3(d)]. Residues 13–19 in Figure 3.3(c) and

residues 42–46 in Figure 3.3(d) correspond to the outermost β-strands contacting the graphene surface in the two predicted orientations, respectively Figure 3.3(a) and Figure 3.3(b)]. Residues 23–36 correspond to the α-helix, part of which contacts the surface in both orientations. This can be seen from the large number of interactions in either the N- [Figure 3.3(c)] or the C-terminal part [Figure 3.3(d)] of the α-helix, respectively [Figure 3.3(a) and Figure 3.3(b)].

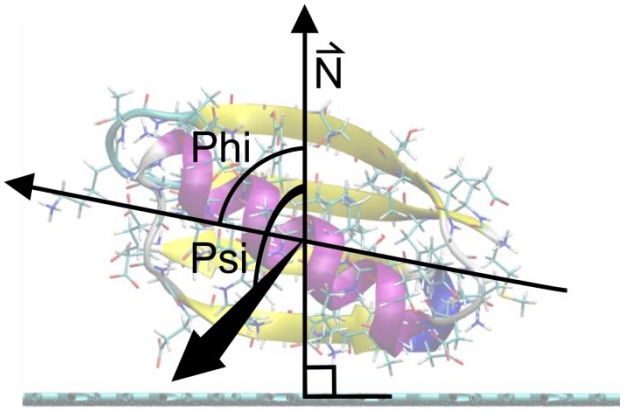

Figure 3.5. Schematic representation of the calculation of the orientation angles. Phi and psi correspond to the angles between the two major principal axes and the surface normal (N).

To further quantify the two predicted orientations of protein G B1 on graphene, a free energy heatmap was created using as collective variables the angles (phi and psi) between the two major principal axes and the surface normal vector (Figure 3.5). The free energy was calculated by taking the negative natural logarithm of the number of times a particular orientation was sampled and multiplying it by the thermal fluctuations, G = –kT ln (N), where N is the count for each orientation (Figure 3.6). Two free energy minima were identified: phi = 80–90 and psi = 110–120; phi = 100–110 and psi = 70–90 (Figure 3.6). These minima corresponded to the two orientations toward which the simulations converged [Figure 3.3(a) and Figure 3.3(b), respectively].

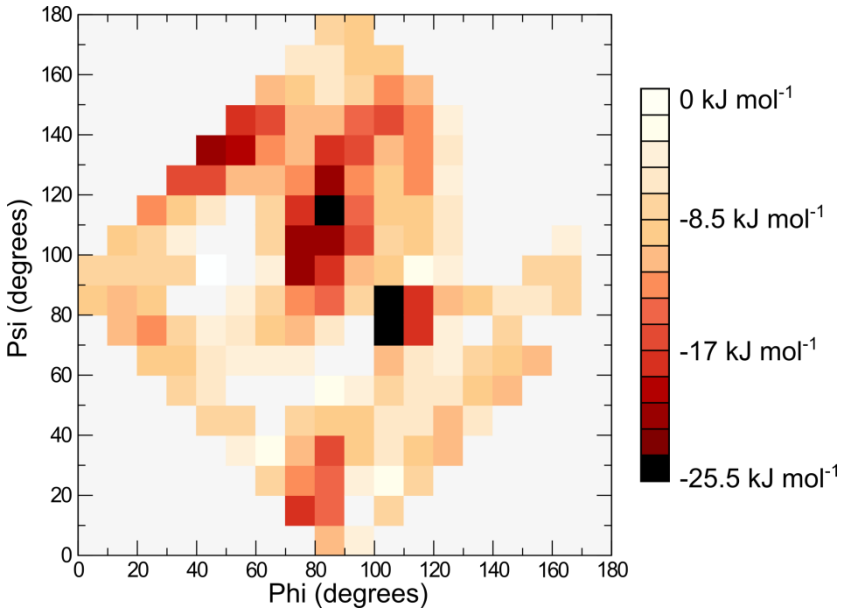

Figure 3.6. Free energy heatmap for all 12 simulated Monte Carlo runs of protein G B1 on graphene. Ranges of 10˚ are shown.

3.4.3 *Verification of the Assumption that Protein G B1 can be Treated as a Rigid Body*

One of the assumptions we have used in the development of the Monte Carlo simulations is that the protein is rigid and does not undergo significant conformational changes upon adsorption onto hydrophobic surfaces. To experimentally validate this assumption, we utilized quartz crystal microbalance with dissipation monitoring. This technique monitors the amount of protein immobilized onto a piezoelectric quartz crystal and how the viscoelasticity/rigidity of the proteins changes upon immobilization. In the QCM-D study, protein G B1 was adsorbed onto hydrophobic polystyrene-coated quartz crystals. The frequency (F) and dissipation (D) during protein G B1 adsorption was monitored, and no significant changes in dissipation were detected (Figure 3.7), i.e., the ratio of $\Delta D/\Delta F$ was <0.05 as protein G B1 was adsorbed. This suggests that no major conformational changes in protein G B1 occurred during the adsorption process [150-152]. We also examined the binding of IgG antibody to the immobilized layer of protein G B1 to determine whether, when immobilized, protein G B1 was still capable of binding IgG. From the frequency shifts, it was determined using the Sauerbrey equation [82]

that 98 ng/cm^2 of protein G B1 was adsorbed onto the polystyrene surface and 350 ng/cm^2 of IgG bound to the protein G B1 covered surface. This confirms that protein G B1 adsorbed onto the hydrophobic polystyrene surface maintains IgG antibody-binding activity.

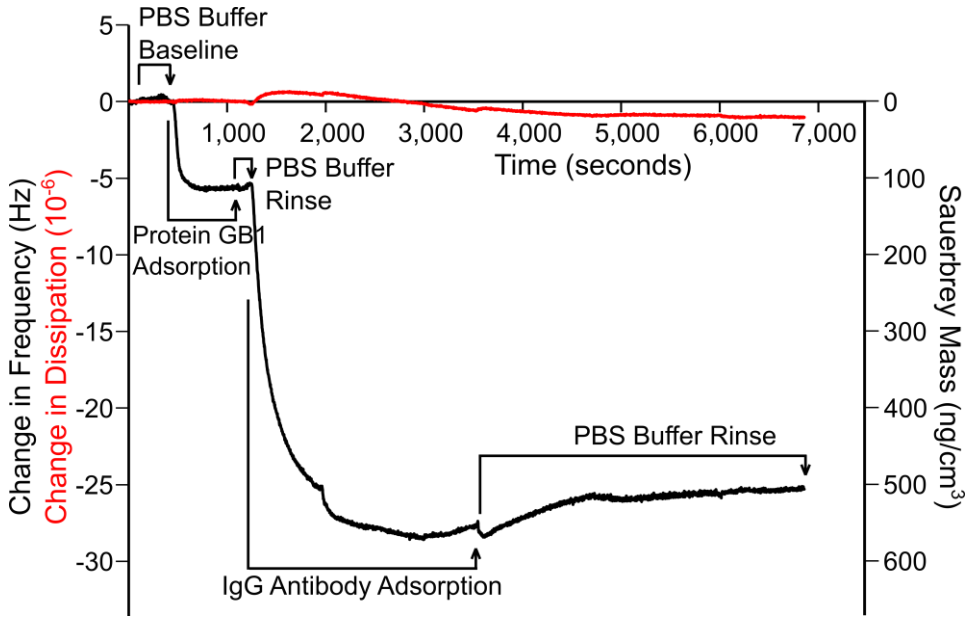

Figure 3.7. Changes in frequency and Sauerbrey mass (black) and dissipation (red) as a function of time during the adsorption of protein G B1 onto a polystyrene surface followed by binding of IgG antibody to the adsorbed protein G B1. After a buffer baseline was established, 5 µg/mL protein G B1 in PBS was introduced for 13 minutes and followed by a buffer rinse. Then 5 µg/mL IgG antibody was introduced for 39 minutes and followed by a final buffer rinse.

3.4.4 *Verification of Predicted Orientations through Sum Frequency Generation Experiments*

SFG spectroscopy was used to experimentally test whether the MC simulations predicted realistic orientations of adsorbed protein G B1. For SFG vibrational spectroscopy, a visible laser beam and a tunable infrared beam are overlapped in time and space at the surface. The sum frequency signal, which is generated at the interface due to nonlinear optical frequency mixing, is enhanced and yields a peak in the spectrum, when interfacial species are in resonance with the infrared light [153]. SFG

has, over the past years, been developed into a reliable tool to determine protein folding and orientation on surfaces *in situ* [48]. Owing to the nonlinear optical selection rules of SFG, only ordered protein layers at the interface are detected. Unbound and disordered proteins, even if close to the surface in solution, cannot not detected. The spectra therefore only represent the ordered proteins within the ensemble of proteins present at the surface. In analogy to Raman or infrared spectroscopy, the amide I modes can provide detailed information about the folding and structure of interfacial proteins.

Amide I SFG spectra of protein G B1 adsorbed onto polystyrene surfaces are shown in Figure 3.8(a) and Figure 3.8(b). The spectra are related to two different polarization combinations: ssp (s-polarized SFG, s-polarized visible, and p-polarized IR) and ppp. The ssp spectra exhibit positive peaks near 1601, 1623, and 1639 cm^{-1} and a negative peak near 1675 cm^{-1}. The ppp spectra contain positive features near 1609, 1634, and 1722 cm^{-1}. The modes near 1630 cm^{-1} and 1675 cm^{-1} are typically assigned to ordered β-sheet structures [32, 70, 154]. The ppp feature near 1722 cm^{-1} is likely related to side chain modes [154]. The low frequency modes below 1610 cm^{-1} are difficult to assign and could be related to side chain modes or caused by interferences of several delocalized backbone modes. The challenges involved with peak assignment in SFG spectra can be traced back to the extensive interference between modes within a complex protein. This is an important difference to linear vibrational spectroscopies, where different adjacent modes overlap but do not influence each other. In SFG, vibrational modes will interfere, which leads to complex spectral shapes [155]. To extract structural information from such spectra, theoretical spectra can be calculated from protein structure files [156] and combined with experimental SFG data [147, 157-159].

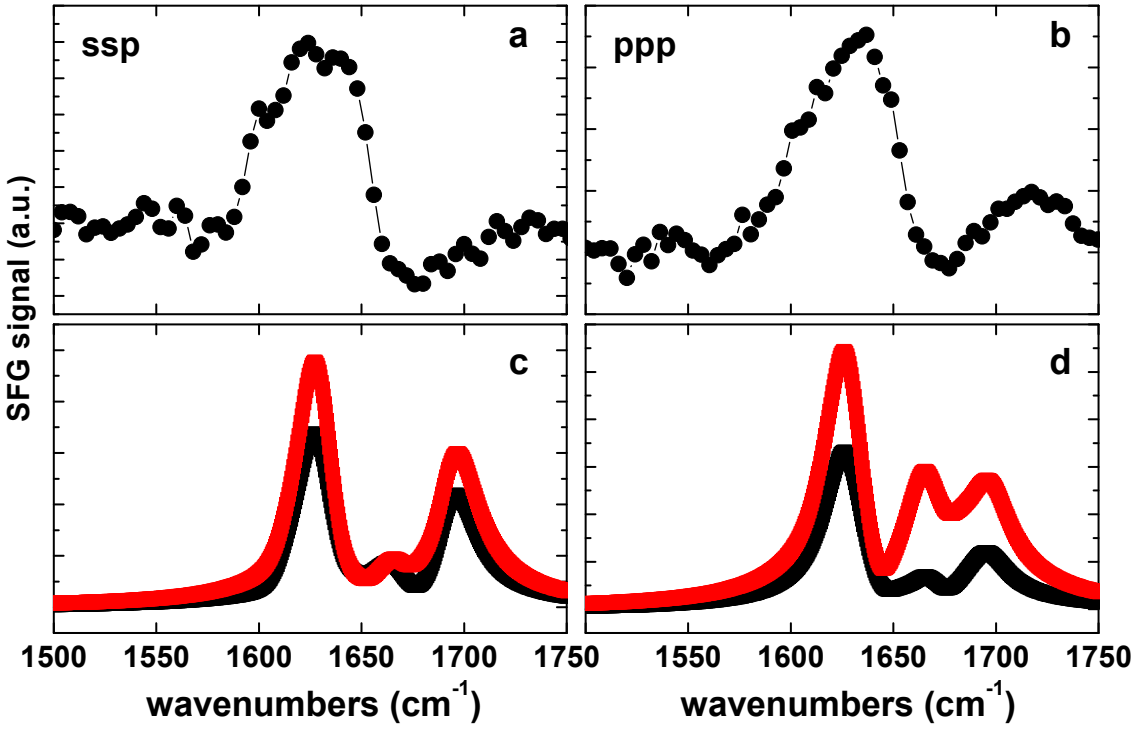

Figure 3.8. Experimental and calculated SFG spectra. (a,b) Experimental spectra for protein G B1 on polystyrene in ssp and ppp polarization combination. (c,d) Spectra calculated from the first predicted orientation shown in Figure 3.3(a) (red) and from the second predicted orientation shown in Figure 3.3(b) (black).

Theoretical SFG spectra were calculated using each of the two adsorbed orientations of protein G B1 determined by the MC simulations [Figure 3.8(c) and Figure 3.8(d)]. Clearly, the calculated spectra do not capture the spectral features of the experimental data well. In ssp, while the calculated spectra capture the main resonance near 1630 cm^{-1}, they also produce an unexpected feature near 1700 cm^{-1} [Figure 3.8(a) and Figure 3.8(c)]. In ppp polarization, the calculations reproduce the main peak near 1630 cm^{-1} but miss any low frequency shoulders and produce two high-energy modes, which are not visible in the experimental data [Figure 3.8(b) and Figure 3.8(d)]. It should be noted that tests with several other orientations yielded no improvements in the agreement between theory and experiment.

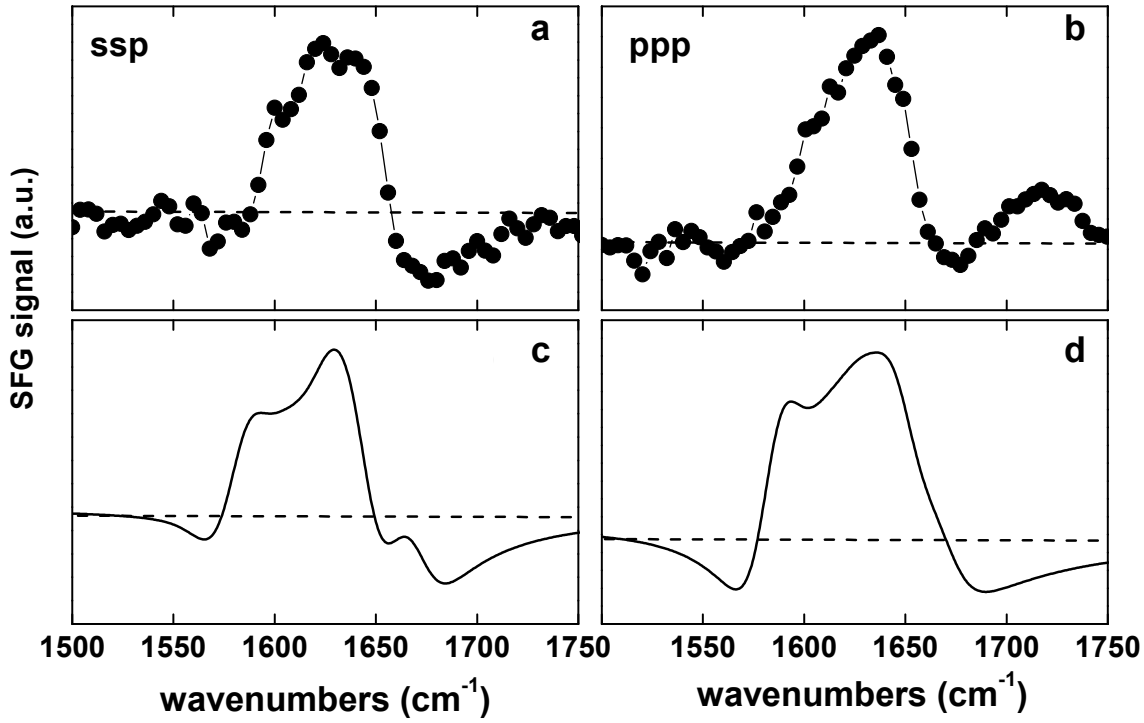

Figure 3.9. Experimental and calculated SFG spectra. (a,b) Experimental spectra for protein G B1 adsorbed onto polystyrene in the ssp and ppp polarization combinations. (c,d) Spectra calculated for a 50/50 mixture of the two predicted orientations.

Since the two orientations predicted by the MC simulations are close in energy it is likely that both orientations will be present on the surface. We therefore calculated the SFG response of a monolayer of protein G B1 with a 50/50 mixture of both orientations. When using a 50/50 mixture of both orientations for the spectra calculations, the peaks around the main feature near 1630 cm^{-1}, including the low energy features, as well as the negative feature near 1675 cm^{-1}, are now captured by the theoretical spectra (Figure 3.9). Therefore, the results of the calculations match the experimental data better than either of the two orientations individually.

3.4.5 *Stability of the Protein G B1 Predicted Orientations in MD Simulations*

To test the conformational stability of protein G B1 adsorbed onto a graphene surface, four 50-ns long MD simulations in explicit water were started from the predicted orientations of protein G B1. Two of the simulations (MD1 and MD2) were started from one of the predicted orientations [Figure 3.3(b)] and two (MD3 and MD4) from the other predicted orientation [Figure 3.3(a)]. In all four simulations, the protein remained within 2.5 Å from the surface [Figure 3.10(a)]. However, in MD2, the protein tilted to an orientation with one of its smaller sides contacting the surface and the rest of it solvent exposed. This is indicated by its relatively larger average distance between the center of geometry (COG) and the surface [Figure 3.10(a)] and the smaller angle Phi between its major axis and the normal to the surface [Figure 3.10(b)]. In the other three runs, the protein maintained its initial orientation throughout the entire simulation length, as indicated by the similar distance between the COG and the surface [Figure 3.10(a)] and the similar angles Phi and Psi between its two major axes and the normal to the surface [Figure 3.10(b)]. Generally, the protein maintained its three-dimensional structure and the α-helix was conserved throughout the simulations as indicated by their backbone Cα atom root mean square deviations from the initial conformation [Figure 3.10(a)].

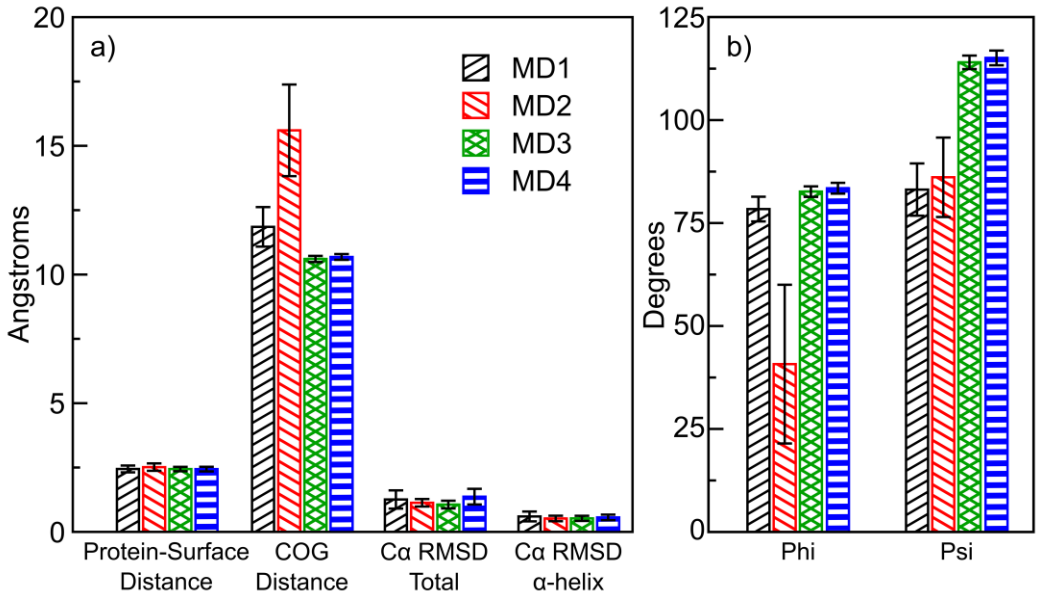

Figure 3.10. Averages of quantities measured during the molecular dynamics simulations started from the Monte Carlo predicted orientations of protein G B1 on the graphene surface. The bars show a time average along the simulations, while error bars represent the standard deviation.

Interestingly, a slight distortion was observed in MD1 where the α-helix briefly tilted outward away from the rest of the protein while generally maintaining its secondary structure but returned to its native position after ca. 12 ns (Figure 3.11). It is plausible that protein G B1 might undergo slight adjustments of its three-dimensional structure upon adsorption to a hydrophobic surface. However, this was an isolated and short-lived event, and thus, no strong conclusions can be drawn. The fact that the protein tilted in one out of four runs could be an artifact of the force field used in the simulations and current force fields might need to be optimized for protein–surface simulations [160, 161], or it could indicate that the protein probes alternative but less populated orientations upon adsorption. It would be interesting to investigate these events in longer time-scale MD simulations in a future study. It also needs to be noted that while the experiments were performed with polystyrene, the simulations were performed with graphene. This does not affect the Monte Carlo calculations since the protein is treated as a rigid body and both surface types are hydrophobic. However, one might want to consider using a polystyrene surface for long timescale MD simulations.

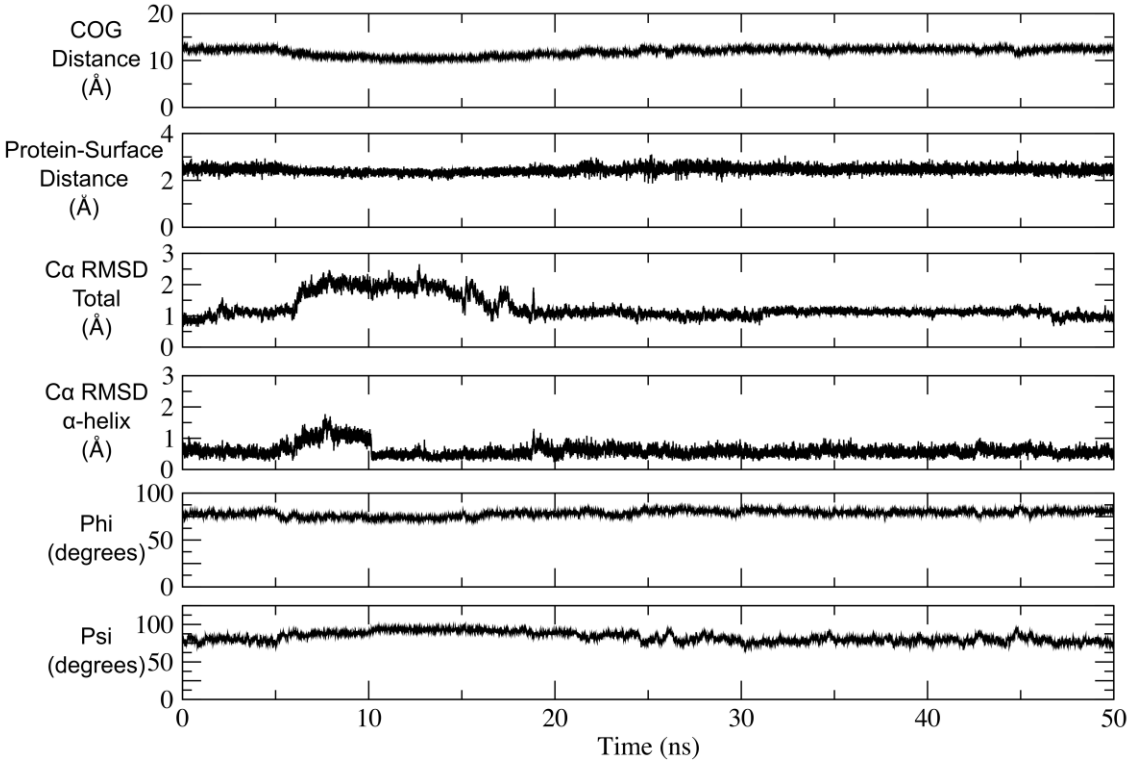

Figure 3.11. Time series of quantities measured during the molecular dynamics simulation MD1 started from one of the Monte Carlo predicted orientations of protein G B1 on the graphene surface [Figure 3.3(b)].

3.5 DISCUSSION

Determining the orientation and structure of proteins adsorbed onto the surface of materials is challenging because although well-established surface analysis methods such as ToF-SIMS provide important details about adsorbed proteins, they do not provide structural information at the atomic level. It would be desirable to have methods that directly determine the composition of biofilms at atomic level of detail, as it is, for example, already the case for proteins in solution and crystals. Because of this technological gap, there is a need for computational tools that can complement and extend experimental surface analysis techniques by providing atomistic details about the protein adsorption process [48]. Computational predictions can then be validated through experimental measurements, and the combination of computations and experiments can provide a detailed and realistic model about the structure of protein films.

Here, a Monte Carlo-based algorithm was developed by combining existing molecular dynamics simulation and visualization software with a SASA based implicit solvation model to determine the orientation of protein G B1 adsorbed onto hydrophobic surfaces. The simulations converged toward two distinct orientations (Figure 3.3) that corresponded to two minima with roughly equal free energy values (Figure 3.6). Strikingly, SFG experiments confirmed that protein G B1 indeed has a roughly 50% probability of being found in either one of the two predicted orientations on a polystyrene surface (Figure 3.9). This highlights the importance of complementing current surface analysis techniques with atomistic computational predictions, since, as shown in this case, it would have been hard to uniquely determine from SFG data alone the number of orientations that were present. Finally, MD simulations in explicit water illustrated how the MC-based method developed here can be used to efficiently generate a starting system for studying conformational fluctuations of adsorbed proteins.

The atomistic understanding of the protein adsorption process can provide insight how different surface materials can differentially influence the function of proteins. For example, recently it has been shown that the coagulation protein von Willebrand factor

(VWF) is activated when adsorbed on a polystyrene surface but inactive on a glass surface [162]. A combination of Monte Carlo and MD simulations as presented here could help discriminate whether this is due to different orientations or to conformational changes of VWF on a hydrophobic versus a hydrophilic surface. It needs to be noted that the method presented here does not take into account that protein molecules can also interact with each other besides with the surface and that this could influence their orientation or conformation. However, since the polypeptides used here are soluble, it is likely that during the adsorption process the protein–surface interaction will be more dominant than any interprotein interactions. Consistent with this, in a recently published simulation, the LK peptide was observed to assume a similar surface orientation whether it was isolated or whether another LK peptide was present [163]. Nonetheless, more complex algorithms could be developed to take interprotein interactions into account for cases where these effects are suspected to play a major role in the system under study.

In the future, it will be necessary to also predict protein orientations on hydrophilic surfaces. Unlike in the case of nonpolar surfaces such as graphene, electrostatic interactions need to be accounted for when studying adsorption onto hydrophilic surfaces. Since the energy evaluation in the Monte Carlo algorithm is based on an implicit solvation model, screening effects of the water will also have to be considered, either by using a constant or a distance-dependent dielectric coefficient. This is challenging because distance-dependent dielectric constants are known to overestimate electrostatic interactions between charged side chains in protein folding studies with implicit solvent models [113, 164]. Another challenge is that more advanced implicit solvation models based on Generalized Born [145, 146] are not adequate to study the interaction between molecules and surfaces. Finally, in cases of surfaces that are known to order water, it might be necessary to include water molecules explicitly. Overall, the development of better implicit solvation models along with the implementation of Monte Carlo algorithms to predict the orientation of proteins on surfaces presents an interesting and exciting challenge.

3.6 CONCLUSIONS

The following conclusions can be drawn from this work:

(1) The Monte Carlo simulations predicted two distinct orientations of protein G B1 on hydrophobic graphene surfaces.

(2) The QCM-D results indicated that upon adsorption onto polystyrene surfaces protein G B1 did not undergo major conformational changes and maintained its IgG antibody binding activity. This justifies the assumption that the protein can be treated as a rigid body in Monte Carlo simulations.

(3) Calculated SFG spectra based on a 50/50 mixture of the two Monte Carlo predicted orientations agreed with experimental data of protein G B1 adsorbed onto polystyrene confirming that an ensemble containing at least the two predicted orientations was present on the surface.

(4) In MD simulations started from the predicted Monte Carlo orientations, the protein was generally stable, remained in contact with the surface, and in three out of four runs it maintained the predicted orientation.

The Monte Carlo simulations developed here can provide atomic-level detail of protein–surface interactions that are not typically available from experimental surface analysis techniques. The predicted orientations can be used to complement results from surface analysis experiments and as starting structure for more accurate explicit solvent molecular dynamics simulations to study conformational changes of the protein at the protein–surface interface.

3.7 ACKNOWLEDGEMENTS

The authors would like to thank Jim Pfaendtner and Wendy Thomas for interesting and helpful discussions. The authors also thank Amedeo Caflisch at the University of Z€urich, Switzerland for helpful discussions about implicit solvation models. Tobias Weidner acknowledges funding by the Deutsche Forschungsgemeinschaft (WE4478/4-1) and European Union Marie Curie Program for support of this work (CIG Grant No. 322124) and thanks Steven Roeters and Sander Woutersen for providing code for the spectra calculations. Recombinant protein G B1 used in this work was obtained from the Institute for Protein Design, University of Washington, Seattle, WA. This study was financially supported by NIH Grant No. R03EB014516 (GI), a NIH career development Award No. K25HL118137 to GI, and NIH Grant No. P41EB002027 (NESAC/BIO).

Chapter 4. `Controlling the Orientation of Five Different Cysteine Mutants of Protein G B1 via Covalent Attachment to a Maleimide Surface

Elisa T. Harrison
Department of Chemical Engineering, University of Washington, Seattle, Washington 98195

Lauren Carter
Department of Bioengineering, University of Washington, Seattle, Washington 98195

David G. Castner
Department of Chemical Engineering, University of Washington, Seattle, Washington 98195 and Department of Bioengineering, University of Washington, Seattle, Washington 98195

4.1 Introduction

Control of protein immobilization onto surfaces is essential for the development of *in vitro* binding protein devices, such as enzyme-linked immunosorbent assays (ELISA) and protein microarrays [12-14]. Controlled adsorption of proteins onto surfaces, via hydrophobic interactions, electrostatic interactions, or covalent attachment, has been used to improve the antibody binding capabilities of binding assays. Specifically, the orientation of proteins can play a vital role in the function and performance of such binding assays [14-22]. When developing methods to understand protein-surface interactions, e.g., controlling immobilization, orientation, conformation and binding activity, it is best to start with simple, model systems and then increase their complexity.

The need to control the immobilization of proteins onto surfaces motivates the necessity for developing methods capable of fully analyzing protein-surface interactions. Thus, surface analytical techniques are being developed to gain a more detailed understanding of immobilized proteins. Qualitative techniques are currently used to

obtain information about immobilized proteins on surfaces. In binding assays, such as sandwich ELISAs, the structure and activity of proteins are indirectly determined by measuring how the proteins bind to other proteins and/or antibodies [4, 5, 22, 23]. Oftentimes, many layers of proteins and antibodies are formed on top of the protein of interest or labels are required before any information can be gathered. Proteins that would otherwise be ruled out because of a lack of signal may, in fact, be useful if researchers could fully control the structure and activity of the adsorbed protein. To take the empirical trial and error aspect out of the design of diagnostic tools, highly sensitive, quantitative, and label-free tools are required. Surface analytical techniques, such as X-ray photoelectron spectroscopy (XPS), quartz crystal microbalance with dissipation monitoring (QCM-D), and time-of-flight secondary ion mass spectrometry (ToF-SIMS) can provide information on the composition, mass of adsorbed proteins, orientation, activity, and adsorption/binding kinetics of immobilized proteins [32-36, 39, 40, 42, 44, 57, 63, 86, 89, 103, 114, 165, 166]. While one technique alone can't provide a full understanding of protein-surface interactions, combining many label-free, surface-sensitive techniques can provide the molecular-level information of protein-surface systems lacking in other techniques that rely on indirect measurements, the use of labels, or comparison to solution or crystalline phases.

In this work, we have utilized the surface analytical methods of XPS, QCM-D, and ToF-SIMS to characterize immobilized proteins and control the orientation of cysteine mutants of protein G B1 covalently attached to a maleimide surface. Protein G B1, a 6 kDa, 56 amino acid immunoglobulin (IgG) binding domain of protein G, was used in this study because of its stability, both in solution and immobilized on surfaces, and the availability of experimental data [25, 31, 32, 53, 70-76]. Self-assembled monolayers (SAMs) were used to modify the surface due to their ease of preparation, precision of surface control, and wide variety of possible surface chemistries [35, 58, 60, 63-69]. To control orientation, cysteine mutants of protein G B1 were immobilized on maleimide-oligo(ethylene glycol)-functionalized (MEG) SAMs and bare gold surfaces. XPS was used to verify the quality of the substrates and to quantify protein adsorption. QCM-D was used to measure changes in mass and viscoelastic properties of immobilized proteins as a function of time [3, 4, 37, 38, 63, 79]. The orientation of immobilized

protein films was determined using ToF-SIMS intensity peak ratio analysis [12, 31, 32, 70, 86-88].

4.2 MATERIALS AND METHODS

4.2.1 *SUBSTRATE PREPARATION AND MODIFICATION*

Gold-coated silicon wafers (XPS and ToF-SIMS) and gold-coated quartz crystal sensors (QCM-D) were used as substrates for protein immobilization studies. Silicon wafers (Silicon Valley Microelectronics Inc., San Jose, CA) were diced into 1×1 cm^2 substrates using a diamond saw. Gold substrates were fabricated by depositing a 5 nm titanium adhesion layer followed by depositing a 100 nm gold layer onto the diced and cleaned silicon substrates via electron-beam deposition at room temperature and pressures <1 $x10^{-6}$ torr. Gold-coated quartz crystal sensors (Q-Sense, Gothenburg, Sweden) were cleaned using the UV-Ozone cleaner and a 75˚C heated piranha solution (5:1:1 water:hydrogen peroxide:ammonium hydroxide solution; caution: piranha solution reacts violently with organic compounds) prior to surface modification.

The SAM substrates used in this work were prepared by submerging the gold-coated substrates in a solution of 1 mM maleimide-oligo(ethylene glycol) (MEG) dissulfides (HO-EG4-C11-S-S-C11-EG6-NHCO-Maleimide, Prochimia, Sopot, Poland) in 200-proof ethanol (Fisher Scientific) for at least 16 hours. The substrates were then rinsed and sonicated in ethanol to remove unbound molecules. Bare gold-coated substrates used in the protein adsorption experiment were submerged in 200-proof ethanol in a separate hood to avoid vapor deposition of thiols or disulfides.

4.2.2 *PROTEIN SYNTHESIS*

Protein G B1, wildtype and the various cysteine point mutants, used in this work were synthesized by the Baker group (Protein Design, University of Washington, Seattle, WA). Recombinant protein G B1 was expressed in E. coli and purified using IMAC and the SMT3/ULP1 protease to cleave the 10xHis tag, then verified for identity using intact mass spectrometry. The amino acids chosen for the point mutations were selected

based on location, ease of synthesis, and predicted binding site of protein G B1 to the IgG antibody.

4.2.3 *Protein Immobilization*

Depending on the instrument used, protein immobilization was done in either a static or flow mode. Protein immobilization for X-ray photoelectron spectroscopy (XPS) and time-of-flight secondary ion mass spectrometry (ToF-SIMS) studies was done using static adsorption while protein immobilization for quartz crystal microbalance with dissipation monitoring (QCM-D) studies was done in a flow regime.

Protein G B1 solutions ranging from 50 µg/mL to 1000 µg/mL were prepared in bicarbonate/carbonate buffer (50 mM, pH 9.5). The buffer was degassed and sonicated for an hour prior to use. Substrates used for static protein immobilization were hydrated in 0.5 mL degassed buffer in a 24-well plate for 30 min at room temperature prior to adding protein solution and then allowing the immobilization to occur for 2 hours at room temperature. After protein immobilization, substrates were rinsed by serial dilution in buffer and then submerged in a series of two buffer and three water solutions for 5 min each while mixing with a stir bar. Substrates were then dried and stored under nitrogen gas.

4.2.4 *X-ray Photoelectron Spectroscopy*

XPS data were acquired on a SSI S-Probe XPS system (Surface Science Instruments, Mountain View, CA) using a monochromatic Al $Ka_{1,2}$ X-ray source (hv =1486.6eV). Survey and detailed scans were collected with analyzer pass energy of 150 eV and a 100 ms dwell time. The survey step size was 1 eV, while 0.4 eV was used for detail scans. High-resolution spectra were acquired with analyzer pass energy of 50 eV and a step size of 0.065 eV. Binding energy scales were calibrated by setting the CH_x peak in the C1s region to 284.6 eV, and a linear background was subtracted for all peak area quantifications. Elemental compositions (atomic percentages) were calculated using the Hawk Data Analysis 7 software (Service Physics, Inc., Bend, Oregon). The C1s, O1s,

and Au4f peak areas were obtained from the survey spectra (0-1100 eV). The N1s (390-410 eV) and S2p (155-173 eV) peak areas were obtained from the detailed scans.

4.2.5 *Quartz Crystal Microbalance with Dissipation Monitoring*

Adsorption and binding of protein G B1 was monitored using the E4 QCM-D (Q-Sense, Gothenburg, Sweden) system. Frequency and dissipation measurements were made on gold-coated quartz crystals with fundamental frequencies of 4.95 MHz (Q-Sense, Gothenburg, Sweden). Replicates were conducted for each protein and substrate combination. The temperature was maintained at 22˚C. During the course of a typical QCM-D experiment, protein G B1 was immobilized onto the sensors at a concentrations ranging from 50 µg/mL to 1000 µg/mL in buffer at a flow rate of 300 µL/min. Following protein G B1 adsorption, the system was rinsed with buffer at 300 µL/min to remove any excess protein. Prior to the QCM-D experiment, the temperature was stabilized for at least 30 min and the PBS buffer baseline was established for at least 30 min.

4.2.6 *Time-of-Flight Secondary Ion Mass Spectrometry*

Negative and positive secondary ion spectra were acquired on a TOF.SIMS 5-100 instrument (ION-TOF, Munster, Germany) using a pulsed 25 keV Bi^{3+} primary ion beam under static conditions (primary ion dose < 10^{12} ions/cm^2). Spectra were collected from five 100 µm x 100 µm regions for each sample. Secondary ions were collected over a range of 0–800 m/z at a mass resolution (m/Δm) between 4000–8000. Positive spectra m/z values were mass calibrated using CH_3^+, $C_2H_3^+$, and $C_3H_5^+$ peaks, and negative spectra using CH^-, OH^-, C_2H^-, C_3^-, C_4H^- and C_5^- peaks. Mass calibration errors were typically below 20 ppm.

4.3 RESULTS

4.3.1 *CONTROLLING PROTEIN G B1 CYSTEINE MUTANT ORIENTATION*

The five cysteine mutants of protein G B1 listed in Table 4.1 and shown in Figure 4.1(a) were synthesized to vary the site of immobilization to the MEG SAM [Figure 4.1(b)] and bare gold substrates. A single cysteine amino acid replaced an amino acid in the protein sequence and was selected based on location, ease of synthesis, and predicted binding site of protein G B1 to the IgG antibody. The proteins used in this work were protein G B1 wildtype (containing no cysteine amino acids) and five cysteine mutants: threonine11 to cysteine (T11C), valine21 to cysteine (V21C), asparatic-acid35 to cysteine (D35C), glutamic-acid42 to cysteine (E42C), and threonine49 to cysteine (T49C).

Table 4.1. Five cysteine mutants synthesized for this work. The predicted orientation and location of cysteine mutation are listed.

Amino acid replaced and residue number	Abbreviation	Predicted Orientation	Cysteine Location
Threonine 11	T11C	End-on	C-terminus
Valine 21	V21C	End-on	N-terminus
Asparatic-acid 35	D35C	Side-on	C-terminus
Glutamic-acid 42	E42C	Side-on	Side
Threonine 49	T49C	End-on	N-terminus

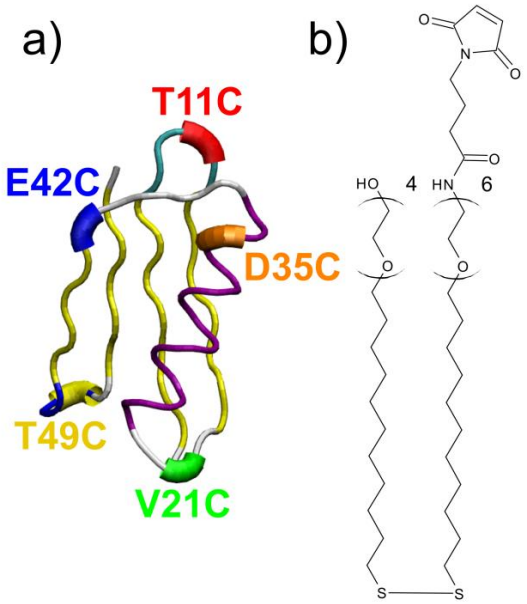

Figure 4.1. (a) Location of cysteine point mutations on protein G B1 (red: T11C, green: V21C, orange: D35C, blue: E42C, and yellow: T49C) will covalently attach to (b) maleimide-poly(ethylene glycol) (MEG) disulfide self-assembled monolayers (SAMs).

Samples prepared for XPS and ToF-SIMS required drying and exposure to ultra-high vacuum conditions while samples prepared in the QCM-D were conducted in solution. Substrates were analyzed by XPS and ToF-SIMS within a week of preparation. Replicates were prepared on different days using freshly prepared protein solutions.

4.3.2 *Correlating Atomic Percentage of Nitrogen and Sauerbrey Mass*

XPS can determine the elemental composition of the top 10 nm of the substrate surface [42, 77]. In this work, XPS was used to verify the quality of the substrates and to quantify protein adsorption. In the development of a protein film, each layer was fully analyzed using XPS in a step-wise fashion. This way, the quality of the substrate can be determined and the quantity of protein adsorbed can be calculated. The XPS determined elemental compositions measured for the MEG SAM and bare gold substrates and each of the cysteine mutants of protein G B1 immobilized onto the MEG SAM and bare gold substrates are listed in Table 4.2.

Table 4.2. XPS elemental compositions for the substrates (bare gold and MEG) and immobilized protein G B1 cysteine mutants (T11C, V21C, D35C, E42C, and T49C). The XPS determined elemental compositions of the organic overlayer were calculated by excluding Au 4f and renormalizing the remaining signals to 100%. The Au 4f atomic percentages shown are prior to this normalization. The Au 4f signal is monitored to assess the overlayer thickness and coverage since the gold signal will be attenuated as the thickness or coverage increases. For samples with immobilized protein, the N1s atomic percentage was monitored since the protein has a larger nitrogen signal compared to the MEG SAM or bare gold substrate. The N1s percentages are corrected (Natt) to remove substrate contribution to the nitrogen signal and are calculated prior to removing the Au contribution. QCM-D Sauerbrey mass calculated from the 7th frequency overtone of immobilized protein G B1 cysteine mutants (T11C, V21C, D35C, E42C, and T49C) onto MEG SAMs and bare gold sensors. The calculated Sauerbrey mass is shown, but note that the Sauerbrey equation can only be used if the change in dissipation is low. The calculated mass includes water associated with the protein film.

	XPS atomic % of organic overlayer								
Sample (protein, temperature, concentration, substrate)	C 1s	O 1s	N 1s	S 2p	Au 4f	N_{att}	QCM-D Frequency (Hz)	QCM-D Dissipation ($x10^{-6}$)	Sauerbrey mass (ng/cm^2)
MEG	68.8 ± 1.5	24.8 ± 0.9	2.1 ± 0.7	4.3 ± 0.6	49.1 ± 0.8				
T11C, RT, 900ug/mL, MEG	70.2 ± 2.4	23.5 ± 1.9	4.2 ± 1.0	2.0 ± 0.6	35.8 ± 3.4	1.7 ± 0.6	-3.9 ± 0.1	0.7 ± 0.2	68.5 ± 1.9
V21C, RT, 1000ug/mL, MEG	66.1 ± 3.1	18.5 ± 2.4	10.8 ± 1.0	4.5 ± 0.4	40.3 ± 2.0	5.3 ± 0.4	-6.5 ± 2.9	0.7 ± 0.5	113.4 ± 51
D35C, RT, 1000ug/mL, MEG	68.3 ± 1.3	21.1 ± 1.1	6.4 ± 0.6	4.2 ± 0.5	48.4 ± 2.5	1.9 ± 0.3	-7.2 ± 0.1	0.7 ± 0.1	126.3 ± 2.7
D35C, RT, 50ug/mL, MEG	69.0 ± 1.5	22.7 ± 1.3	3.5 ± 0.5	4.8 ± 0.7	55.2 ± 1.2	0.0 ± 0.3	-2.4 ± 0.1	0.3 ± 0.1	41.6 ± 2.1
D35C, RT, 250ug/mL, MEG	71.0 ± 5.0	21.7 ± 4.1	3.3 ± 0.9	4.0 ± 0.9	54.6 ± 1.3	-0.1 ± 0.4	-2.6 ± 0.1	0.5 ± 0.1	45.7 ± 2.1
D35C, 37C, 250ug/mL, MEG	68.2 ± 2.4	19.6 ± 2.7	7.8 ± 0.8	4.4 ± 1.2	44.9 ± 2.6	3.0 ± 0.7	-1.9 ± 0.4	0.4 ± 0.1	32.5 ± 6.8
D35C, RT, 500ug/mL, MEG	69.8 ± 1.7	19.2 ± 1.2	6.2 ± 0.8	4.8 ± 0.5	44.1 ± 0.9	2.2 ± 0.4	-4.6	0.6	81.4
D35C, RT, 1000ug/mL, MEG overnight hydrolysis							-1.6	-2.5	27.4
E42C, RT, 1000ug/mL, MEG	68.6 ± 2.0	21.3 ± 1.3	6.5 ± 0.5	3.6 ± 0.4	47.1 ± 1.6	2.1 ± 0.2	-3.1 ± 1.1	0.3 ± 0.1	53.7 ± 18.7
T49C, RT, 1000ug/mL, MEG	66.0 ± 1.7	19.7 ± 2.2	8.9 ± 0.3	5.3 ± 0.5	41.9 ± 2.8	4.0 ± 0.3	-6.9	1.1	121.7
WT, RT, 1000ug/mL, MEG	72.6 ± 1.9	22.1 ± 3.1	2.9 ± 0.8	2.4 ± 0.3	45.4 ± 1.2	0.3 ± 0.4	-1.5 ± 0.3	0.2 ± 0.01	26.4 ± 4.4
Bare Au	95.0 ± 3.9	5.0 ± 3.9	n.d.	n.d.	77.9 ± 2.6				
T11C, RT, 900ug/mL, bare Au	70.1 ± 1.9	16.2 ± 1.2	13.7 ± 1.1	n.d.	42.6 ± 2.3	7.9 ± 0.3	-16.0 ± 1.6	1.4 ± 0.01	279.5 ± 28.1
V21C, RT, 600ug/mL, bare Au	69.6 ± 2.4	16.9 ± 1.9	13.1 ± 1.0	0.5 ± 0.6	37.3 ± 1.4	5.4 ± 0.6	-14.1 ± 0.8	0.8 ± 0.01	246.8 ± 14.4
D35C, RT, 1000ug/mL, bare Au	66.4 ± 2.7	20.4 ± 1.3	13.2 ± 1.5	n.d.	45.8 ± 3.1	7.3 ± 0.5	-19.6 ± 3.2	1.8 ± 0.6	343.4 ± 56.3
E42C, RT, 1000ug/mL, bare Au	66.4 ± 0.6	18.1 ± 0.4	15.5 ± 0.8	n.d.	44.6 ± 1.1	8.7 ± 0.3	-16.5 ± 7.2	1.0 ± 0,4	289.8 ± 126.6
T49C, RT, 1000ug/mL, bare Au							-14.9 ± 1.5	1.3 ± 0.3	260.9 ± 26.7
WT, RT, 1000ug/mL, bare Au	67.3 ± 0.9	18.0 ± 1.1	12.9 ± 0.6	1.8 ± 0.2	39.9 ± 2.2	7.7 ± 0.2	-24.0 ± 3.1	2.5 ± 0.5	420.3 ± 54.9

n.d. = not detected

The C1s, O1s, N1s, and S2p atomic percentages were renormalized to 100 % to remove the Au4f signal to investigate the organic overlayer composition. The gold signal is monitored to access the overlayer thickness and coverage since the gold signal will be attenuated as the overlayer thickness or coverage increases. For protein adsorption, the atomic percentage of N1s was monitored since the protein (~10 at.% N) has a larger nitrogen concentration compared to the MEG SAM (~2 at.% N) or bare gold substrate (no N). Proteins immobilized on bare gold substrates exhibited atomic percentages of N1s of 6-10 at.%, suggesting a monolayer of protein G B1 was formed [165]. Protein immobilized on the MEG SAM substrates had a lower atomic percentage of N1s, of 2-5 at.%, suggesting either sub-monolayer coverage due to the protein-resistant ethylene glycol background preventing non-specific adsorption or a protein layer with a thickness that is smaller than the XPS sampling depth due to the small size of the protein (~4 nm in diameter) [167]. For protein immobilization onto MEG SAM substrates, the nitrogen signal could originate from both the protein overlayer and the MEG SAM. Therefore, the nitrogen signal was corrected to remove the nitrogen signal contributed by the MEG SAM substrate using the methods discussed in ref. [167]. The corrected nitrogen signals, N_{att}, are listed in Table 4.2. For protein G B1 wildtype, which contains no cysteine amino acids and should not result in minimal immobilization to MEG SAM substrates, the corrected nitrogen atomic percentage decreases from 2.9 at.% to trace amounts of nitrogen (<1 at.%).

The changes in frequency and dissipation resulting from protein G B1 immobilization onto the MEG SAM and bare gold substrates are listed in Table 4.2. The mass adsorbed, in ng/cm^2, was calculated with the Sauerbrey [82, 168] equation using the seventh overtone. The Sauerbrey equation can only be used if the dissipation is low. If dissipation occurs, the Sauerbrey model will underestimate the mass. If the dissipation is too large to use the Sauerbrey model, the Voigt model can be used, which models the changes in viscoelastic properties as a damper and spring [83-85]. For protein G B1 immobilization onto both MEG SAM and bare gold substrates, the Sauerbrey equation was used to calculate the mass of protein G B1 immobilized since the change in dissipation remained low compared to the change in frequency (<1%) suggesting a rigid film was formed.

To compare results from XPS and QCM-D, the concentration of the D35C cysteine mutant was varied to create concentration isotherm curves (Figure 4.2). The corrected nitrogen signal, after removing the nitrogen contribution from the MEG SAM substrate, and the calculated Sauerbrey mass was plotted as a function of D35C concentration in buffer solution. At the lowest concentrations (50 and 250 µg/mL D35C in buffer solution), the calculated Sauerbrey mass was ~40 ng/cm^2 and only trace amounts of nitrogen were detected. Therefore, a Sauerbrey mass of ~40 ng/cm^2 will be considered as the XPS detection limit for protein G B1 adsorption. Both the corrected nitrogen atomic percentage and the Sauerbrey mass increased as the protein solution concentration was increase from 50 to 1000 µg/mL. We would expect the curves to eventually level off as the protein solution is increased above 1000 µg/mL, however the risk of aggregation in solution increases as the protein concentration increases, so for the remaining protein G B1 cysteine mutant adsorption experiments, the concentration was prepared at or slightly below 1000 µg/mL.

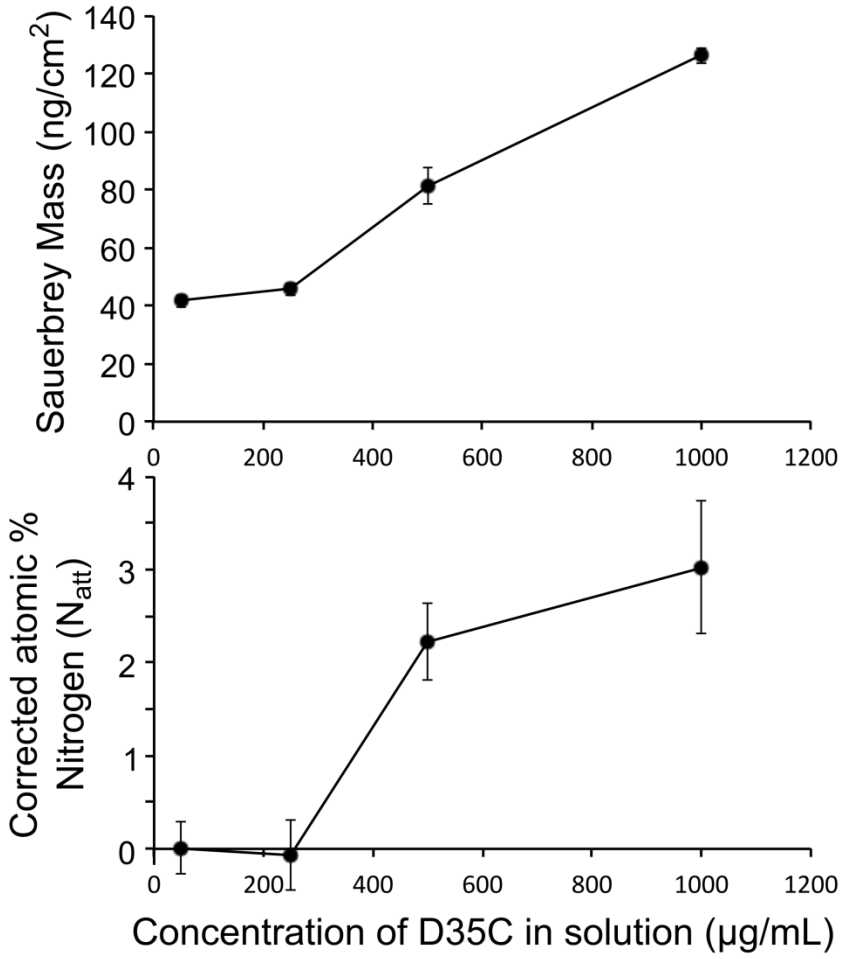

Figure 4.2. Concentration isotherms of the D35C cysteine mutant of protein G B1 to compare changes in atomic percentage of nitrogen measured using XPS and Sauerbrey mass calculated using QCM-D. Both XPS and QCM-D show immobilization of the protein G B1 D35C cysteine mutant to the MEG surface increased as the protein solution concentration was increased from 50 to 1000 µg/mL.

The correlation between the XPS corrected atomic percentage of nitrogen and the QCM-D calculated Sauerbrey mass for all protein G B1 cysteine mutants immobilized onto MEG SAM substrates is shown in Figure 4.3. The corrected nitrogen atomic percentage and the Sauerbrey mass were only correlated if the same protein solution was used since the protein solution was shown to affect the amount of protein adsorbed.

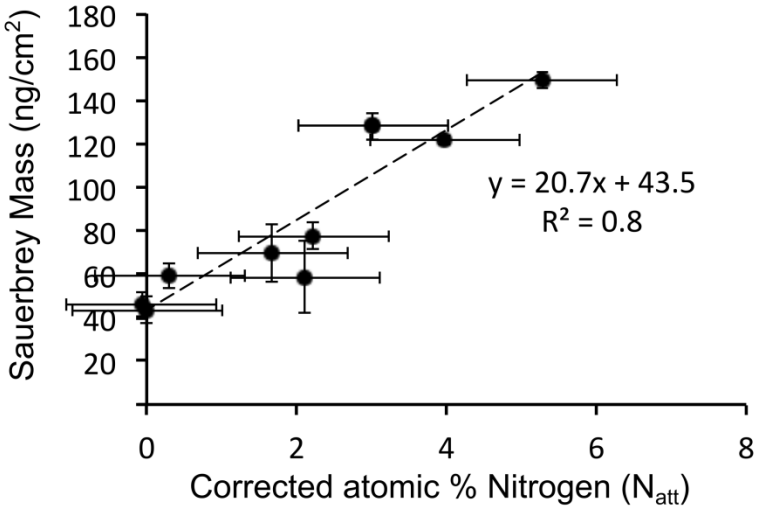

Figure 4.3. Correlation between the XPS corrected atomic percentage of nitrogen and the QCM-D calculated Sauerbrey mass for immobilization of the Protein G B1 cysteine mutants onto the MEG SAM substrates.

Additionally, hydrolysis of the maleimide group on the MEG SAM substrate was investigated by allowing the MEG SAM substrate to be submerged in buffer overnight for 17 hours. The hydrated MEG SAM substrate was then dried and placed in the QCM-D flow modules for protein G B1 D35C cysteine mutant adsorption. The change in frequency, dissipation, and calculated Sauerbrey mass for the D35C mutant after overnight hydrolysis of the MEG SAM substrate are listed in Table 4.2. Using the same 1000 µg/mL protein G B1 D35C cysteine mutant solution as previous runs, the calculated Sauerbrey mass of the adsorbed protein was 29 ng/cm^2, compared to 130 ng/cm^2 with only 30 min buffer exposure. The calculated Sauerbrey mass after 17 hours exposure to a water-based buffer was similar to the calculated Sauerbrey mass for WT Protein G B1 on the MEG SAM and below the minimum detection limit (~40 ng/cm^2), indicating hydrolysis of the MEG SAM substrate occurred from the 17 hour buffer exposure and prevented protein adsorption.

4.3.3 *ToF-SIMS Peak Ratio Analysis to Determine Protein Orientation*

The orientation of immobilized protein films can be determined using ToF-SIMS [12, 31, 32, 70, 86-88]. Peak ratio analysis of ToF-SIMS spectra used a peak list consisting of only protein amino acid-derived mass fragments. The amino acids with asymmetric distributions in the protein G B1 3D structure (Ile/Leu, Gly, Asn, Tyr, Phe, and Trp) used to calculate peak intensity ratios from ToF-SIMS data to determine the orientation of the cysteine mutants of protein G B1 covalently attached to the MEG SAM surface are shown in Figure 4.4. Figure 4.4(a) lists the amino acids, the mass of the characteristic amino acid ion fragments, and the amino acid distribution in the crystal structure visualized using VMD in the C-terminus, N-terminus and the center of the protein. High concentrations of protein G B1 were necessary for ToF-SIMS peak ratio analysis to achieve close to monolayer coverage when calculating protein orientation. Remaining ToF-SIMS experiments used protein G B1 concentrations at or slightly below 1000 µg/mL.

a)

	C-terminus			N-terminus	Center	
Amino Acid:	Ile/Leu	Gly	Asn	Tyr	Phe	Trp
Mass of ion fragments (m/z):	86.10	85.04 113.04	88.04 98.02	55.02 107.05	120.08 132.06	130.07 159.09 170.06
AA distributions on Protein G B1:	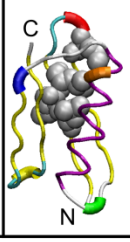	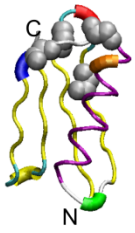	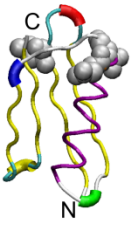	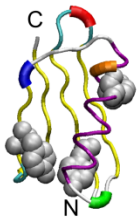	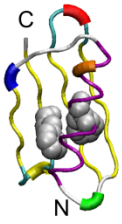	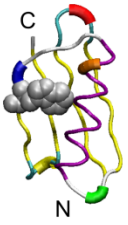

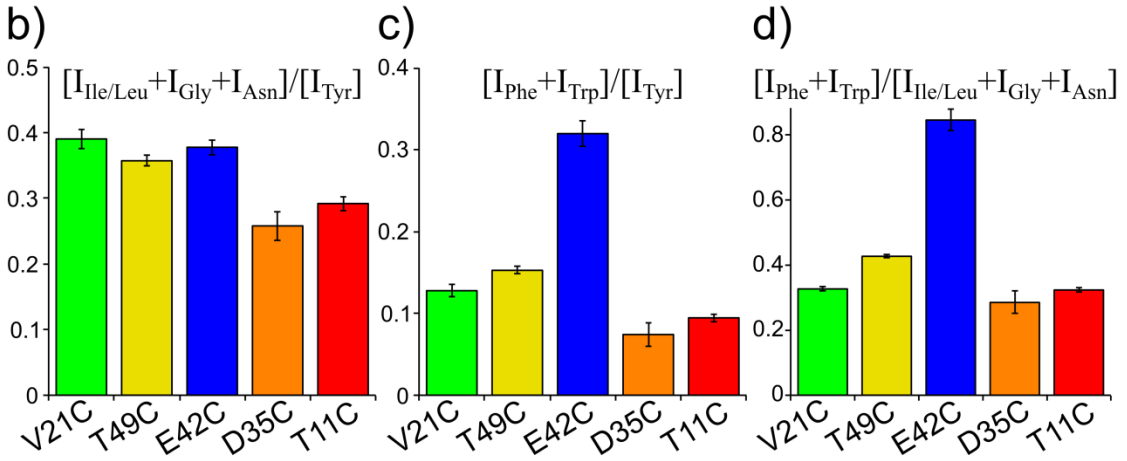

Figure 4.4. (a) Amino acids with asymmetric distributions used to calculate peak intensity ratios from ToF-SIMS data are listed with the characteristic mass of the ion fragments and highlighted in the crystal structure of protein G B1 as shown by VMD. ToF-SIMS peak intensity ratios were calculated as (b) the sum of intensities of chosen amino acids from the C-terminus divided by the sum of intensities of chosen amino acids from the N-terminus ($[I_{Ile/Leu}+I_{Gly}+I_{Asn}]/[I_{Tyr}]$), (c) the sum of intensities of chosen amino acids from the center divided by the sum of intensities of chosen amino acids from the N-terminus ($[I_{Phe}+I_{Trp}]/[I_{Tyr}]$), and (d) the sum of intensities of chosen amino acids from the center divided by the sum of intensities of chosen amino acids from the C-terminus ($[I_{Phe}+I_{Trp}]/[I_{Ile/Leu}+I_{Gly}+I_{Asn}]$).

Ratios of intensities of peaks from amino acids on opposite ends of the protein can be used to suggest a preferred end-on protein orientation when immobilized onto a surface [22, 31, 32, 70]. End-on orientation peak intensity ratios were calculated as the sum of intensities of chosen amino acids from the C-terminus (Ile/Leu: 86.10; Gly: 85.04, 113.04; Asn: 88.04, 98.02) divided by the sum of intensities of chosen amino acids from the N-terminus (Tyr: 55.02, 107.05). These peak ratios for the five-cysteine mutants are shown in Figure 4.4(b). Similar to the results shown in refs. [31, 32, 70], the end-on orientation peak ratio was higher for the V21C (green) mutant compared to the T11C (red) mutant [Figure 4.4(b)]. This was expected since the cysteine in the V21C mutant is located opposite the C-terminus while the cysteine in the T11C mutant is located opposite the N-terminus [Figure 4.1(a)]. The end-on orientation peak ratio for the D35C mutant was similar to T11C, while the end-on orientation peak ratio for T49C and E42C were similar V11C. Due to the T49C cysteine location in protein G B1, T49C should have a similar orientation to V11C. Although D35C was designed for side-on binding, the D35C cysteine was reasonably close to T11C cysteine location, so it is not surprising that D35C and T11C have similar orientations. However, it was surprising the end-on orientation peak ratio value for the E42C was similar to V21C, so differences in side-on orientations were investigated.

Similar to end-on orientation peak ratio analysis, ratios of intensities of peaks from amino acids in the center of the protein to either the C- or N-terminus can be used to suggest a preferred side-on protein orientation when immobilized onto a surface. Side-on orientation peak intensity ratios were calculated as the sum of intensities of chosen amino acids from the center of the protein (Phe: 120.08, 132.06; Trp: 130.07, 159.09, 170.06) divided by the sum of intensities of chosen amino acids from the C- or N-terminus. The peak ratios for the five cysteine mutants were calculated to determine preferential side-on orientations and are shown in Figure 4.4(c,d). As expected, the E42C (blue) mutant is preferentially orienting in a side-on orientation suggested by the increase in the side-on orientation peak ratio compared to the other four cysteine mutants (V21C, T49C, D35C, and T11C). This trend is clear whether the C- or the N-terminus [Figure 4.4(c or d, respectively)] is used to calculate side-on orientation peak ratios.

4.4 CONCLUSIONS

Methods to immobilize cysteine mutants of protein G B1 onto MEG SAMs were developed to achieve control of the accessibility of the antibody binding sites on the protein. In this work, XPS, QCM-D, and ToF-SIMS were used to characterize the orientation of five different cysteine mutants of protein G B1 covalently attached to a MEG SAM substrate. Controlling the orientation of immobilized proteins can ultimately aid in the development and optimization of in vitro binding protein devices, such as enzyme-linked immunosorbent assays.

The following conclusions can be drawn from this work:

(1) Cysteine mutants of protein G B1 with varying cysteine locations were successfully synthesized and immobilized onto MEG SAM and bare gold substrates. The amount of immobilized cysteine mutants of protein G B1 was determined using XPS and QCM-D.

(2) The maleimide group on the MEG SAM substrate is susceptible to hydrolysis and extended exposure to buffer must be avoided to maximize protein G B1 cysteine mutant immobilization.

(3) The corrected atomic percentage of nitrogen using XPS, after removing the contribution from the MEG SAM substrate, was linearly correlated to the Sauerbrey mass calculated from the QCM-D for Protein G B1 cysteine mutants immobilized onto MEG SAM substrates.

(4) The surface sensitivity of ToF-SIMS was used to determine protein orientation by monitoring the changes in intensity of characteristic amino acid mass fragments. ToF-SIMS peak ratio analysis was calculated using asymmetrically distributed amino acids on the C-terminus, N-terminus, and the center of protein G B1. The T11C and D35C mutants are preferentially orienting in an end-on orientation with the N-terminus at the sample surface. The V21C and T49C mutants are preferentially orienting in an end-on orientation with the C-terminus at the sample surface. The E42C mutant is preferentially orienting in a side-on orientation.

4.5 ACKNOWLEDGEMENTS

Recombinant protein G B1 used in this work was obtained from the Institute for Protein Design, University of Washington, Seattle, WA. This study was financially supported by NIH Grant No. P41EB002027 (NESAC/BIO).

Chapter 5. Analyzing the Effect of Protein G B1 Orientation on Antibody Binding in Complex, Multilayer Protein Systems

Elisa T. Harrison
Department of Chemical Engineering, University of Washington, Seattle, Washington 98195

David G. Castner
Department of Chemical Engineering, University of Washington, Seattle, Washington 98195 and Department of Bioengineering, University of Washington, Seattle, Washington 98195

5.1 Introduction

Methods of studying multilayer systems have been studied so extensively that model multilayer systems, such as Irganox delta-layers, are used to calibrate and test the resolution in depth profiling experiments [114, 115, 166, 169, 170]. Well-known markers have been identified in these systems which make studying these model multilayer systems relatively simple. Protein multilayers, on the other hand, do not naturally contain characteristic markers so oftentimes labels are required to obtain information on multilayer protein systems. One such example is binding assays (e.g. sandwich enzyme-linked immunosorbent assays) which are commonly used to obtain information indirectly about immobilized proteins on surfaces. Many layers are formed on top of the protein of interest or labels are required before any information can be gathered.

Unfortunately, a databank for adsorbed protein structures has not been established because the structure of proteins adsorbed onto a surface is not well understood and no atomic level structures of surface-bound proteins exist. This particular lack of scientific data emphasizes the need for techniques to analyze immobilized protein multilayers. Combining many label-free, surface-sensitive techniques can provide the molecular-level information of protein-surface systems lacking in other traditional biochemistry

techniques that rely on indirect measurements, the use of labels, or comparison to solution or crystalline phases.

The focus of this study was to distinguish between proteins and antibodies in multicomponent protein films and to measure the effect of protein orientation on antibody binding using a variety of surface analytical techniques. Protein G B1, a 6 kDa, 56 amino acid immunoglobulin (IgG)-binding domain of protein G, was used in this study because of its stability, known structure, and amenability to protein engineering. Multicomponent protein films were formed using protein G B1 and IgG antibodies, both whole IgG (H+L) antibodies and IgG F(ab')$_2$ fragments, immobilized onto bare gold. Cysteine mutants of protein G B1 were immobilized onto maleimide-oligo(ethylene glycol)-functionalized (MEG) self-assembled monolayers (SAMs) to study the effect of protein orientation on antibody binding.

X-ray photoelectron spectroscopy (XPS) was used to detect amounts of proteins and antibodies immobilized onto surfaces. However, since the atomic composition of proteins and antibodies do not significantly differ, distinguishing between proteins and antibodies in multicomponent films can be challenging [14]. The chemical specificity and increased surface sensitively of secondary ion mass spectrometry (SIMS), especially with the introduction of cluster ion sources [93-96, 171, 172], may be used to distinguish between proteins and antibodies in multicomponent protein films [44, 47, 86, 103, 104, 169, 173, 174]. Additionally, the binding capabilities of proteins and antibodies in the formation of multicomponent protein films was detected in real time using quartz crystal microbalance with dissipation monitoring (QCM-D). This work directly addresses the challenges in studying complex, multicomponent protein/antibody films by advancing our ability to obtain detailed information about the structure, orientation, and binding of immobilized proteins and antibodies.

5.2 MATERIALS AND METHODS

5.2.1 *SUBSTRATE PREPARATION AND MODIFICATION*

Gold-coated silicon wafers and gold-coated quartz crystal sensors were used as substrates for protein immobilization studies. Gold-coated silicon wafers were used for XPS and ToF-SIMS studies and gold-coated quartz crystal sensors were used in QCM-D experiments. Silicon wafers (Silicon Valley Microelectronics Inc., San Jose, CA) were diced into 1×1 cm^2 substrates using a diamond saw. Gold substrates were fabricated by depositing a 5 nm titanium adhesion layer followed by depositing a 100 nm gold layer onto the diced and cleaned silicon substrates via electron-beam deposition at room temperature and pressures <1 $x10^{-6}$ torr. Gold-coated quartz crystal sensors (Q-Sense, Gothenburg, Sweden) were cleaned using the UV-Ozone cleaner and a 75˚C heated piranha solution (5:1:1 water:hydrogen peroxide:ammonium hydroxide solution; caution: piranha solution reacts violently with organic compounds) prior to surface modification.

The SAM substrates used in this work were prepared by submerging the gold-coated substrates in a solution of 1 mM maleimide-oligo(ethylene glycol) (MEG) dissulfides (HO-EG4-C11-S-S-C11-EG6-NHCO-Maleimide, Prochimia, Sopot, Poland) in 200-proof ethanol (Fisher Scientific) for at least 16 hours. The substrates were then rinsed and sonicated in ethanol to remove unbound molecules. To prepare bare gold substrates, the gold-coated substrates were submerged in 200-proof ethanol in a separate hood to avoid vapor deposition of thiols or disulfides.

5.2.2 *PROTEIN SYNTHESIS*

Protein G B1, wildtype (WT) and the various cysteine point mutants, used in this work were synthesized using methods discussed in Chapter 4. Cysteine mutants of protein G B1 were synthesized to vary the site of immobilization. The proteins used in this work were protein G B1 WT and five cysteine mutants: threonine11 to cysteine (T11C), valine21 to cysteine (V21C), asparatic-acid35 to cysteine (D35C), glutamic-acid42 to cysteine (E42C), and threonine49 to cysteine (T49C). Whole IgG (H+L) antibody and

IgG F(ab')$_2$ fragment of the IgG antibody were purchased from Jackson ImmunoResearch (West Grove, PA).

5.2.3 *Protein Adsorption*

Depending on the instrument used, protein immobilization was done in either a static or flow mode. Protein immobilization for X-ray photoelectron spectroscopy (XPS) and time-of-flight secondary ion mass spectrometry (ToF-SIMS) studies was done using static adsorption while protein immobilization for quartz crystal microbalance with dissipation monitoring (QCM-D) studies was done in a flow regime.

Protein G B1, whole IgG (H+L) antibody, and IgG F(ab')$_2$ fragment antibody solutions were prepared in bicarbonate/carbonate buffer (50 mM, pH 9.5). The buffer was degassed and sonicated for an hour prior to use. Substrates used for static protein/antibody immobilization were hydrated in 0.5 mL degassed buffer in a 24-well plate for 30 min at room temperature prior to adding protein or antibody solution and then allowing the immobilization to occur for 2 hours at room temperature. After protein/antibody immobilization, substrates were rinsed by serial dilution in buffer and then submerged in a series of two buffer and three water solutions for 5 min each while mixing with a stir bar. Substrates were then dried and stored under nitrogen gas. Samples prepared for XPS and ToF-SIMS required drying and exposure to ultra-high vacuum (UHV) conditions while samples prepared in the QCM-D were conducted in solution. Substrates were analyzed by XPS and ToF-SIMS within a week of preparation. Replicates were prepared on different days using freshly prepared protein solutions.

5.2.4 *X-ray Photoelectron Spectroscopy*

XPS data were acquired on a SSI S-Probe XPS system (Surface Science Instruments, Mountain View, CA) using a monochromatic Al $Ka_{1,2}$ X-ray source (hv =1486.6eV). Survey and detailed scans were collected with analyzer pass energy of 150 eV and a 100 ms dwell time. The survey step size was 1 eV, while 0.4 eV was used for detail scans. High-resolution spectra were acquired with analyzer pass energy of 50 eV and a step size of 0.065 eV. Binding energy scales were calibrated by setting the CH_x peak in

the C1s region to 284.6 eV, and a linear background was subtracted for all peak area quantifications. Elemental compositions (atomic percentages) were calculated using the Hawk Data Analysis 7 software (Service Physics, Inc., Bend, Oregon). The C1s, O1s, and Au4f peak areas were obtained from the survey spectra (0-1100 eV). The N1s (390-410 eV) and S2p (155-173 eV) peak areas were obtained from the detailed scans.

5.2.5 *Time-of-Flight Secondary Ion Mass Spectrometry*

Positive ion spectra were acquired using a J105 imager (Ionoptika, Southhampton, UK) using an argon gas cluster gun (GCIB). The GCIB was operated at 40 keV using argon 4000 clusters, containing 15% CO_2 to improve cluster formation (Matheson Tri-Gas, Fife, Washington). Spectra were collected from a 500 micron x 500 micron area with a dose of ~$3.6x10^{11}$ ions/cm^2). The instrument was mass calibrated using a thin film of Irganox 1010 using peaks at masses m/z 219, 527, and 731. Calibration errors were below 5 ppm.

5.2.6 *Quartz Crystal Microbalance with Dissipation Monitoring*

Adsorption and binding of protein G B1 was monitored using the E4 QCM-D (Q-Sense, Gothenburg, Sweden) system. Frequency and dissipation measurements were made on gold-coated quartz crystals with fundamental frequencies of 4.95 MHz (Q-Sense, Gothenburg, Sweden). Replicates were conducted for each protein and substrate combination. The temperature was maintained at 22˚C. During the course of a typical QCM-D experiment, protein G B1 was immobilized onto the sensors at a concentrations ranging from 50 µg/mL to 1000 µg/mL in buffer at a flow rate of 300 µL/min. Following protein G B1 adsorption, the system was rinsed with buffer at 300 µL/min to remove any excess protein. Prior to the QCM-D experiment, the temperature was stabilized for at least 30 min and the buffer baseline was established for at least 30 min.

5.3 RESULTS

5.3.1 *FORMATION OF LAYERED MULTICOMPONENT PROTEIN/ANTIBODY FILMS*

Multicomponent protein/antibody films were formed on bare gold substrates with the goal of forming three distinct layers of different proteins. To distinguish between the different layers, each protein or antibody was either immobilized individually or in a layer-by-layer fashion (1 layer: protein G B1 D35C cysteine mutant on bare gold substrates, 2 layers: whole IgG (H+L) antibody on protein G B1 on bare gold substrates, and 3 layers: IgG F(ab')$_2$ fragment antibody on whole IgG (H+L) antibody on protein G B1 on bare gold substrates). The final multicomponent protein/antibody film (3 layers) is shown as a cartoon in Figure 5.1.

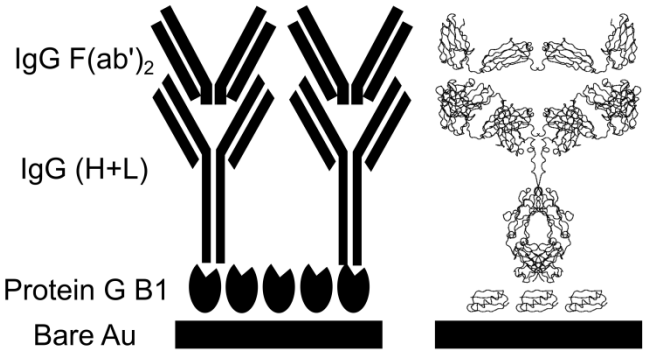

Figure 5.1. Protein G B1, whole IgG (H+L), and IgG F(ab')$_2$ fragments were immobilized on bare gold substrates layer-by-layer. The multicomponent protein/antibody films are depicted as a cartoon and using the crystal structures of the proteins and antibodies visualized using Visual Molecular Dynamics (VMD) Visual Molecular Dynamics (VMD) [17].

The elemental compositions, determined using XPS, for the bare gold substrates and layer-by-layer multicomponent protein/antibody film formation on gold (1 layer, 2 layers, and 3 layers) are listed in Table 5.1. Adventitious atmospheric hydrocarbons were detected on the bare gold substrates since the samples were exposed to the laboratory environment before introduction into ultra-high vacuum [175-178]. With each layer of the

multicomponent protein/antibody formation, the measured nitrogen signal increased, due to higher concentration of nitrogen in the proteins and antibodies, and the gold signal decreased, due to attenuation of the gold surface when increasing the thickness of the organic overlayer. This suggests that multiple layers of protein were formed rather than a mixed monolayer of the three proteins/antibodies.

Table 5.1. XPS elemental composition of bare gold substrate and immobilized protein G B1 D35C cysteine mutant (1 layer), whole IgG (H+L) on protein G B1 (2 layer), and IgG F(ab')$_2$ fragment antibody on whole IgG (H+L) on protein G B1 (3 layer) on bare gold substrates. The Au 4f signal was normalized out to show the elemental composition of the organic overlayer. The remaining signal, excluding Au 4f, was renormalized to 100%. The Au 4f atomic percentages shown are prior to normalization. The Au 4f signal is monitored to access the overlayer thickness and coverage since the gold signal will be attenuated as the thickness or coverage increases. For protein adsorption, the atomic percentage of N1s was monitored since the protein will contribute to a larger nitrogen signal compared to the MEG SAM or bare gold substrate.

	XPS atomic % of organic overlayer				
Sample	C 1s	O 1s	N 1s	S 2p	Au 4f
Bare gold	84.9 ± 6.8	15.1 ± 6.8	n.d.	n.d.	76.5 ± 2.3
1 layer	69.4 ± 1.3	18.1 ± 1.6	8.5 ± 0.4	4.0 ± 0.2	53.6 ± 1.0
2 layers	67.5 ± 3.6	18.5 ± 3.4	10.3 ± 0.3	3.6 ± 0.3	50.2 ±1.5
3 layers	65.3 ± 1.1	19.4 ± 0.7	13.0 ± 0.3	2.3 ± 0.5	40.8 ± 1.4

5.3.2 *Distinguishing between Proteins in Layered Multicomponent Protein/Antibody Films using ToF-SIMS*

XPS is useful for quantifying amounts of proteins immobilized onto surfaces by determining the elemental composition of the top 10 nm of the substrate [35, 40, 42, 86, 165]. However, XPS alone cannot distinguish between the layers of proteins and antibodies used in this work because the proteins and antibodies contain similar amino acids and the sampling depth of XPS encompasses the multiple proteins. The increased surface sensitivity of ToF-SIMS was used to detect slight differences in the intensities of characteristic amino acid mass fragments [34, 39, 44, 86]. Principal component analysis

(PCA) was used to reduce the dimensions of the ToF-SIMS data into principal components (PC) [34, 86]. PC1 captured the majority of variation in the ToF-SIMS data. For proteins immobilized individually and for layer-by-layer formation, PCA identified spectral differences between the protein G B1 D35C cysteine mutant, whole IgG (H+L) antibodies, and IgG F(ab')$_2$ fragment antibodies from protein-only characteristic amino acid mass fragments. The PCA results are shown in Figure 5.2.

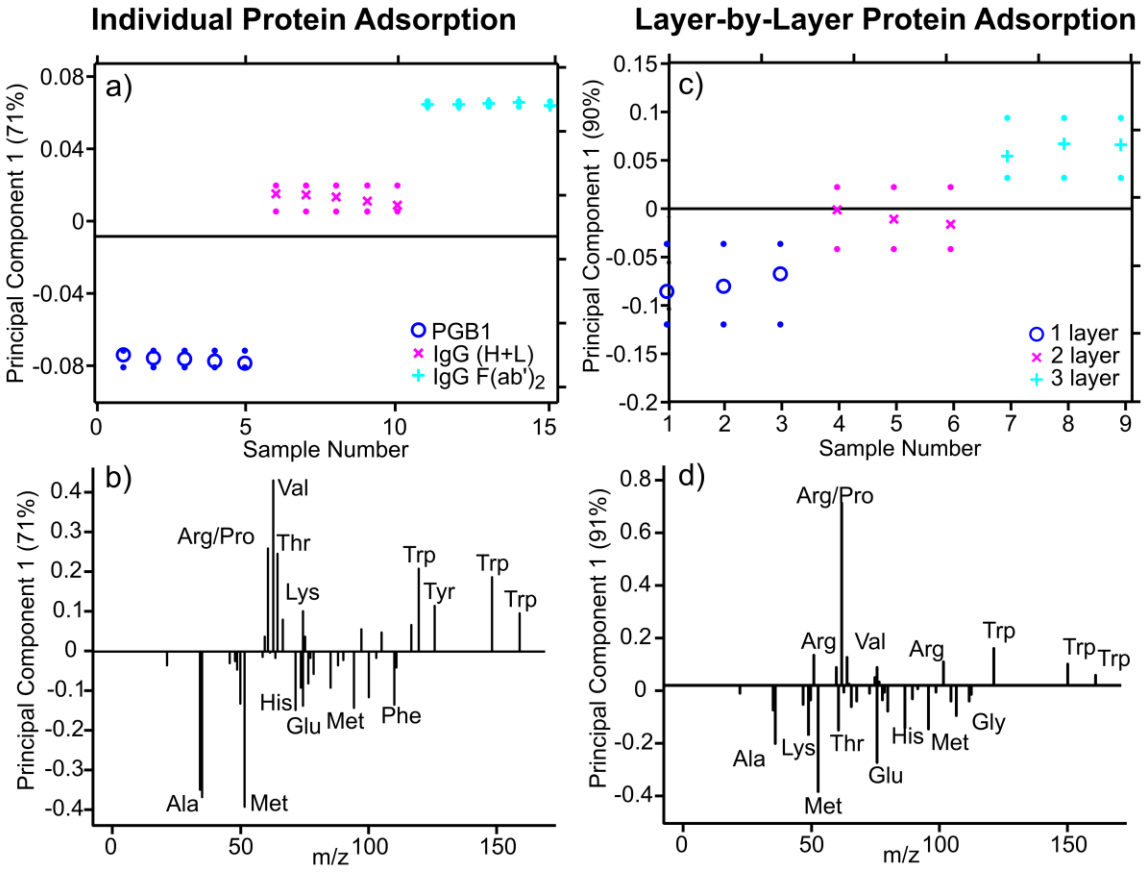

Figure 5.2. PCA results for positive ion ToF-SIMS data from the immobilization of (a,b,c) individual protein G B1 D35C cysteine mutant (PGB1), whole IgG (H+L), and IgG F(ab')$_2$ fragment onto bare gold substrates and (d, e, f) layer-by-layer adsorption of PGB1 onto bare gold substrates (1 layer), whole IgG (H+L) on PGB1 on bare gold substrates (2 layer), and IgG F(ab')$_2$ fragment onto whole IgG (H+L) onto PGB1 onto bare gold substrates (3 layer). Principal component one (PC1) scores (a, d) and loadings (b, c, e, f) were generated from a set of protein-only peaks. PC1 accounted for 71 and 91% of the total variance between spectra, and separated PGB1, whole IgG (H+L), and IgG F(ab')$_2$ fragment when the proteins were immobilized individually and when the proteins were sequentially immobilized layer-by-layer.

For proteins and antibodies immobilized individually and layer-by-layer on bare gold substrates, PC1 captured 70-90% of the variance in the spectra using characteristic protein-only peaks [44, 47, 87]. The positive and negative loading peaks are shown in Figure 5.2(b,d). Among the highest loading peaks, similar positively loading amino acid peaks (Trp, Arg, Pro, Val) and similar negatively loading amino acid peaks (Ala, Met, Glu) loaded high whether the proteins and antibodies are immobilized individually or layer-by-layer. Since the IgG antibodies (whole (H+L) and $F(ab')_2$ fragment) load positively and PGB1 loads negatively, amino acids with a higher percentage in the sequence of the IgG antibodies (whole (H+L) and $F(ab')_2$ fragment) are expected to load positively and amino acids with a higher percentage in the sequence of protein G B1 are expected to load negatively. Two amino acids are not present in protein G B1 (Pro and Arg), which explains the higher positively loading Pro and Arg characteristic peaks. To explain the remaining high loading amino acid peaks, the distribution of amino acids in the sequence of the proteins and antibodies was investigated. The numbers and percentages of each amino acid in the sequence of the proteins and antibodies are listed in Table 5.2.

Table 5.2. Amino acid distributions of protein G B1 (PGB1), whole IgG (H+L) antibody, and IgG $F(ab')_2$ fragment antibody. Amino acids with high positive (a) and negative (b) loading in ToF-SIMS analysis using PCA are labeled.

Amino acid	Number in PGB1	% in PGB1	Number in IgG (H+L)	% in IgG (H+L)	Number in IgG $F(ab')_2$	% in IgG $F(ab')_2$
[b]Alanine (Ala)	6	11	72	5	34	8
Cysteine (Cys)	1	2	36	3	10	2
Aspartic acid (Asp)	4	7	54	4	12	3
[b]Glutamic acid (Glu)	5	9	56	4	22	5
Phenylalanine (Phe)	2	4	42	3	8	2
Glycine (Gly)	4	7	98	7	32	7
Histodine (His)	0	0	26	2	4	1
Isoleucine (Ile)	1	2	30	2	12	3
Lysine (Lys)	6	11	82	6	24	6
Leucine (Leu)	3	5	90	7	26	6
[b]Methionine (Met)	1	2	14	1	4	1
Asparagine (Asn)	3	5	50	4	16	4
[a]Proline (Pro)	0	0	102	8	32	7
Glutamine (Gln)	1	2	62	5	18	4
[a]Arginine (Arg)	0	0	38	3	10	2
Serine (Ser)	0	0	178	13	66	15
Threonine (Thr)	11	20	106	8	44	10
[a]Valine (Val)	4	7	122	9	32	7
[a]Tryptophan (Trp)	1	2	26	2	8	2
Tyrosine (Tyr)	3	5	52	4	18	4
Total number of amino acids:	56		1336		432	

Amino acid fragments of Ala, Glu, and Met are among the highest negatively loading amino acid fragments. While PGB1 only contains 6 Ala (compared to 72 in IgG (H+L) and 34 in IgG F(ab')$_2$), 5 Glu amino acids (compared to 56 in IgG (H+L) and 22 in IgG F(ab')$_2$), and 2 Met amino acids (compared to 14 in IgG (H+L) and 4 in IgG F(ab')$_2$), these three amino acids combined are responsible for 22% of PGB1 sequence compared to only 10% of IgG (H+L) and 14% of IgG F(ab')$_2$. On the other hand, amino acid fragments of Pro, Arg, Val, and Trp are among the highest positively loading amino acid fragments. These three amino acids combined are responsible for only 9% of the PGB1 sequence, compared to 22% in IgG (H+L) and 18% in IgG F(ab')$_2$. Since amino acids from only the top 2-3 nm are being probed using ToF-SIMS, this ToF-SIMS analysis complements the XPS results suggesting that the proteins are immobilizing in layers, instead of forming mixed monolayers of proteins.

5.3.3 *Orientation Effects of Protein G B1 on IgG Binding*

To test the effects of protein G B1 orientation on IgG antibody binding, the orientation of protein G B1 was controlled using methods described in ref. [31, 32] and Chapter 4. Cysteine mutants of protein G B1, with a single amino acid on the C- and N-terminus, was replaced with a cysteine amino acid for covalent attachment to maleimide surfaces [31, 32, 40]. ToF-SIMS has been used previously to characterize the conformation and orientation of protein G B1 cysteine mutants immobilized onto MEG SAM substrates. This work has been expanded to determine the effect of protein G B1 orientation on IgG antibody binding. To accomplish this, we have utilized QCM-D to monitor the amount of IgG antibodies (both whole (H+L) and F(ab')$_2$ fragments) that bind to the V21C cysteine mutant, T11C cysteine mutant, and the wildtype of protein G B1, which contains no cysteine amino acids, immobilized onto MEG SAMs substrates. The change in frequency and dissipation during protein G B1 adsorption was monitored. The mass adsorbed, in ng/cm^2, was calculated using the Sauerbrey [82, 168] equation using the seventh overtone. The Sauerbrey equation can only be used if the dissipation is low. If dissipation occurs, the Sauerbrey model will underestimate the mass. The change in frequency, dissipation, and mass for the adsorption of protein G B1 (V21C, T11C, and WT) and IgG antibodies (whole (H+L) and F(ab')$_2$ fragments) are listed in Table 5.3.

Table 5.3. Changes in frequency, dissipation, and Sauerbrey mass for the immobilization of protein G B1 (T11C and V21C mutants and WT) onto a MEG SAM surface followed by binding of whole IgG (H+L) antibody followed by binding of IgG F(ab')$_2$ fragment antibody. After a buffer baseline was established, protein G B1 was introduced and followed by a buffer rinse. Then 100 µg/mL whole IgG (H+L) antibody was introduced and followed by another buffer rinse. Finally, 100 µg/mL IgG F(ab')$_2$ fragment antibody was introduced and followed by a final buffer rinse.

Sample	Change in Frequency (Hz)	Change in Dissipation (x10-6)	Change in Sauerbrey mass (ng/cm^2)
V21C, 1000 µg/mL, on MEG	-4.4	0.3	77.3
+ IgG (H+L), 100 µg/mL	-25.2	1.2	443
+ IgG F(ab')$_2$, 100 µg/mL	-3.2	0.3	56.4
T11C, 800 µg/mL, on MEG	-3.8	0.6	65.9
+ IgG (H+L), 100 µg/mL	-0.8	0.1	14.4
+ IgG F(ab')$_2$, 100 µg/mL	-0.1	0.2	2.0
WT, 1000 µg/mL, on MEG	-1.5	0.2	26.4
+ IgG (H+L), 100 µg/mL	-0.2	0.1	4.1
+ IgG F(ab')$_2$, 100 µg/mL	-0.5	0.04	8.5

The change in frequency and Sauerbrey mass as a function of time is shown in Table 5.3. After the buffer baseline was established for about 10 min, 1000 µg/mL of V21C, 800 µg/mL of T11C, or 1000 µg/mL of WT protein G B1 was added at 300 µL/min for about one hour followed by a buffer rinse. Then, 100 µg/mL of whole IgG (H+L) antibody was introduced at 300 µL/min for about an hour followed by another buffer rinse. Finally, 100 µg/mL of IgG F(ab')$_2$ fragment antibody was introduced at 300 µL/min for about a half hour followed by a final buffer rinse. From the change in frequency, a mass of 66-77 ng/cm^2 of protein G B1 cysteine mutants immobilized, as compared to only 26 ng/cm^2 of protein G B1 wildtype, onto MEG SAM substrates. The mass of whole IgG (H+L) antibody bound to the protein G B1 was about 30 times greater on V21C compared to T11C and about 100 times greater than on WT. The agrees with the difference in molecular weights of the protein and IgG antibody; the molecular weight of the whole IgG antibody (150 kDa) is 25 times more than the molecular weight of protein G B1 (6 kDa). This suggests the orientation of protein G B1 cysteine mutant effects IgG antibody binding and that the V21C mutant has the IgG binding site more accessible than the T11C when immobilized onto MEG SAM substrates. The fact that no

detectable IgG antibody immobilizes onto WT on MEG SAM substrates also demonstrates that absence of nonspecific IgG antibody binding. As expected, the increase in IgG binding on V21C cysteine mutants of protein G B1 increases the subsequent binding of the IgG F(ab')$_2$ fragment antibody, which again binds about 30 times more on V21C compared to T11C.

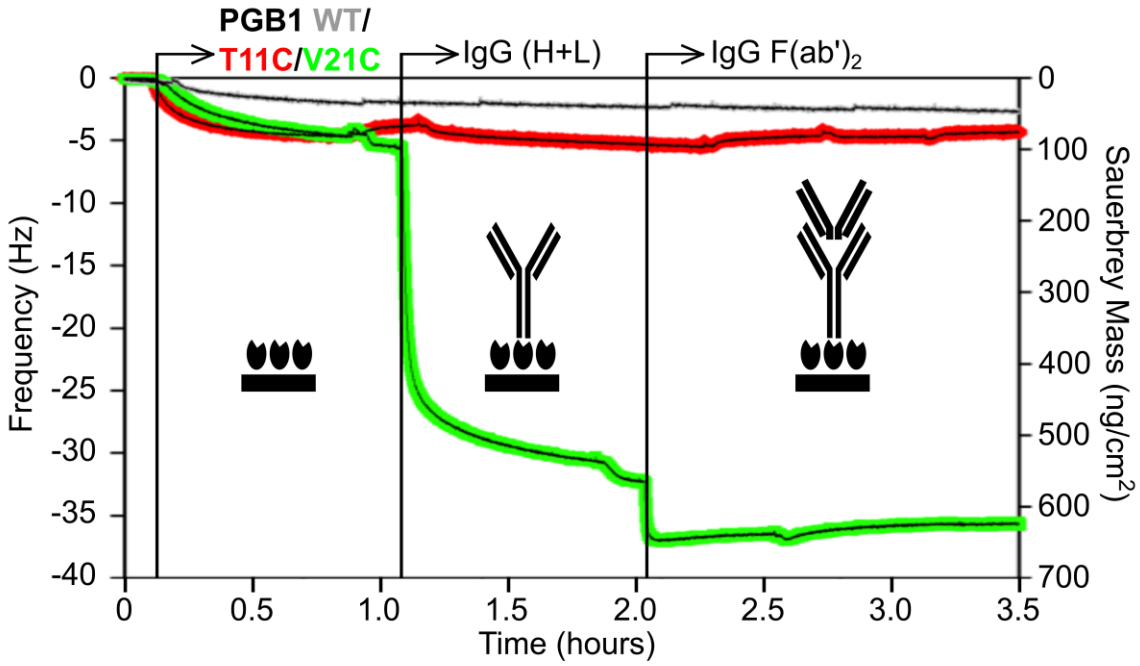

Figure 5.3. Changes in frequency and Sauerbrey mass as a function of time during the immobilization of protein G B1 (T11C and V21C mutants) onto a MEG SAM surface followed by binding of whole IgG (H+L) antibody followed by binding of IgG F(ab')$_2$ fragment antibody. After a buffer baseline was established, protein G B1 in buffer was introduced and followed by a buffer rinse. Then 100 µg/mL whole IgG (H+L) antibody was introduced and followed by another buffer rinse. Then 100 µg/mL IgG F(ab')$_2$ fragment antibody was introduced and followed by a final buffer rinse.

5.4 CONCLUSIONS

Layered multicomponent protein films were successfully formed and characterized using XPS, ToF-SIMS, and QCM-D. Control of the accessibility of the antibody binding sites on the protein was demonstrated by measuring the amount of IgG antibody bound to cysteine mutants of protein G B1 on MEG SAMs.

The following conclusions can be drawn from this work:

(1) The formation of layer-by-layer multicomponent protein films, by immobilizing protein G B1, whole IgG (H+L) antibodies, and IgG F(ab')$_2$ fragment antibodies, were confirmed using XPS. The nitrogen signal increased, due to higher concentration of nitrogen in the proteins and antibodies, and the gold signal decreased, due to attenuation of the gold surface when increasing the thickness of the organic overlayer.

(2) The surface sensitivity of ToF-SIMS enabled us distinguish between proteins and antibodies. PCA of the ToF-SIMS spectra of protein only peaks suggested that the proteins and antibodies are immobilizing in layers instead of forming a mixed monolayer of proteins and antibodies.

(3) The orientation of protein G B1 cysteine mutants immobilized onto MEG SAM substrates effects IgG antibody binding. In fact, the IgG antibody binds 30 times more on the V21C mutant of protein G B1 immobilized onto MEG SAM substrates compared to the T11C mutant.

5.5 ACKNOWLEDGEMENTS

Recombinant protein G B1 used in this work was obtained from the Institute for Protein Design, University of Washington, Seattle, WA. This study was financially supported by NIH Grant No. P41EB002027 (NESAC/BIO).

Chapter 6. CONCLUDING REMARKS

6.1 SCIENTIFIC/TECHNOLOGICAL MOTIVATION

Binding assays (e.g. sandwich ELISAs) are commonly used to obtain information indirectly about immobilized proteins on surfaces. The structure and activity of proteins are inferred by measuring how proteins bind to other proteins and/or antibodies. Oftentimes, many layers are formed on top of the protein of interest or labels are required before any information can be gathered. Alternatively, combining many label-free, surface-sensitive techniques and computational methods can provide the molecular-level information of protein-surface systems lacking in other traditional biochemistry techniques that rely on indirect measurements, the use of labels, or comparison to solution or crystalline phases.

6.2 SCIENTIFIC/TECHNOLOGICAL IMPACT

A full understanding of the interactions between proteins and surfaces, especially at the molecular level, is essential in the development of many diverse applications including biosensors, medical devices, pharmaceutical drugs, and environmental test devices. Since proteins will immediately adsorb onto any material when it comes in contact with a biological fluid, the function of the material can be affected by the structure, activity, and orientation of immobilized proteins.

Controlling the immobilization of proteins on the surface is necessary for the development of *in vitro* binding protein devices, such as enzyme-linked immunosorbent assays and protein microarrays. Controlled adsorption of proteins on surfaces, via hydrophobic interactions, electrostatic interaction, or covalent attachment, has been used to improve the antibody binding capabilities of binding assays. Specifically, the orientation of proteins can play a vital role in the function and performance of such binding assays.

The need to control the immobilization of proteins on surfaces motivates the necessity for developing methods capable of fully analyzing protein-surface interactions.

Quantitative techniques, such as nuclear magnetic resonance (NMR) and X-ray diffraction (XRD), have been developed to analyze the structure of proteins in solution or in its crystalline phase. The Research Collaboratory for Structural Bioinformatics (RCSB) protein databank contains protein structures of over 116,000 proteins. Unfortunately, a databank for adsorbed protein structures has not been established because the structure of proteins adsorbed onto a surface is not well understood and no atomic level structures of surface-bound proteins exist. This particular lack of scientific data emphasizes the need for techniques to analyze immobilized proteins. This research project directly addresses these challenges by advancing our ability to obtain detailed information about the structure of immobilized proteins.

6.3 Summary of Dissertation and Future Work

Surface analytical and computational techniques were developed to obtain a more detailed structural understanding of immobilized proteins. The goal was to stress the importance of using a multi-technique approach, combining both surface analytical and computational methods, to fully characterize protein structure on surfaces. The work outlined in this dissertation focused on two main aspects of protein immobilization: (1) the orientation and conformation of immobilized proteins and (2) the formation of complex, multicomponent protein films.

The focus of this work was to control the orientation of protein G B1, an antibody-binding protein, on well-defined surfaces as well as determining the effect of protein G B1 orientation on antibody binding. Protein G B1, a 6 kDa, 56 amino acid immunoglobulin-binding domain of protein G, was used in this study because of its stability, known structure, and amenability to protein engineering.

Surface analytical techniques, such as X-ray photoelectron spectroscopy (XPS), time-of-flight secondary ion mass spectrometry (ToF-SIMS), quartz crystal microbalance with dissipation monitoring (QCM-D), and sum frequency generation (SFG), were used to provide information on the composition, mass of adsorbed proteins, orientation, activity, and adsorption/binding kinetics of immobilized proteins. To control orientation, five cysteine point mutations of protein G B1 were immobilized onto maleimide-

oligo(ethylene glycol)-functionalized (MEG) self-assembled monolayers (SAMs) and bare gold surfaces.

XPS was used to verify the quality of the substrates and to quantify protein adsorption. QCM-D was used to measure changes in mass and viscoelastic properties of immobilized proteins as a function of time. QCM-D detected protein coverages of 70 - 130 ng/cm^2. Amino acids with asymmetric distributions in the protein G B1 3D structure (Ile/Leu, Gly, Asn, Tyr, Phe, and Trp) were used to calculate peak intensity ratios from ToF-SIMS data to determine the orientation of the cysteine mutants of protein G B1 covalently attached to a MEG SAM surface. QCM-D and XPS analysis revealed that packing density along with orientation affected the antibody binding process. Spectra from ToF-SIMS using large Ar gas cluster ion beam (GCIB) sources were used to distinguish the different proteins present in multilayer protein systems. This work can be expanded by using large Ar GCIB sources to depth profile through multilayer protein films.

Additionally, development of computational methods to study proteins on surfaces complemented surface analytical data. A Monte Carlo (MC) algorithm was developed to predict protein orientation on surfaces. MC techniques allowed the sampling of protein orientations on surfaces at a lower computational cost than conventional Molecular Dynamics simulations. Two preferred and distinct orientations of protein G B1 adsorbed in side-on configurations onto a hydrophobic surface were predicted and characterized as two mutually exclusive sets of amino acids on the outermost β-sheets contacting the surface. This prediction was consistent with SFG vibrational spectroscopy results. In fact, theoretical SFG spectra calculated from an equal combination of the two predicted orientations exhibited reasonable agreement with measured spectra of protein G B1 on polystyrene surfaces. This method can be expanded to predict protein G B1 orientations on more complex surfaces, such as self-assembled monolayers.

BIBLIOGRAPHY

1. Wu, P., D.G. Castner, and D.W. Grainger, *Diagnostic devices as biomaterials: a review of nucleic acid and protein microarray surface performance issues.* Journal of Biomaterials Science, Polymer Edition, 2008. **19**(6): p. 725-753.
2. Zaera, F., *Probing liquid/solid interfaces at the molecular level.* Chemical reviews, 2012. **112**(5): p. 2920-2986.
3. Costa, D., P.A. Garrain, and M. Baaden, *Understanding small biomolecule-biomaterial interactions: A review of fundamental theoretical and experimental approaches for biomolecule interactions with inorganic surfaces.* Journal of Biomedical Materials Research Part A, 2013. **101**(4): p. 1210-1222.
4. Pei, X., B. Zhang, J. Tang, B. Liu, W. Lai, and D. Tang, *Sandwich-type immunosensors and immunoassays exploiting nanostructure labels: A review.* Analytica chimica acta, 2013. **758**: p. 1-18.
5. Mashaghi, A., S. Mashaghi, I. Reviakine, R.M. Heeren, V. Sandoghdar, and M. Bonn, *Label-free characterization of biomembranes: from structure to dynamics.* Chemical Society Reviews, 2014. **43**(3): p. 887-900.
6. Welch, N.G., J.A. Scoble, B.W. Muir, and P.J. Pigram, *Orientation and characterization of immobilized antibodies for improved immunoassays (Review).* Biointerphases, 2017. **12**(2): p. 02D301.
7. Haynes, C.A. and W. Norde, *Structures and stabilities of adsorbed proteins.* Journal of colloid and interface science, 1995. **169**(2): p. 313-328.
8. Green, R., I. Hopkinson, and R. Jones, *Unfolding and intermolecular association in globular proteins adsorbed at interfaces.* Langmuir, 1999. **15**(15): p. 5102-5110.
9. Gray, J.J., *The interaction of proteins with solid surfaces.* Current opinion in structural biology, 2004. **14**(1): p. 110-115.
10. Dickinson, E., *Adsorbed protein layers at fluid interfaces: interactions, structure and surface rheology.* Colloids and Surfaces B: Biointerfaces, 1999. **15**(2): p. 161-176.
11. Dalgicdir, C. and M. Sayar, *Conformation and Aggregation of LKα14 Peptide in Bulk Water and at the Air/Water Interface.* The Journal of Physical Chemistry B, 2015. **119**(49): p. 15164-15175.
12. Wang, H., D.G. Castner, B.D. Ratner, and S. Jiang, *Probing the orientation of surface-immobilized immunoglobulin G by time-of-flight secondary ion mass spectrometry.* Langmuir, 2004. **20**(5): p. 1877-1887.
13. Soellner, M.B., K.A. Dickson, B.L. Nilsson, and R.T. Raines, *Site-specific protein immobilization by Staudinger ligation.* Journal of the American Chemical Society, 2003. **125**(39): p. 11790-11791.
14. Peluso, P., D.S. Wilson, D. Do, H. Tran, M. Venkatasubbaiah, D. Quincy, B. Heidecker, K. Poindexter, N. Tolani, and M. Phelan, *Optimizing antibody immobilization strategies for the construction of protein microarrays.* Analytical biochemistry, 2003. **312**(2): p. 113-124.
15. Den Braber, E., J. De Ruijter, L. Ginsel, A. Von Recum, and J. Jansen, *Orientation of ECM protein deposition, fibroblast cytoskeleton, and attachment complex components on silicone microgrooved surfaces.* Journal of biomedical materials research, 1998. **40**(2): p. 291-300.

16. Edmiston, P.L., J.E. Lee, S.-S. Cheng, and S.S. Saavedra, *Molecular orientation distributions in protein films. 1. Cytochrome c adsorbed to substrates of variable surface chemistry.* Journal of the American Chemical Society, 1997. **119**(3): p. 560-570.
17. Marchesi, V., T. Tillack, R. Jackson, J. Segrest, and R. Scott, *Chemical characterization and surface orientation of the major glycoprotein of the human erythrocyte membrane.* Proceedings of the National Academy of Sciences, 1972. **69**(6): p. 1445-1449.
18. Okumura, T. and G. Jamieson, *Platelet glycocalicin. I. Orientation of glycoproteins of the human platelet surface.* Journal of Biological Chemistry, 1976. **251**(19): p. 5944-5949.
19. Cha, T., A. Guo, and X.Y. Zhu, *Enzymatic activity on a chip: the critical role of protein orientation.* Proteomics, 2005. **5**(2): p. 416-419.
20. Seong, S.y. and C.y. Choi, *Current status of protein chip development in terms of fabrication and application.* Proteomics, 2003. **3**(11): p. 2176-2189.
21. Turkova, J., *Oriented immobilization of biologically active proteins as a tool for revealing protein interactions and function.* Journal of Chromatography B: Biomedical Sciences and Applications, 1999. **722**(1): p. 11-31.
22. Kanno, S., Y. Yanagida, T. Haruyama, E. Kobatake, and M. Aizawa, *Assembling of engineered IgG-binding protein on gold surface for highly oriented antibody immobilization.* Journal of biotechnology, 2000. **76**(2): p. 207-214.
23. O'Neil, K.T., R.H. Hoess, D.P. Raleigh, and W.F. DeGrado, *Thermodynamic genetics of the folding of the B1 immunoglobulin-binding domain from streptococcal protein G.* Proteins: Structure, Function, and Bioinformatics, 1995. **21**(1): p. 11-21.
24. Achari, A., S.P. Hale, A.J. Howard, G.M. Clore, A.M. Gronenborn, K.D. Hardman, and M. Whitlow, *1.67-. ANG. X-ray structure of the B2 immunoglobulin-binding domain of streptococcal protein G and comparison to the NMR structure of the B1 domain.* Biochemistry, 1992. **31**(43): p. 10449-10457.
25. Stone, M.J., S. Gupta, N. Snyder, and L. Regan, *Comparison of protein backbone entropy and β-sheet stability: NMR-derived dynamics of protein G B1 domain mutants.* Journal of the American Chemical Society, 2001. **123**(1): p. 185-186.
26. Franks, W.T., D.H. Zhou, B.J. Wylie, B.G. Money, D.T. Graesser, H.L. Frericks, G. Sahota, and C.M. Rienstra, *Magic-angle spinning solid-state NMR spectroscopy of the β1 immunoglobulin binding domain of protein G (GB1): 15N and 13C chemical shift assignments and conformational analysis.* Journal of the American Chemical Society, 2005. **127**(35): p. 12291-12305.
27. Blanco, F.J., M.A. Jimenez, A. Pineda, M. Rico, J. Santoro, and J.L. Nieto, *NMR Solution Structure of the Isolated N-Terminal Fragment of Protein-G B1 Domain. Evidence of Trifluoroethanol Induced Native-Like. beta.-Hairpin Formation.* Biochemistry, 1994. **33**(19): p. 6004-6014.
28. Weidner, T., N.F. Breen, K. Li, G.P. Drobny, and D.G. Castner, *Sum frequency generation and solid-state NMR study of the structure, orientation, and dynamics of polystyrene-adsorbed peptides.* Proceedings of the National Academy of Sciences, 2010. **107**(30): p. 13288-13293.
29. Gallagher, T., P. Alexander, P. Bryan, and G.L. Gilliland, *Two crystal structures of the B1 immunoglobulin-binding domain of streptococcal protein G and comparison with NMR.* Biochemistry, 1994. **33**(15): p. 4721-4729.
30. Berman, H.M., J. Westbrook, Z. Feng, G. Gilliland, T. Bhat, H. Weissig, I.N. Shindyalov, and P.E. Bourne, *The protein data bank.* Nucleic acids research, 2000. **28**(1): p. 235-242.

31. Baio, J., T. Weidner, N. Samuel, K. McCrea, L. Baugh, P.S. Stayton, and D.G. Castner, *Multitechnique characterization of adsorbed peptide and protein orientation: LK310 and Protein G B1*. Journal of Vacuum Science & Technology B, 2010. **28**(4): p. C5D1-C5D8.
32. Baugh, L., T. Weidner, J. Baio, P.-C.T. Nguyen, L.J. Gamble, P.S. Stayton, and D.G. Castner, *Probing the orientation of surface-immobilized protein G B1 using ToF-SIMS, sum frequency generation, and NEXAFS spectroscopy.* Langmuir, 2010. **26**(21): p. 16434-16441.
33. Benninghoven, A., *Surface investigation of solids by the statical method of secondary ion mass spectroscopy (SIMS).* Surface Science, 1973. **35**: p. 427-457.
34. Brüning, C., S. Hellweg, S. Dambach, D. Lipinsky, and H. Arlinghaus, *Improving the interpretation of ToF-SIMS measurements on adsorbed proteins using PCA.* Surface and Interface Analysis, 2006. **38**(4): p. 191-193.
35. Cheng, F., L.J. Gamble, and D.G. Castner, *XPS, TOF-SIMS, NEXAFS, and SPR characterization of nitrilotriacetic acid-terminated self-assembled monolayers for controllable immobilization of proteins.* Analytical chemistry, 2008. **80**(7): p. 2564-2573.
36. Delcroix, M., S. Demoustier-Champagne, and C.C. Dupont-Gillain, *Quartz crystal microbalance study of ionic strength and pH-dependent polymer conformation and protein adsorption/desorption on PAA, PEO, and mixed PEO/PAA brushes*. Langmuir, 2013. **30**(1): p. 268-277.
37. Dixon, M.C., *Quartz crystal microbalance with dissipation monitoring: enabling real-time characterization of biological materials and their interactions.* J Biomol Tech, 2008. **19**(3): p. 151-158.
38. Dolatshahi-Pirouz, A., K. Rechendorff, M.B. Hovgaard, M. Foss, J. Chevallier, and F. Besenbacher, *Bovine serum albumin adsorption on nano-rough platinum surfaces studied by QCM-D.* Colloids and Surfaces B: Biointerfaces, 2008. **66**(1): p. 53-59.
39. Dubey, M., J. Brison, D.W. Grainger, and D.G. Castner, *Comparison of Bi1+, Bi3+ and C60+ primary ion sources for ToF-SIMS imaging of patterned protein samples.* Surface and Interface Analysis, 2011. **43**(1-2): p. 261-264.
40. Foster, R.N., E.T. Harrison, and D.G. Castner, *ToF-SIMS and XPS Characterization of Protein Films Adsorbed onto Bare and Sodium Styrene Sulfonate Grafted Gold Substrates.* Langmuir, 2016.
41. Green, R.J., R.A. Frazier, K.M. Shakesheff, M.C. Davies, C.J. Roberts, and S.J. Tendler, *Surface plasmon resonance analysis of dynamic biological interactions with biomaterials.* Biomaterials, 2000. **21**(18): p. 1823-1835.
42. McArthur, S.L., *Applications of XPS in bioengineering.* Surface and Interface Analysis, 2006. **38**(11): p. 1380-1385.
43. Michel, R. and D.G. Castner, *Advances in time-of-flight secondary ion mass spectrometry analysis of protein films.* Surface and Interface Analysis, 2006. **38**(11): p. 1386-1392.
44. Muramoto, S., D.J. Graham, M.S. Wagner, T.G. Lee, D.W. Moon, and D.G. Castner, *ToF-SIMS analysis of adsorbed proteins: principal component analysis of the primary ion species effect on the protein fragmentation patterns.* The Journal of Physical Chemistry C, 2011. **115**(49): p. 24247-24255.
45. Nakanishi, K., T. Sakiyama, and K. Imamura, *On the adsorption of proteins on solid surfaces, a common but very complicated phenomenon.* Journal of Bioscience and Bioengineering, 2001. **91**(3): p. 233-244.

46. Tidwell, C.D., D.G. Castner, S.L. Golledge, B.D. Ratner, K. Meyer, B. Hagenhoff, and A. Benninghoven, *Static time-of-flight secondary ion mass spectrometry and x-ray photoelectron spectroscopy characterization of adsorbed albumin and fibronectin films.* Surface and Interface Analysis, 2001. **31**(8): p. 724-733.
47. Wagner, M.S. and D.G. Castner, *Analysis of adsorbed proteins by static time-of-flight secondary ion mass spectrometry.* Applied surface science, 2004. **231**: p. 366-376.
48. Weidner, T. and D.G. Castner, *SFG analysis of surface bound proteins: a route towards structure determination.* Physical Chemistry Chemical Physics, 2013. **15**(30): p. 12516-12524.
49. Xia, N., C.J. May, S.L. McArthur, and D.G. Castner, *Time-of-flight secondary ion mass spectrometry analysis of conformational changes in adsorbed protein films.* Langmuir, 2002. **18**(10): p. 4090-4097.
50. Zheng, J., L. Li, H.-K. Tsao, Y.-J. Sheng, S. Chen, and S. Jiang, *Strong repulsive forces between protein and oligo (ethylene glycol) self-assembled monolayers: a molecular simulation study.* Biophysical journal, 2005. **89**(1): p. 158-166.
51. He, Y., J. Hower, S. Chen, M.T. Bernards, Y. Chang, and S. Jiang, *Molecular simulation studies of protein interactions with zwitterionic phosphorylcholine self-assembled monolayers in the presence of water.* Langmuir, 2008. **24**(18): p. 10358-10364.
52. Collier, G., N.A. Vellore, J.A. Yancey, S.J. Stuart, and R.A. Latour, *Comparison between empirical protein force fields for the simulation of the adsorption behavior of structured LK peptides on functionalized surfaces.* Biointerphases, 2012. **7**(1): p. 24.
53. Liu, J., C. Liao, and J. Zhou, *Multiscale simulations of protein G B1 adsorbed on charged self-assembled monolayers.* Langmuir, 2013. **29**(36): p. 11366-11374.
54. Rohl, C.A., C.E. Strauss, K.M. Misura, and D. Baker, *Protein structure prediction using Rosetta.* Methods in enzymology, 2004. **383**: p. 66-93.
55. Makrodimitris, K., D.L. Masica, E.T. Kim, and J.J. Gray, *Structure prediction of protein-solid surface interactions reveals a molecular recognition motif of statherin for hydroxyapatite.* Journal of the American Chemical Society, 2007. **129**(44): p. 13713-13722.
56. Harrison, E.T., T. Weidner, D.G. Castner, and G. Interlandi, *Predicting the orientation of protein G B1 on hydrophobic surfaces using Monte Carlo simulations.* Biointerphases, 2017. **12**(2): p. 02D401.
57. Fang, F., J. Satulovsky, and I. Szleifer, *Kinetics of protein adsorption and desorption on surfaces with grafted polymers.* Biophysical journal, 2005. **89**(3): p. 1516-1533.
58. Chen, S., J. Zheng, L. Li, and S. Jiang, *Strong resistance of phosphorylcholine self-assembled monolayers to protein adsorption: insights into nonfouling properties of zwitterionic materials.* Journal of the American Chemical Society, 2005. **127**(41): p. 14473-14478.
59. Baszkin, A. and D.J. Lyman, *The interaction of plasma proteins with polymers. I. Relationship between polymer surface energy and protein adsorption/desorption.* Journal of biomedical materials research, 1980. **14**(4): p. 393-403.
60. Li, L., S. Chen, and S. Jiang, *Protein interactions with oligo (ethylene glycol)(OEG) self-assembled monolayers: OEG stability, surface packing density and protein adsorption.* Journal of Biomaterials Science, Polymer Edition, 2007. **18**(11): p. 1415-1427.
61. Norde, W. and J. Lyklema, *Protein adsorption and bacterial adhesion to solid surfaces: a colloid-chemical approach.* Colloids and Surfaces, 1989. **38**(1): p. 1-13.

62. Rabe, M., D. Verdes, and S. Seeger, *Understanding protein adsorption phenomena at solid surfaces.* Advances in colloid and interface science, 2011. **162**(1): p. 87-106.
63. Phan, H.T., S. Bartelt-Hunt, K.B. Rodenhausen, M. Schubert, and J.C. Bartz, *Investigation of Bovine Serum Albumin (BSA) Attachment onto Self-Assembled Monolayers (SAMs) Using Combinatorial Quartz Crystal Microbalance with Dissipation (QCM-D) and Spectroscopic Ellipsometry (SE).* PloS one, 2015. **10**(10): p. e0141282.
64. Li, L., S. Chen, J. Zheng, B.D. Ratner, and S. Jiang, *Protein adsorption on oligo (ethylene glycol)-terminated alkanethiolate self-assembled monolayers: the molecular basis for nonfouling behavior.* The Journal of Physical Chemistry B, 2005. **109**(7): p. 2934-2941.
65. Graham, D.J., D.D. Price, and B.D. Ratner, *Solution assembled and microcontact printed monolayers of dodecanethiol on gold: a multivariate exploration of chemistry and contamination.* Langmuir, 2002. **18**(5): p. 1518-1527.
66. Boeckl, M. and D. Graham, *Self-Assembled Monolayers: Advantages of Pure Alkanethiols.* Material Matters, 2006. **1**(2): p. 3-5.
67. Belu, A.M., D.J. Graham, and D.G. Castner, *Time-of-flight secondary ion mass spectrometry: techniques and applications for the characterization of biomaterial surfaces.* Biomaterials, 2003. **24**(21): p. 3635-3653.
68. Cooper, E. and G.J. Leggett, *Static secondary ion mass spectrometry studies of self-assembled monolayers: influence of adsorbate chain length and terminal functional group on rates of photooxidation of alkanethiols on gold.* Langmuir, 1998. **14**(17): p. 4795-4801.
69. Li, L., S. Chen, and S. Jiang, *Protein adsorption on alkanethiolate self-assembled monolayers: nanoscale surface structural and chemical effects.* Langmuir, 2003. **19**(7): p. 2974-2982.
70. Baio, J.E., T. Weidner, L. Baugh, L.J. Gamble, P.S. Stayton, and D.G. Castner, *Probing the orientation of electrostatically immobilized protein G B1 by time-of-flight secondary ion spectrometry, sum frequency generation, and near-edge X-ray adsorption fine structure spectroscopy.* Langmuir, 2011. **28**(4): p. 2107-2112.
71. Blanco, F.J., A.R. Ortiz, and L. Serrano, *Role of a nonnative interaction in the folding of the protein G B1 domain as inferred from the conformational analysis of the α-helix fragment.* Folding and Design, 1997. **2**(2): p. 123-133.
72. Blanco, F.J. and L. Serrano, *Folding of protein G B1 domain studied by the conformational characterization of fragments comprising its secondary structure elements.* European Journal of Biochemistry, 1995. **230**(2): p. 634-649.
73. Chiu, H.-P., B. Kokona, R. Fairman, and R.P. Cheng, *Effect of highly fluorinated amino acids on protein stability at a solvent-exposed position on an internal strand of protein G B1 domain.* Journal of the American Chemical Society, 2009. **131**(37): p. 13192-13193.
74. Fesinmeyer, R.M., F.M. Hudson, and N.H. Andersen, *Enhanced hairpin stability through loop design: the case of the protein G B1 domain hairpin.* Journal of the American Chemical Society, 2004. **126**(23): p. 7238-7243.
75. Goehlert, V.A., E. Krupinska, L. Regan, and M.J. Stone, *Analysis of side chain mobility among protein G B1 domain mutants with widely varying stabilities.* Protein science, 2004. **13**(12): p. 3322-3330.
76. Sloan, D.J. and H.W. Hellinga, *Dissection of the protein G B1 domain binding site for human IgG Fc fragment.* Protein science, 1999. **8**(08): p. 1643-1648.

77. Vickerman, J.C. and I.S. Gilmore, *Surface analysis: the principal techniques*. Vol. 2. 2009: Wiley Online Library.
78. Castner, D.G., K. Hinds, and D.W. Grainger, *X-ray photoelectron spectroscopy sulfur 2p study of organic thiol and disulfide binding interactions with gold surfaces.* Langmuir, 1996. **12**(21): p. 5083-5086.
79. Speight, R.E. and M.A. Cooper, *A survey of the 2010 quartz crystal microbalance literature.* Journal of Molecular Recognition, 2012. **25**(9): p. 451-473.
80. Fee, C.J., *Label-free, real-time interaction and adsorption analysis 2: Quartz crystal microbalance.* Protein Nanotechnology: Protocols, Instrumentation, and Applications, Second Edition, 2013: p. 313-322.
81. Hirotsugu, O., *Wireless-electrodeless quartz-crystal-microbalance biosensors for studying interactions among biomolecules: A review.* Proceedings of the Japan Academy. Series B, Physical and biological sciences, 2013. **89**(9): p. 401.
82. Sauerbrey, G., *Use of quartz vibration for weighing thin films on a microbalance.* J. Physik, 1959. **155**: p. 206-212.
83. Iruthayaraj, J., G. Olanya, and P.M. Claesson, *Viscoelastic Properties of Adsorbed Bottle-brush Polymer Layers Studied by Quartz Crystal Microbalance□ Dissipation Measurements.* The Journal of Physical Chemistry C, 2008. **112**(38): p. 15028-15036.
84. Donnelly, B. and J. Medige, *Shear properties of human brain tissue.* Journal of biomechanical engineering, 1997. **119**(4): p. 423-432.
85. Constantinides, G., Z.I. Kalcioglu, M. McFarland, J.F. Smith, and K.J. Van Vliet, *Probing mechanical properties of fully hydrated gels and biological tissues.* Journal of biomechanics, 2008. **41**(15): p. 3285-3289.
86. Lhoest, J.B., M.S. Wagner, C.D. Tidwell, and D.G. Castner, *Characterization of adsorbed protein films by time of flight secondary ion mass spectrometry.* J Biomed Mater Res, 2001. **57**(3): p. 432-40.
87. Canavan, H.E., D.J. Graham, X. Cheng, B.D. Ratner, and D.G. Castner, *Comparison of native extracellular matrix with adsorbed protein films using secondary ion mass spectrometry.* Langmuir, 2007. **23**(1): p. 50-56.
88. Mantus, D.S., B.D. Ratner, B.A. Carlson, and J.F. Moulder, *Static secondary ion mass spectrometry of adsorbed proteins.* Analytical chemistry, 1993. **65**(10): p. 1431-1438.
89. Benninghoven, A., *Surface analysis by secondary ion mass spectrometry (SIMS).* Surface Science, 1994. **299**: p. 246-260.
90. Chilkoti, A., B.D. Ratner, and D. Briggs, *Static secondary ion mass spectrometric investigation of the surface chemistry of organic plasma-deposited films created from oxygen-containing precursors. 3. Multivariate statistical modeling.* Analytical chemistry, 1993. **65**(13): p. 1736-1745.
91. Benninghoven, A., F. Rudenauer, and H.W. Werner, *Secondary ion mass spectrometry: basic concepts, instrumental aspects, applications and trends.* 1987.
92. Benninghoven, A., D. Jaspers, and W. Sichtermann, *Secondary-ion emission of amino acids.* Applied physics, 1976. **11**(1): p. 35-39.
93. Hill, R., P. Blenkinsopp, S. Thompson, J. Vickerman, and J.S. Fletcher, *A new time-of-flight SIMS instrument for 3D imaging and analysis.* Surface and Interface Analysis, 2011. **43**(1-2): p. 506-509.
94. Vickerman, J.C., *Molecular imaging and depth profiling by mass spectrometry—SIMS, MALDI or DESI?* Analyst, 2011. **136**(11): p. 2199-2217.

95. Rabbani, S., J. Fletcher, N. Lockyer, and J. Vickerman, *Exploring subcellular imaging on the buncher-ToF J105 3D chemical imager.* Surface and Interface Analysis, 2011. **43**(1-2): p. 380-384.
96. Rabbani, S., A.M. Barber, J.S. Fletcher, N.P. Lockyer, and J.C. Vickerman, *TOF-SIMS with argon gas cluster ion beams: a comparison with C60+.* Analytical chemistry, 2011. **83**(10): p. 3793-3800.
97. Bailey, J., R. Havelund, J.S. Sharp, A.G. Shard, I.S. Gilmore, M.R. Alexander, and D.J. Scurr, *3D ToF-SIMS Imaging of Polymer Multi-layer Films using Argon Cluster Sputter Depth Profiling.* ACS applied materials & interfaces, 2015.
98. Kayser, S., D. Rading, R. Moellers, F. Kollmer, and E. Niehuis, *Surface spectrometry using large argon clusters.* Surface and Interface Analysis, 2013. **45**(1): p. 131-133.
99. Lee, J., S. Ninomiya, J. Matsuo, I. Gilmore, M. Seah, and A. Shard, *Organic depth profiling of a nanostructured delta layer reference material using large argon cluster ions.* Analytical chemistry, 2009. **82**(1): p. 98-105.
100. Miyayama, T., N. Sanada, S.R. Bryan, J.S. Hammond, and M. Suzuki, *Removal of Ar+ beam-induced damaged layers from polyimide surfaces with argon gas cluster ion beams.* Surface and Interface Analysis, 2010. **42**(9): p. 1453-1457.
101. Ninomiya, S., K. Ichiki, H. Yamada, Y. Nakata, T. Seki, T. Aoki, and J. Matsuo, *Molecular depth profiling of multilayer structures of organic semiconductor materials by secondary ion mass spectrometry with large argon cluster ion beams.* Rapid Communications in Mass Spectrometry, 2009. **23**(20): p. 3264-3268.
102. Oshima, S., I. Kashihara, K. Moritani, N. Inui, and K. Mochiji, *Soft-sputtering of insulin films in argon-cluster secondary ion mass spectrometry.* Rapid Communications in Mass Spectrometry, 2011. **25**(8): p. 1070-1074.
103. Wehbe, N., T. Tabarrant, J. Brison, T. Mouhib, A. Delcorte, P. Bertrand, R. Moellers, E. Niehuis, and L. Houssiau, *TOF-SIMS depth profiling of multilayer amino-acid films using large Argon cluster Arn+, C60+ and Cs+ sputtering ions: A comparative study.* Surface and Interface Analysis, 2013. **45**(1): p. 178-180.
104. Wagner, M. and D.G. Castner, *Characterization of adsorbed protein films by time-of-flight secondary ion mass spectrometry with principal component analysis.* Langmuir, 2001. **17**(15): p. 4649-4660.
105. Boyd, R.W., *Nonlinear optics*, in *Handbook of Laser Technology and Applications (Three-Volume Set)*2003, Taylor & Francis. p. 161-183.
106. Roeters, S., C. van Dijk, A. Torres-Knoop, E.H. Backus, R.K. Campen, M. Bonn, and S. Woutersen, *Determining in situ protein conformation and orientation from the amide-i sum-frequency generation spectrum: theory and experiment.* The Journal of Physical Chemistry A, 2013. **117**(29): p. 6311-6322.
107. Berendsen, H.J., D. van der Spoel, and R. van Drunen, *GROMACS: A message-passing parallel molecular dynamics implementation.* Computer Physics Communications, 1995. **91**(1): p. 43-56.
108. David Van Der, S., L. Erik, H. Berk, E. Alan, and J. Herman, *Gromacs: Fast, Flexible, and Free.* J. Comput. Chem, 2005. **26**: p. 1701-1718.
109. Hess, B., C. Kutzner, D. Van Der Spoel, and E. Lindahl, *GROMACS 4: algorithms for highly efficient, load-balanced, and scalable molecular simulation.* Journal of chemical theory and computation, 2008. **4**(3): p. 435-447.

110. Bjelkmar, P., P. Larsson, M.A. Cuendet, B. Hess, and E. Lindahl, *Implementation of the CHARMM force field in GROMACS: Analysis of protein stability effects from correction maps, virtual interaction sites, and water models.* Journal of chemical theory and computation, 2010. **6**(2): p. 459-466.
111. Levitt, M., M. Hirshberg, R. Sharon, and V. Daggett, *Potential energy function and parameters for simulations of the molecular dynamics of proteins and nucleic acids in solution.* Computer physics communications, 1995. **91**(1-3): p. 215-231.
112. Bartell, L., *Molecular geometry: Bonded versus nonbonded interactions.* Journal of Chemical Education, 1968. **45**(12): p. 754.
113. Ferrara, P., J. Apostolakis, and A. Caflisch, *Evaluation of a fast implicit solvent model for molecular dynamics simulations.* Proteins: Structure, Function, and Bioinformatics, 2002. **46**(1): p. 24-33.
114. Hassan, S.A. and P.J. Steinbach, *Water-exclusion and liquid-structure forces in implicit solvation.* The Journal of Physical Chemistry B, 2011. **115**(49): p. 14668-14682.
115. Lazaridis, T. and M. Karplus, *Effective energy functions for protein structure prediction.* Current opinion in structural biology, 2000. **10**(2): p. 139-145.
116. Onufriev, A., D. Bashford, and D.A. Case, *Exploring protein native states and large-scale conformational changes with a modified generalized born model.* Proteins: Structure, Function, and Bioinformatics, 2004. **55**(2): p. 383-394.
117. Hawkins, G.D., C.J. Cramer, and D.G. Truhlar, *Parametrized models of aqueous free energies of solvation based on pairwise descreening of solute atomic charges from a dielectric medium.* The Journal of Physical Chemistry, 1996. **100**(51): p. 19824-19839.
118. Li, Z. and H.A. Scheraga, *Monte Carlo-minimization approach to the multiple-minima problem in protein folding.* Proceedings of the National Academy of Sciences, 1987. **84**(19): p. 6611-6615.
119. Hansmann, U.H. and Y. Okamoto, *New Monte Carlo algorithms for protein folding.* Current opinion in structural biology, 1999. **9**(2): p. 177-183.
120. Metropolis, N. and S. Ulam, *The monte carlo method.* Journal of the American statistical association, 1949. **44**(247): p. 335-341.
121. Pronk, S., S. Páll, R. Schulz, P. Larsson, P. Bjelkmar, R. Apostolov, M.R. Shirts, J.C. Smith, P.M. Kasson, and D. van der Spoel, *GROMACS 4.5: a high-throughput and highly parallel open source molecular simulation toolkit.* Bioinformatics, 2013. **29**(7): p. 845-854.
122. MacKerell, A.D., N. Banavali, and N. Foloppe, *Development and current status of the CHARMM force field for nucleic acids.* Biopolymers, 2000. **56**(4): p. 257-265.
123. Humphrey, W., A. Dalke, and K. Schulten, *VMD: visual molecular dynamics.* Journal of molecular graphics, 1996. **14**(1): p. 33-38.
124. MacKerell Jr, A.D., D. Bashford, M. Bellott, R.L. Dunbrack Jr, J.D. Evanseck, M.J. Field, S. Fischer, J. Gao, H. Guo, and S. Ha, *All-atom empirical potential for molecular modeling and dynamics studies of proteins†.* The Journal of Physical Chemistry B, 1998. **102**(18): p. 3586-3616.
125. MacKerell Jr, A.D., M. Feig, and C.L. Brooks, *Improved treatment of the protein backbone in empirical force fields.* Journal of the American Chemical Society, 2003. **126**(3): p. 698-699.
126. MacKerell, A.D., M. Feig, and C.L. Brooks, *Extending the treatment of backbone energetics in protein force fields: Limitations of gas-phase quantum mechanics in*

reproducing protein conformational distributions in molecular dynamics simulations. Journal of computational chemistry, 2004. **25**(11): p. 1400-1415.
127. Best, R.B., X. Zhu, J. Shim, P.E. Lopes, J. Mittal, M. Feig, and A.D. MacKerell Jr, *Optimization of the additive CHARMM all-atom protein force field targeting improved sampling of the backbone ϕ, ψ and side-chain $\chi 1$ and $\chi 2$ dihedral angles.* Journal of chemical theory and computation, 2012. **8**(9): p. 3257-3273.
128. Darden, T., D. York, and L. Pedersen, *Particle mesh Ewald: An N· log (N) method for Ewald sums in large systems.* The Journal of chemical physics, 1993. **98**(12): p. 10089-10092.
129. Nosé, S., *A unified formulation of the constant temperature molecular dynamics methods.* The Journal of chemical physics, 1984. **81**(1): p. 511-519.
130. Hoover, W.G., *Canonical dynamics: equilibrium phase-space distributions.* Physical Review A, 1985. **31**(3): p. 1695.
131. Hess, B., H. Bekker, H.J. Berendsen, and J.G. Fraaije, *LINCS: a linear constraint solver for molecular simulations.* Journal of computational chemistry, 1997. **18**(12): p. 1463-1472.
132. Griesser, H.J., P.G. Hartley, S.L. McArthur, K.M. McLean, L. Meagher, and H. Thissen, *Interfacial properties and protein resistance of nano-scale polysaccharide coatings.* Smart materials and structures, 2002. **11**(5): p. 652.
133. Rao, S.V., K.W. Anderson, and L.G. Bachas, *Oriented immobilization of proteins.* Microchimica Acta, 1998. **128**(3-4): p. 127-143.
134. Norde, W., *Adsorption of proteins from solution at the solid-liquid interface.* Advances in colloid and interface science, 1986. **25**: p. 267-340.
135. Thyparambil, A.A., Y. Wei, Y. Wu, and R.A. Latour, *Determination of orientation and adsorption-induced changes in the tertiary structure of proteins on material surfaces by chemical modification and peptide mapping.* Acta biomaterialia, 2014. **10**(6): p. 2404-2414.
136. Norde, W., *The behavior of proteins at interfaces, with special attention to the role of the structure stability of the protein molecule*, in *Biologically Modified Polymeric Biomaterial Surfaces*1992, Springer. p. 85-91.
137. Xia, N., Y. Hu, D.W. Grainger, and D.G. Castner, *Functionalized poly (ethylene glycol)-grafted polysiloxane monolayers for control of protein binding.* Langmuir, 2002. **18**(8): p. 3255-3262.
138. Vidal, F. and A. Tadjeddine, *Sum-frequency generation spectroscopy of interfaces.* Reports on Progress in Physics, 2005. **68**(5): p. 1095.
139. Yan, E.C., Z. Wang, and L. Fu, *Proteins at interfaces probed by chiral vibrational sum frequency generation spectroscopy.* The Journal of Physical Chemistry B, 2015. **119**(7): p. 2769-2785.
140. Roy, S., P.A. Covert, W.R. FitzGerald, and D.K. Hore, *Biomolecular structure at solid–liquid interfaces as revealed by nonlinear optical spectroscopy.* Chemical reviews, 2014. **114**(17): p. 8388-8415.
141. Sheinerman, F.B. and C.L. Brooks, *A molecular dynamics simulation study of segment B1 of protein G.* Proteins: Structure, Function, and Bioinformatics, 1997. **29**(2): p. 193-202.

142. Roccatano, D., A. Amadei, A.D. Nola, and H.J. Berendsen, *A molecular dynamics study of the 41-56 β-hairpin from B1 domain of protein G.* Protein science, 1999. **8**(10): p. 2130-2143.
143. DeGrado, W. and J. Lear, *Induction of peptide conformation at apolar water interfaces. 1. A study with model peptides of defined hydrophobic periodicity.* Journal of the American Chemical Society, 1985. **107**(25): p. 7684-7689.
144. Metropolis, N., A.W. Rosenbluth, M.N. Rosenbluth, A.H. Teller, and E. Teller, *Equation of state calculations by fast computing machines.* The journal of chemical physics, 1953. **21**(6): p. 1087-1092.
145. Still, W.C., A. Tempczyk, R.C. Hawley, and T. Hendrickson, *Semianalytical treatment of solvation for molecular mechanics and dynamics.* Journal of the American Chemical Society, 1990. **112**(16): p. 6127-6129.
146. Onufriev, A., D.A. Case, and D. Bashford, *Effective Born radii in the generalized Born approximation: the importance of being perfect.* Journal of computational chemistry, 2002. **23**(14): p. 1297-1304.
147. Roeters, S.J., C.N. van Dijk, A. Torres-Knoop, E.H. Backus, R.K. Campen, M. Bonn, and S. Woutersen, *Determining in situ protein conformation and orientation from the amide-I sum-frequency generation spectrum: theory and experiment.* J Phys Chem A, 2013. **117**(29): p. 6311-22.
148. Weidner, T., N.T. Samuel, K. McCrea, L.J. Gamble, R.S. Ward, and D.G. Castner, *Assembly and structure of α-helical peptide films on hydrophobic fluorocarbon surfaces.* Biointerphases, 2010. **5**(1): p. 9-16.
149. Deighan, M. and J. Pfaendtner, *Exhaustively sampling peptide adsorption with metadynamics.* Langmuir, 2013. **29**(25): p. 7999-8009.
150. Janshoff, A. and C. Steinem, *Quartz crystal microbalance for bioanalytical applications.* Sensors update, 2001. **9**(1): p. 313-354.
151. Höök, F., J. Vörös, M. Rodahl, R. Kurrat, P. Böni, J. Ramsden, M. Textor, N. Spencer, P. Tengvall, and J. Gold, *A comparative study of protein adsorption on titanium oxide surfaces using in situ ellipsometry, optical waveguide lightmode spectroscopy, and quartz crystal microbalance/dissipation.* Colloids and Surfaces B: Biointerfaces, 2002. **24**(2): p. 155-170.
152. Feiler, A.A., A. Sahlholm, T. Sandberg, and K.D. Caldwell, *Adsorption and viscoelastic properties of fractionated mucin (BSM) and bovine serum albumin (BSA) studied with quartz crystal microbalance (QCM-D).* Journal of colloid and interface science, 2007. **315**(2): p. 475-481.
153. Boyd, R.W., *Nonlinear Optics*. 1 ed1992, London: Academic Press.
154. Nguyen, K.T., J.T. King, and Z. Chen, *Orientation Determination of Interfacial beta-Sheet Structures in Situ.* Journal of Physical Chemistry B, 2010. **114**(25): p. 8291-8300.
155. Lambert, A.G., P.B. Davies, and D.J. Neivandt, *Implementing the Theory of Sum Frequency Generation Vibrational Spectroscopy: A Tutorial Review.* Appl. Spectrosc. Rev., 2005. **40**: p. 103-145.
156. Liang, C., M. Louhivuori, S.J. Marrink, T.L.C. Jansen, and J. Knoester, *Vibrational Spectra of a Mechanosensitive Channel.* The Journal of Physical Chemistry Letters, 2013. **4**(3): p. 448-452.

157. Hennig, R., J. Heidrich, M. Saur, L. Schmuser, S.J. Roeters, N. Hellmann, S. Woutersen, M. Bonn, T. Weidner, J. Markl, and D. Schneider, *IM30 triggers membrane fusion in cyanobacteria and chloroplasts.* Nature Communications, 2015. **6**.
158. Schach, D., C. Globisch, S.J. Roeters, S. Woutersen, A. Fuchs, C.K. Weiss, E.H.G. Backus, K. Landfester, M. Bonn, C. Peter, and T. Weidner, *Sticky water surfaces: Helix-coil transitions suppressed in a cell-penetrating peptide at the air-water interface.* The Journal of Chemical Physics, 2014. **141**(22): p. 22D517.
159. Bellucci, L., A. Ardevol, M. Parrinello, H. Lutz, H. Lu, T. Weidner, and T. Corni, *The interaction with a gold surface suppresses fiber-like conformations of the Amyloid Aβ16-22 peptide.* Nanoscale, 2016. **8**: p. 8737-8748.
160. Latour, R.A., *Perspectives on the simulation of protein–surface interactions using empirical force field methods.* Colloids and Surfaces B: Biointerfaces, 2014. **124**: p. 25-37.
161. Biswas, P.K., N.A. Vellore, J.A. Yancey, T.G. Kucukkal, G. Collier, B.R. Brooks, S.J. Stuart, and R.A. Latour, *Simulation of multiphase systems utilizing independent force fields to control intraphase and interphase behavior.* Journal of computational chemistry, 2012. **33**(16): p. 1458-1466.
162. Tronic, E.H., O. Yakovenko, T. Weidner, J.E. Baio, R. Penkala, D.G. Castner, and W.E. Thomas, *Differential surface activation of the A1 domain of von Willebrand factor.* Biointerphases, 2016. **11**(2): p. 029803.
163. Lutz, H., V. Jaeger, R. Berger, M. Bonn, J. Pfaendtner, and T. Weidner, *Biomimetic Growth of Ultrathin Silica Sheets Using Artificial Amphiphilic Peptides.* Advanced Materials Interfaces, 2015. **2**(17).
164. Lazaridis, T. and M. Karplus, *Effective energy function for proteins in solution.* Proteins: Structure, Function, and Bioinformatics, 1999. **35**(2): p. 133-152.
165. Paynter, R., B.D. Ratner, T. Horbett, and H. Thomas, *XPS studies on the organization of adsorbed protein films on fluoropolymers.* Journal of colloid and interface science, 1984. **101**(1): p. 233-245.
166. Shard, A., R. Foster, I. Gilmore, J. Lee, S. Ray, and L. Yang, *VAMAS interlaboratory study on organic depth profiling. Part I: Preliminary report.* Surface and Interface Analysis, 2011. **43**(1-2): p. 510-513.
167. Michel, R., S. Pasche, M. Textor, and D.G. Castner, *The influence of PEG architecture on protein adsorption and conformation.* Langmuir: the ACS journal of surfaces and colloids, 2005. **21**(26): p. 12327.
168. Kankare, J., *Sauerbrey equation of quartz crystal microbalance in liquid medium.* Langmuir, 2002. **18**(18): p. 7092.
169. Fletcher, J.S., N.P. Lockyer, and J.C. Vickerman, *Developments in molecular SIMS depth profiling and 3D imaging of biological systems using polyatomic primary ions.* Mass spectrometry reviews, 2011. **30**(1): p. 142-174.
170. Shard, A., P. Brewer, F. Green, and I. Gilmore, *Measurement of sputtering yields and damage in C60 SIMS depth profiling of model organic materials.* Surface and Interface Analysis, 2007. **39**(4): p. 294-298.
171. Rading, D., R. Moellers, H.G. Cramer, and E. Niehuis, *Dual beam depth profiling of polymer materials: Comparison of C60 and Ar cluster ion beams for sputtering.* Surface and Interface Analysis, 2013. **45**(1): p. 171-174.

172. Taylor, M., D. Scurr, M. Lutolf, L. Buttery, M. Zelzer, and M. Alexander, *3D chemical characterization of frozen hydrated hydrogels using ToF-SIMS with argon cluster sputter depth profiling.* Biointerphases, 2016. **11**(2): p. 02A301.
173. Graham, D.J., M.S. Wagner, and D.G. Castner, *Information from complexity: Challenges of TOF-SIMS data interpretation.* Applied surface science, 2006. **252**(19): p. 6860-6868.
174. Wagner, M., T. Horbett, and D.G. Castner, *Characterization of the structure of binary and ternary adsorbed protein films using electron spectroscopy for chemical analysis, time-of-flight secondary ion mass spectrometry, and radiolabeling.* Langmuir, 2003. **19**(5): p. 1708-1715.
175. Smith, G.C., *Evaluation of a simple correction for the hydrocarbon contamination layer in quantitative surface analysis by XPS.* Journal of electron spectroscopy and related phenomena, 2005. **148**(1): p. 21-28.
176. Evans, S., *Correction for the effects of adventitious carbon overlayers in quantitative XPS analysis.* Surface and Interface Analysis, 1997. **25**(12): p. 924-930.
177. Cheng, F., L.J. Gamble, D.W. Grainger, and D.G. Castner, *X-ray photoelectron spectroscopy, time-of-flight secondary ion mass spectrometry and principal component analysis of the hydrolysis, regeneration and reactivity of NHS-containing organic thin films.* Analytical chemistry, 2007. **79**(22): p. 8781.
178. Lee, C.-Y., P. Gong, G.M. Harbers, D.W. Grainger, D.G. Castner, and L.J. Gamble, *Surface coverage and structure of mixed DNA/alkylthiol monolayers on gold: characterization by XPS, NEXAFS, and fluorescence intensity measurements.* Analytical chemistry, 2006. **78**(10): p. 3326.

APPENDIX

TOF-SIMS AND XPS CHARACTERIZATION OF PROTEIN FILMS ADSORBED ONTO BARE AND SODIUM STYRENESULFONATE-GRAFTED GOLD SUBSTRATES

For full text, see ref. [40]

Rami N. Foster,† Elisa T. Harrison,† and David G. Castner*,†,‡

† National ESCA and Surface Analysis Center for Biomedical Problems, Department of Chemical Engineering, and ‡ National ESCA and Surface Analysis Center for Biomedical Problems, Department of Bioengineering, University of Washington, Seattle, Washington 98195, United States

DOI: 10.1021/acs.langmuir.5b04743

Langmuir, 2016, 32 (13), pp 3207–3216

Publication Date (Web): March 15, 2016

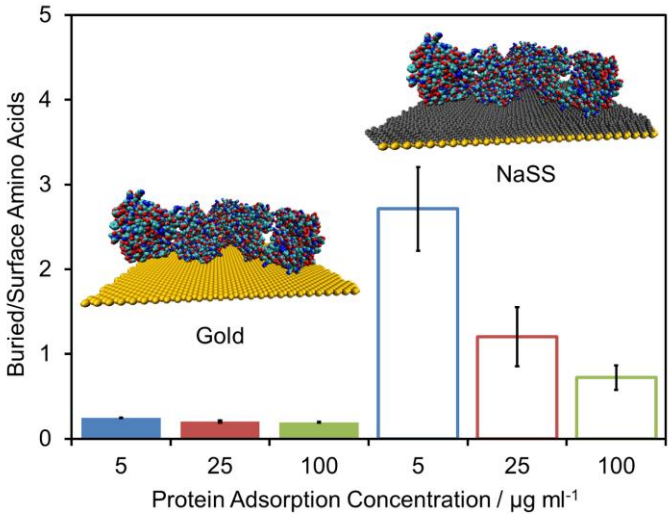

ABSTRACT

The adsorption of single-component bovine serum albumin (BSA), bovine fibrinogen (Fgn), and bovine immunoglobulin G (IgG) films as well as multicomponent bovine plasma films onto bare and sodium styrenesulfonate (NaSS)-grafted gold substrates was characterized. The adsorption isotherms, measured via X-ray photoelectron spectroscopy, showed that at low solution concentrations all three single-component proteins adsorb with higher affinity onto gold surfaces compared to NaSS surfaces. However, at higher concentrations, NaSS surfaces adsorb the same or more total protein than gold surfaces. This may be because proteins that adsorb onto NaSS undergo structural rearrangements, resulting in a larger fraction of irreversibly adsorbed species over time. Still, with the possible exception of BSA adsorbed onto gold, neither surface appeared to have saturated at the highest protein solution concentration studied. Principal component (PC) analysis of amino acid mass fragments from time-of-flight secondary ion mass spectra distinguished between the same protein adsorbed onto NaSS and gold surfaces, suggesting that proteins adsorb differently on NaSS and gold surfaces. Explored further using peak ratios for buried/surface amino acids for each protein, we found that proteins denature more on NaSS surfaces than on gold surfaces. Also, using peak ratios for asymmetrically distributed amino acids, potential structural differences were postulated for BSA and IgG adsorbed onto NaSS and gold surfaces. PC modeling, used to track changes in plasma adsorption with time, suggests that plasma films on NaSS and Au surfaces become more Fgn-like with increasing adsorption time. However, the PC models included only three proteins, where plasma is composed of hundreds of proteins. Therefore, while both gold and NaSS appear to adsorb more Fgn with time, further study is required to confirm that this is representative of the final state of the plasma films.

VITA

Elisa Harrison received a B.S. from Florida State University (FSU) in Chemical-Biomedical Engineering in April 2012. She participated in two undergraduate research experiences at FSU including a tissue engineering laboratory under Dr. Teng Ma and a protein engineering laboratory under Dr. Anant Paravastu. Elisa received Honors in the Major after defending a thesis based on a year and a half of research involving the characterization of a protein using solid-state NMR.

Elisa joined the departments of Chemical Engineering and Bioengineering under Dr. David Castner at the University of Washington in autumn of 2012. She joined the National ESCA and Surface Analysis Center for Biomedical Problems (NESAC/BIO) in January 2013.